CHARACTERIZATION OF DOMAINS WITHIN THE CORONAVIRUS SPIKE GLYCOPROTEIN UTILIZED FOR ENTRY

A Dissertation

Presented to the Faculty of the Graduate School

Of Cornell University

In Partial Fulfillment of the Requirements for the Degree of

Doctor of Philosophy

by

Ikenna Madu

February 2010

CHARACTERIZATION OF DOMAINS WITHIN THE CORONAVIRUS SPIKE GLYCOPROTEIN UTILIZED FOR ENTRY

Ikenna Madu, Ph.D

Cornell University 2010

Enveloped viruses utilize their spike glycoproteins to mediate entry into the target cells. The first step requires binding of the viral spike to the receptor on the surface of the target cells. The binding of the virus to the host receptor is further enhanced in the presence of attachment factors. The final process in the entry event requires the fusion of the host and cell membranes to deliver the viral payload. This is mediated by the fusion machinery of the viral spike and can be triggered by receptor binding, proteolytic activity and/or low pH.

The virus family *Coronavirdae* is a representative of enveloped viruses that cause respiratory disease in a wide range of animal hosts. Coronaviruses like the severe acute respiratory syndrome (SARS) virus and the infectious bronchitis virus (IBV) represent some of the common coronaviruses that have had a negative impact on the health of humans and the poultry industry. It is therefore key that we understand the mechanisms by which these viruses gain entry into their hosts in order to develop specific therapeutics in the event of an outbreak.

In this dissertation, we analyzed two domains within the S2 domain of the severe acute respiratory syndrome (SARS) virus spike protein. We employed a series of mutagenic analysis as well as fusion and pseudoviral infection assays to observe that not only are these domains conserved across the *Coronaviridae,* but they may function as a potential viral fusion peptide in one domain and a critical member of the fusion signaling process in another domain.

We also investigated the entry requirements of the infectious bronchitis virus (IBV). This work combined FACS, fluorescence and competitive assays to observe the use of heparan sulfate as an attachment factor for the Beaudette strain of IBV. This work may further add to the rationale for the promiscuity of this lab-adapted strain of IBV because the virus can infect primary chicken cells as well as most cells exposed to the virus.

BIOGRAPHICAL SKETCH

Ikenna Madu was born and raised in Lagos, Nigeria. For his secondary school education he attended King's college Lagos and graduated in 1996. He moved to the United states of America in 1998 .In 2001 he enrolled into California State University Los Angeles (CSULA) where he received his Bachelor of Science degree in Biochemistry in the spring of 2005. In CSULA, Ikenna participated in the department of Chemistry and Biochemistry minorities in research program. In the Analytical Chemistry laboratory of Dr. Feimeng Zhou, he participated in research characterizing electron and metal transfer involving metallothioneins using electrochemistry combined on-line with inductively coupled plasma-mass spectrometry.

In the fall of 2005, Ikenna enrolled into Cornell University to pursue a Ph.D in the field of Biochemistry, Molecular and Cell Biology in the department of Molecular Biology and Genetics. In 2006, Ikenna began his doctoral research in the laboratory Dr. Gary R. Whittaker in the department of Microbiology and Immunology, in the College of veterinary medicine.

Upon completion of his Ph.D, Ikenna plans to pursue a career in science policy first by participating in the AAAS Science & Technology Policy 2010-2011 Fellowships.

ACKNOWLEDGEMENTS

I would like to thank my advisor Dr. Gary R. Whittaker for all of the support and mentorship. No words can express my gratitude to Dr. Whittaker for taking me into his laboratory and helping me get to the stage of presenting a Ph.D dissertation a feat I that would be impossible if not for his guidance. I am especially grateful for his patience, calmness and belief in my abilities as a researcher, all of which has reinforced me while in his lab and I will take with me as I continue to grow.

I would also like to thank my special committee members Dr. Joel Baines and Dr. Gerald Feigenson. I have benefited immensely from their advice on my research. They have always provided their time and fresh perspective to my training and for that I am grateful. Dr Volker Vogt and his lab were also very supportive in my initial transition from CSULA to Cornell University and for that I will always be thankful.

I would also like to thank the Whittaker group past and present : Shoshannah Roth, Sandrine Belouzard, Victor Chu, Xiangjie Sun, Yueting Zhang, Michele Bialecki, Victor Tse, Andrew Regan, Beth Licitra, Damon Ferguson and Nadia Chapman not only for all their support, ideas and feedback but for their most important contribution, their friendship. I have especially gained a wealth of experience from having many collaborations and discussions with Sandrine and Shoshannah and even better for all the techniques they have shared with me. I also extend my thanks to the laboratory of Dr. Ruth Collins as past and present lab members have also helped me in my graduate research, and Dr. Collins has played a valuable role in my graduate advancement.

In the non-scientific aspects of graduate school, I would like to say thank you to Mary linton, Walter Iddings, Sachiko Funaba, Janna Lamey, and Casey Isham for all their help and support while at the College of Veterinary medicine.

I also would like to thank my family for all the love and support they have showered on me through out my studies they have never failed to show me the what it is to be loved and for that I will always love you all.

Finally I would like to dedicate my graduate work to my wife. I am touched by the love, sacrifice and support she has shown me. I am grateful for all the nights she came to lab with me at odd hours of the night and all the times I lost her as I rambled on. I have known nothing but love from her so this one is for you Idorenyin.

TABLE OF CONTENTS

LIST OF FIGURES

LIST OF TABLES

CHAPTER 1

INTRODUCTION

Viral surface glycoproteins and their roles in mediating entry through receptor binding and membrane fusion.

Viral entry refers to the sum of processes evolved by viruses to efficiently deliver their genome and accessory proteins in a replication competent form into the host cell.

In enveloped viruses, this process of entry initially begins when the virus attaches itself to a receptor or attachment factor via the viral spike glycoprotein. These receptors and attachment factors are usually cellular proteins, carbohydrates or lipids on host cells. Receptors and attachment factors may differ from virus to virus and present themselves in a manner that is abundant or cell specific. Attachment factors like heparan sulfate proteoglycans usually help concentrate viruses like the avian coronavirus Infectious bronchitis virus (IBV), herpes, dengue, papilloma and Sindbis viruses on the surface of cells (9, 11, 15, 20, 46, 53, 80) or in the case of HIV which utilizes cell surface lectins like DC-SIGN and L-SIGN through high mannose N-linked glycans in the envelope protein (gp120) (5, 65). True receptors on the other hand, not only bind the virus and guide the virus down a selective cellular pathway but also serve as cues for conformational changes within the spike protein that may result in membrane fusion. One example is the HIV glycoprotein 120, which despite binding to lectins only undergoes conformational changes when a subunit of the virus protein binds to the receptor CD4 that in turn allows for interaction with co-receptors CXCR4 or CCR5 to ultimately assume a fusion competent conformation (12, 27).

Following receptor binding, overcoming the membrane barrier of the host is the next agenda of the enveloped virus. This is possible through the fusion of the viral and host membranes mediated by the fusion protein component of the spike glycoprotein. Sometimes this fusion protein is a single glycoprotein working in

concert with a receptor binding glycoprotein. The membrane fusion event can occur at the plasma membrane in a neutral pH environment were receptor binding is a trigger, or intracellularly after endocytosis where low pH and/or proteolysis also acts as additional triggers for membrane fusion. For the endocytic route, transport is usually by coated and non-coated clathrin pits/vesicles, caveolae, and macropinocytosis (74). Viruses that use the plasma membrane to gain entry can also use the endocytic route – for example HIV-1 and the severe acute respiratory syndrome (SARS) coronavirus. In both entry routes, conformational changes result in the fusion of host and viral membranes as the viral fusion protein assumes a stable hairpin conformation.

Due to the diversity within the pathway to establish a stable hairpin conformation, there are three different classes of viral fusion proteins (Table 1.1). Class I fusion proteins, of which the influenza HA is the best studied, are trimers of hairpins with a central alpha-helical coiled-coil structure (34, 48, 75) Class II fusion proteins, which occur in flaviviruses and alphaviruses, represent trimers of hairpins composed of beta structures (44, 77) and class III fusion proteins found in the rhabdoviruses and herpesviruses, is a combination of some of the elements of I and II as it displays a central alpha-helical trimeric core similar to class I, but the fusion domain exposes fusion loops located at the tip of an elongated beta-sheet in resemblance of the class II fusion protein (35, 67).

Despite the diversity in viral fusion proteins, one common theme is the exposure of a viral fusion peptide or loop (FP). Following such cues as receptor binding, pH or proteolytic cleavage during entry, the FP is exposed and anchors unto the target membrane and as the metastable fusion protein converts to a lower energy conformation, it allows for both the target and viral membrane to be in close proximity to fuse.

Table 1.1 Classifications of Viral Fusion Proteins (selective) (adapted from Weissenhorn et. al, *FEBS lett.*, 2007)

Virus Family	Virus species	PDB code
Class I		
Orthomyxoviridae	Influenza A virus HA	1HA0, 3HMG, 1HTM, 1QUI
Coronaviridae	SARS coronavirus S2	2BEQ, 1WYY
Class II		
Flaviviridae	Dengue 2 and 3 virus E	1OK8, 1UZG, 10AN, 1TG8
Togaviridae	Semliki forest virus E1	1E9W, 1RER
Class III		
Rhabdoviridae	Vesicular stomatitis virus G	2GUM
Herpesviridae	Herpes simplex virus gB	2CMZ

Fusion peptides are generally apolar sequences that are conserved within a virus family. Commonly found within FPs are bulky hydrophobic residues as well as glycine and alanine residues to confer conformational flexibility. Proof of a fusion peptide usually comes from mutating conserved residues within a proposed sequence in the context of the fusion protein and observing marked reductions in fusion activity compared to the wildtype activity (18, 54, 81). Also the ability of a synthetic peptide form of the said sequence to interact with membranes to induce fusion or identification

of the said sequence in membrane cross-linking studies is key to identifying a fusion peptide. Depending on the position of the FP in relation to the fusion unit, FPs can be considered N-terminal or internal (Table 1.2).

FPs destabilize membranes by initiating stalk formation possibly by displacing water from the lipid-water interface which leads to reduced repulsive force between the fusing host and virus membranes (33, 87).

Table 1.2 Amino acid sequences of viral fusion peptides (adapted from Earp, LJ. et. al. *CTMI*, 2004)

N-terminal	Virus	Sequence
Class I	Influenza HA2	GLFGAIAGFIENGWEG
	Sendai F1	FFGAVIGTIALGVATA
	Resp. Syn. F1	FLGFLLGVGSAIASGV
	HIV gp41	AAIGALFLFGLGAAGSTMGAA
Internal		
Class I	Ebola GP	GAAIGLAWIPYFGPAA
	ASLV gp 37	IFASILAPGVAAAQAL
Class II	SFV E1	DYQCKVYTGVYPFMWGGAYCFCD
	TBE E	DRGWGNHCGLFGKGSIVA
Class III	VSV G	QGTWLNPGFPPQSCGYATV

Along with the FP, other parts of the fusion protein play an important role in fusion. Regions like the membrane proximal ectodomain region (MPER), the

transmembrane domain (TMD), and the cytoplasmic tail (60) have all been cited as players in the fusion machinery.

MPERs are located between the C-terminal heptad repeat and the TMD. Mostly characterized in class 1 viral fusion proteins, MPERs conserved within the virus family commonly contain aromatic residues. MPER sequences have been predicted to partition into membrane interfaces (72, 79, 81). In HIV Env, mutated MPER aromatic residues have been shown to cause a reduction in fusion (71). The mutations to the MPER are believed to abrogate the transition from a small fusion pore to a large one (58). HIV Env MPERs have also been shown to be a site of action of the T20 HIV peptide inhibitor (45). In virus fusion proteins of the SARS coronavirus, VSV-G, HSV-1gH, HPIV2 F and FIV, mutations to the MPER residues inhibited fusion (25, 28, 38, 40, 41, 84) and peptides to the regions in SARS and Ebola have been shown to require aromatic residues in order to destabilize membranes (68, 70). It has also been proposed that the hydrophobicity of the MPER may serve as compensation for less hydrophobic FPs as is the case for several herpes virus gB proteins (4).

C-terminal to the MPER is the transmembrane domain (TMD) another region that is reported to be important for membrane fusion. Although studies on the TMD can affect folding, trimerization, surface expression and even incorporation of the glycoprotein into the virion, it is still important for fusion. An example, also seen in other fusion proteins, is the replacement of the influenza HA TMD with a GPI anchor which blocks fusion, particularly at the hemifusion or small pore stage (43, 55, 57, 84). Many studies have cited factors such as key residues that are either conserved, as is the case for the basic residues within the TMD of retroviral glycoproteins (59, 86), or residues like proline or glycine, which contain helix-disrupting properties, such

residues are found in the middle of the TMD (17, 19) and have been reported as important for TMD function. Other factors such as minimal length of residues as a requirement for individual TMDs to function have also been reported (2, 52, 56). Although studies on the TMD sequences required for supporting fusion are inconclusive, other studies leave us with the suggestion that the TMD must span the viral membrane bilayer and be anchored at the inner leaflet to support fusion.

The cytoplasmic tail (60) (CT) of viral fusion proteins play important roles for membrane fusion within virus families. CTs can affect the ectodomain structure and alter fusion. One example is CT proteolytical cleavage lowering the energy barrier for fusion, thus causing virus fusion proteins like the HIV Env or HSV gB lacking a CT or truncations of the CT to fuse faster (1, 64, 82). Studies have also shown that CTs can serve to prevent premature fusion as observed in the interactions of the gp41 CT and the viral capsid gag (89). Interestingly, the membrane proximal regions of the CT have also been implicated to be critical for the late stages of fusion in a manner much like MPERs. One example observed in SARS S and subtypes of influenza HA is palmitoylation of cysteine residues in the membrane proximal regions of the CT have been shown to be important for membrane fusion (13, 62). The loss in fusion function that comes with the deletion of the CT or palmitoylation sites has been linked to the inability of the mutant fusion proteins to transition from small to large pores: the most energy demanding step of fusion.

Coronaviruses

Coronaviruses (CoV) of the family Coronaviridae are enveloped viruses with a single, linear, non-segmented, positive-sense RNA genome (Figure 1.2). The viral genome, which ranges from 26-32 KB, encodes non-structural proteins, and four main structural proteins S, E, M, N and a fifth protein HE is only encoded in a subset of

CoVs. The S glycoprotein is responsible for receptor binding and membrane fusion. The E protein is an integral protein with roles in morphogenesis, assembly and budding. The M protein functions in viral structural integrity and assembly. The N protein is responsible for viral RNA encapsidation. The group 2 subgroup protein HE has hemagglutination, receptor binding and virion release activity. This virus family has a negative impact on the lives of humans and animals as they cause respiratory and enteric disease within the hosts they infect. CoVs are currently divided into three groups based on serological and genetic data, and are further divided into subgroups (61) (Table 1.3). Group 1 represents viruses that infect humans, bats, cats and dogs while group 2 covers cattle, swine, murine, humans and bats with the severe acute respiratory syndrome coronavirus (SARS-CoV) being the prototype virus of this group. The structural protein S is a main focus of this thesis. Finally group 3, which cover the avian coronaviruses. We discuss in chapter 2 a possible attachment factor utilized by the infectious bronchitis virus (IBV).

A distinctive feature of the CoVs is the crown shaped morphology that can be seen in electron microscopy images attributed to the spike glycoprotein S. It is a heavily glycosylated protein of 150-180 kDa and is responsible for receptor binding and membrane fusion. The CoV spike protein S functions in entry is the main focus and in the course of this thesis, we will go into detail on how domains within the spike protein may aid the entry process. As a major protein of importance for entry, the spike protein of coronaviruses has been studied in detail. The protein is dedicated to the delivery of the viral genome to the target cell. In order to achieve this task, it has two functions: binding the receptor on the host cell, and mediating the fusion of host.

Table 1.3 Representative coronavirus species and receptors (adapted from Perlman et. al. *Nature*, 2009)

GROUP	HOST	VIRUS	RECEPTOR
Group1a	Bat	BtCov	Unknown
	Cat	FCoV, FIPV	APN
	Dog	CCoV	APN
	Pig	TGEV	APN
Group 1b	Human	HCoV-229E, NL63*	APN, ACE2*
	Pig	PEDV	Unknown
Group 2a	Cattle	BCoV	9-O-acetylated sialic acid
	Dog	CRCoV	Unknown
	Human	HCoV–HKUI, OC43	Unknown
	Mouse	MHV	CEACAM
	Pig	PHEV	Unknown
Group 2b	Bat	BtCoV	Unknown
	Human	SARS-CoV	ACE2
Group 3a	Chicken	IBV	Unknown
	Pheasant	PhCoV	Unknown
	Turkey	TCoV	Unknown
Group 3b	Beluga whale	SW1	Unknown
Group 3c	Bulbul	BuCoV-HKU11	Unknown

and viral membranes for the efficient delivery of the viral genome. For these roles, the spike protein can be processed into two main domains, S1 and S2 respectively.

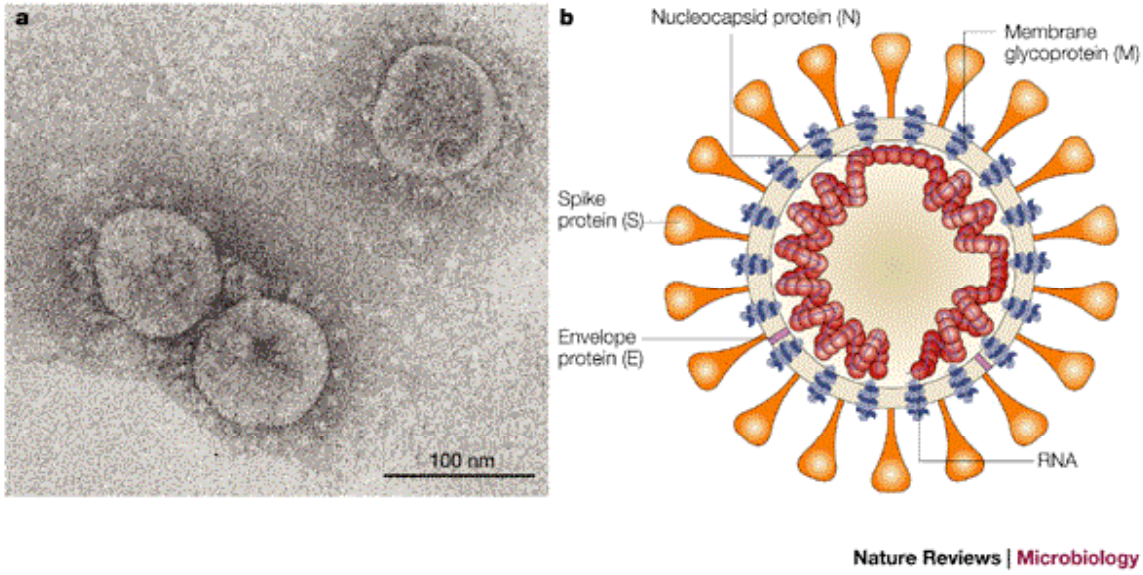

Figure 1.1 a) Electron microscope image and b) Schematic of a Coronavirus.

As CoVs has a wide host range (Table 1.3) the less conserved S1 region (54) defines the host tropism (14, 31, 36, 37, 49, 50, 73, 83, 85). For the S2 domain, undeniable sequence conservation is observed in the fusion component of the protein hinting at a conserved fusion mechanism (16, 54). S2 contains a fusion peptide, heptad repeats (HR1 and HR2), a membrane proximal region, a transmembrane domain and a short C-terminal tail, all of which have been characterized as being important for mediating membrane fusion (8, 10, 38, 62).

Severe acute respiratory syndrome (SARS) coronavirus

The year 2002 marked the introduction of the first new infectious disease of the twenty-first century. A severe respiratory illness, which originated from a province in China, was caused by the severe acute respiratory syndrome coronavirus (SARS-CoV). This new coronavirus with severe disease-causing capabilities in humans was responsible for close to 800 deaths with an overall fatality of 10% until it was brought under control through an effective global quarantine effort in 2003 (21, 24).

The SARS-CoV is a group 2 coronavirus borne out of a zoonotic event from natural reservoir hosts like bats and palm civets (22). Entry into host cells is achieved through the interaction of the viral spike protein S and the host cell receptor, the human angiotensin-converting enzyme 2 (ACE2) (47). As the S protein is key for attachment and entry it is one of the most studied coronavirus proteins in the hopes that detailed studies may lend to the development of therapeutics/prophylactics to combat re-emergence of SARS-CoV or a SARS-like coronavirus into the human population.

SARS-CoV S protein

The SARS-CoV S protein functions as a trimer and is classified as a class 1 viral fusion glycoprotein in the same company as the glycoproteins of HIV, Influenza, and Ebola viruses. This class of fusion proteins is trimeric and alpha-helical in secondary structure and can be triggered to undergo irreversible conformational changes in the presence of a receptor, low pH or a combination of the two (87) .

The structure of the whole S protein has yet to be solved but the minimal receptor-binding domain (RBD) in S1 has been mapped in crystallographic studies to residues 318-510 (3). The crystallographic study of the RBD in complex with the receptor ACE2, revealed the presence of a tyrosine rich receptor binding motif as well

as multiple cysteines in disulphide bonds of which cysteines 479 and 487 are attributed the responsibility of SARS disease progression and tropism (51, 66). SARS-CoV S has also been shown to gain entry with the use of DC-SIGN and L-SIGN (32, 42) however their function as a receptor remains to be further verified.

The fusion component of the S protein lies in the S2 domain. This region is highly conserved within the family and is structurally similar to the other class 1 fusion proteins as S2 contains a fusion peptide, two heptad repeat regions, a membrane proximal region, a transmembrane region and a cytoplasmic tail. S protein of SARS-CoV being mostly proteolytically unprocessed at the boundary of S1/S2 is a character that sets the S protein apart from other class 1 fusion proteins. Also is the fact that the fusion peptide of SARS-CoV and other coronaviruses are internal at a yet unknown location while that of other class 1fusion proteins like HIV and influenza are N-terminal of the membrane anchored subunit. It is considered that the little cleavage that occurs at the S1/S2 boundary is not directly related to fusion peptide exposure for SARS-CoV or any other CoV (7, 76, 90).

Although the mature SARS S protein is proteolytically uncleaved during maturation, proteolysis is required to facilitate membrane fusion. In the presence of proteolytic activity it has been shown that SARS-CoV can gain entry via two pathways: at the cell surface as mediated by trypsin-like enzymes or by the endosomal pathway through the activity of cathepsin L in endosomes (7, 23, 39). Recently, it has been published that within S2 lies a region of proteolysis that has been proposed to be part of a cleavage event that activates the S protein (6, 91).

The multiple investigations on the proteolytic activity occuring within S2, has reopened the controversial discussion about the position of the coronavirus fusion peptide. Previous reports using Wimley and White interfacial hydrophobicity scales

have identified amino acids 770-788 and 858-886 as putative fusion peptides (29, 30, 69). Synthetic peptides corresponding to these regions of S2 were all shown to induce fusion and leakage of vesicles as well as adopt secondary structure in the presence of lipids. Chapter 2 adds to the discussion of the identity of the coronavirus fusion peptide by presenting the region S798-F815 as a putative coronavirus fusion peptide. Our proposal that this region may serve as the fusion peptide is not only based on membrane interactions and secondary structure as seen in previous studies, but also based on the strong conservation within the family and the proximity to the recently publish cleavage site within S2.

Finally the redox status of the S protein during entry has also been taken into consideration. There are 39 cysteines in S capable of disulfide bonds. Studies have shown cysteines have played key roles in receptor binding and membrane fusion (62, 63, 66). Other investigations point to the importance of redox changes occurring during conformational rearrangements of coronavirus proteins (26, 78). In chapter 3, we introduce a cysteine-flanked domain in S2 that is important for membrane fusion. We propose this region forms a disulfide linked loop structure that is part of the fusion machinery within S2 and set out to characterize it.

Infectious Bronchitis virus

The Infectious Bronchitis virus (IBV) is an avian coronavirus that targets the respiratory and uro-genital tract. The virus can spread to different organs throughout the chicken. Infection initially causes respiratory disease in the infected birds but can affect the renal systems of chickens. Poultry industries have suffered great losses as IBV infection causes a reduction in weight gain and also drops egg production in layers and breeders.

The natural receptor for IBV remains unknown but the entry requirements for IBV are still being investigated. To date, the virus entry process has been associated with a low pH environment (16). Cell surface sialic acid has also been reported as a requirement for IBV entry (88) but in the absence of a HE protein in IBV that is required for sialic acid binding, it is most likely interacting with sialic acid as a non specific attachment factor rather than a functional receptor.

IBV can be propagated in embryonated eggs and transiently in primary chicken embryo kidney cells. In contrast to the clinical strains of IBV that infect only primary cells, the Beaudette strain of IBV has an extensive tropism in cell culture and efficiently infects various cell types, including BHK-21 cells and is used as an in vitro infection model.

With the spike protein S being the sole determinant of the extended species tropism, a bioinformatic analysis of the S protein of the Beaudette strain compared to the clinical IBV strains revealed a heparin binding consensus sequence unique to the S protein of Beaudette. In chapter 4, we propose that this region is responsible for binding cell surface heparan sulfate (HS) as an attachment factor aiding extended tropism observed in this strain.

REFERENCES

1. Abrahamyan, L. G., S. R. Mkrtchyan, J. Binley, M. Lu, G. B. Melikyan, and F. S. Cohen. 2005. The cytoplasmic tail slows the folding of human immunodeficiency virus type 1 Env from a late prebundle configuration into the six-helix bundle. Journal of Virology 79:106-115.

2. Armstrong, R. T., A. S. Kushnir, and J. M. White. 2000. The transmembrane domain of influenza hemagglutinin exhibits a stringent length requirement to support the hemifusion to fusion transition. Journal of Cell Biology 151:425-437.

3. Babcock, G. J., D. J. Esshaki, W. D. Thomas, and D. M. Ambrosino. 2004. Amino acids 270 to 510 of the severe acute respiratory syndrome coronavirus spike protein are required for interaction with receptor. Journal of Virology 78:4552-4560.

4. Backovic, M., G. P. Leser, R. A. Lamb, R. Longnecker, and T. S. Jardetzky. 2007. Characterization of EBV gB indicates properties of both class I and class II viral fusion proteins. Virology 368:102-113.

5. Bashirova, A. A., T. B. H. Geijtenbeek, G. C. F. van Duijnhoven, S. J. van Vliet, J. B. G. Eilering, M. P. Martin, L. Wu, T. D. Martin, N. Viebig, P. A. Knolle, V. N. KewalRamani, Y. van Kooyk, and M. Carrington. 2001. A dendritic cell-specific intercellular adhesion molecule 3-grabbing nonintegrin (DC-SIGN)-related protein is highly expressed on human liver sinusoidal endothelial cells and promotes HIV-1 infection. Journal of Experimental Medicine 193:671-678.

6. Belouzard, S., V. C. Chu, and G. R. Whittaker. 2009. Activation of the SARS coronavirus spike protein via sequential proteolytic cleavage at two distinct

sites. Proceedings of the National Academy of Sciences of the United States of America 106:5871-5876.

7. Bosch, B. J., W. Bartelink, and P. J. M. Rottier. 2008. Cathepsin L functionally cleaves the severe acute respiratory syndrome coronavirus class I fusion protein upstream of rather than adjacent to the fusion peptide. Journal of Virology 82:8887-8890.

8. Bosch, B. J., B. E. E. Martina, R. van der Zee, J. Lepault, B. J. Haijema, C. Versluis, A. J. R. Heck, R. de Groot, A. Osterhaus, and P. J. M. Rottier. 2004. Severe acute respiratory syndrome coroavirus (SARS-CoV) infection inhibition using spike protein heptad repeat-derived peptides. Proceedings of the National Academy of Sciences of the United States of America 101:8455-8460.

9. Bose, S., and A. K. Banerjee. 2002. Role of heparan sulfate in human parainfluenza virus type 3 infection. Virology 298:73-83.

10. Broer, R., B. Boson, W. Spaan, F. L. Cosset, and J. Corver. 2006. Important role for the transmembrane domain of severe acute respiratory syndrome coronavirus spike protein during entry. Journal of Virology 80:1302-1310.

11. Brynes, A. P., and D. E. Griffin. 1998. Binding of sindbis virus to cell surface heparan sulfate. Journal of Virology 72:7349-7356.

12. Carr, C. M., and P. S. Kim. 1993. A SPRING-LOADED MECHANISM FOR THE CONFORMATIONAL CHANGE OF INFLUENZA HEMAGGLUTININ. Cell 73:823-832.

13. Chen, B. J., M. Takeda, and R. A. Lamb. 2005. Influenza virus hemagglutinin (H3 subtype) requires palmitoylation of its cytoplasmic tail for assembly: M1

proteins of two subtypes differ in their ability to support assembly. Journal of Virology 79:13673-13684.

14. Chen, D. S., M. Asanaka, F. S. Chen, J. E. Shively, and M. M. C. Lai. 1997. Human carcinoembryonic antigen and biliary glycoprotein can serve as mouse hepatitis virus receptors. Journal of Virology 71:1688-1691.

15. Chen, Y. P., T. Maguire, R. E. Hileman, J. R. Fromm, J. D. Esko, R. J. Linhardt, and R. M. Marks. 1997. Dengue virus infectivity depends on envelope protein binding to target cell heparan sulfate. Nature Medicine 3:866-871.

16. Chu, V. C., L. J. McElroy, V. Chu, B. E. Bauman, and G. R. Whittaker. 2006. The avian coronavirus infectious bronchitis virus undergoes direct low-pH-dependent fusion activation during entry into host cells. Journal of Virology 80:3180-3188.

17. Cleverley, D. Z., and J. Lenard. 1998. The transmembrane domain in viral fusion: Essential role for a conserved glycine residue in vesicular stomatitis virus G protein. Proceedings of the National Academy of Sciences of the United States of America 95:3425-3430.

18. Delos, S. E., and J. M. White. 2000. Critical role for the cysteines flanking the internal fusion peptide of avian sarcoma/leukosis virus envelope glycoprotein. Journal of Virology 74:9738-9741.

19. Dennison, S. M., N. J. Greenfield, J. Lenard, and B. R. Lentz. 2002. VSV transmembrane domain (TMD) peptide promotes PEG-mediated fusion of liposomes in a conformatioanlly sensitive fashion. Biophysical Journal 82:2649.

20. Drobni, P., N. Mistry, N. McMillan, and M. Evander. 2003. Carboxy-fluorescein diacetate, succinimidyl ester labeled papillomavirus virus-like particles fluoresce after internalization and interact with heparan sulfate for binding and entry. Virology 310:163-172.

21. Drosten, C., S. Gunther, W. Preiser, S. van der Werf, H. R. Brodt, S. Becker, H. Rabenau, M. Panning, L. Kolesnikova, R. A. M. Fouchier, A. Berger, A. M. Burguiere, J. Cinatl, M. Eickmann, N. Escriou, K. Grywna, S. Kramme, J. C. Manuguerra, S. Muller, V. Rickerts, M. Sturmer, S. Vieth, H. D. Klenk, A. Osterhaus, H. Schmitz, and H. W. Doerr. 2003. Identification of a novel coronavirus in patients with severe acute respiratory syndrome. New England Journal of Medicine 348:1967-1976.

22. Du, L. Y., Y. X. He, Y. S. Zhou, S. W. Liu, B. J. Zheng, and S. B. Jiang. 2009. The spike protein of SARS-CoV - a target for vaccine and therapeutic development. Nature Reviews Microbiology 7:226-236.

23. Du, L. Y., R. Y. Kao, Y. S. Zhou, Y. X. He, G. Y. Zhao, C. Wong, S. B. Jiang, K. Y. Yuen, D. Y. Jin, and B. J. Zheng. 2007. Cleavage of spike protein of SARS coronavirus by protease factor Xa is associated with viral infectivity. Biochemical and Biophysical Research Communications 359:174-179.

24. Fouchier, R. A. M., T. Kuiken, M. Schutten, G. van Amerongen, J. van Doornum, B. G. van den Hoogen, M. Peiris, W. Lim, K. Stohr, and A. Osterhaus. 2003. Aetiology - Koch's postulates fulfilled for SARS virus. Nature 423:240-240.

25. Galdiero, S., A. Falanga, M. Vitiello, M. D'Isanto, C. Collins, V. Orrei, H. Browne, C. Pedone, and M. Galdiero. 2007. Evidence for a role of the

membrane-proximal region of herpes simplex virus type 1 glycoprotein H in membrane fusion and virus inhibition. Chembiochem 8:885-895.

26. Gallagher, T. M. 1996. Murine coronavirus membrane fusion is blocked by modification of thiols buried within the spike protein. Journal of Virology 70:4683-4690.

27. Gallo, S. A., C. M. Finnegan, M. Viard, Y. Raviv, A. Dimitrov, S. S. Rawat, A. Puri, S. Durell, and R. Blumenthal. 2003. The HIV Env-mediated fusion reaction. Biochimica Et Biophysica Acta-Biomembranes 1614:36-50.

28. Giannecchini, S., F. Bonci, M. Pistello, D. Matteucci, O. Sichi, P. Rovero, and M. Bendinelli. 2004. The membrane-proximal tryptophan-rich region in the transmembrane glycoprotein ectodomain of feline immunodeficiency virus is important for cell entry. Virology 320:156-166.

29. Guillen, J., R. F. M. de Almeida, M. Prieto, and J. Villalain. 2008. Structural and dynamic characterization of the interaction of the putative fusion peptide of the S2SARS-CoV virus protein with lipid membranes. Journal of Physical Chemistry B 112:6997-7007.

30. Guillen, J., A. J. Perez-Berna, M. R. Moreno, and J. Villalain. 2005. Identification of the membrane-active regions of the severe acute respiratory syndrome coronavirus spike membrane glycoprotein using a 16/18-mer peptide scan: Implications for the viral fusion mechanism. Journal of Virology 79:1743-1752.

31. Han, D. P., M. Lohani, and M. W. Cho. 2007. Specific asparagine-linked glycosylation sites are critical for DC-SIGN- and L-SIGN-Mediated severe acute respiratory syndrome coronavirus entry. Journal of Virology 81:12029-12039.

32. Han, D. P., M. Lohani, and M. W. Cho. 2007. Specific asparagine-linked glycosylation sites are critical for DC-SIGN- and L-SIGN-Mediated severe acute respiratory syndrome coronavirus entry. Journal of Virology 81:12029-12039.

33. Han, X., J. H. Bushweller, D. S. Cafiso, and L. K. Tamm. 2001. Membrane structure and fusion-triggering conformational change of the fusion domain from influenza hemagglutinin. Nature Structural Biology 8:715-720.

34. Harrison, S. C. 2005. Mechanism of membrane fusion by viral envelope proteins, p. 231-261, Virus Structure and Assembly, vol. 64.

35. Heldwein, E. E., H. Lou, F. C. Bender, G. H. Cohen, R. J. Eisenberg, and S. C. Harrison. 2006. Crystal structure of glycoprotein B from herpes simplex virus 1. Science 313:217-220.

36. Hensley, L. E., and R. S. Baric. 1998. Human biliary glycoproteins function as receptors for interspecies transfer of Mouse Hepatitis virus, p. 43-52. *In* L. Enjuanes, S. G. Siddell, and W. Spaan (ed.), Coronaviruses and Arteriviruses, vol. 440.

37. Hofmann, H., G. Simmons, A. J. Rennekamp, C. Chaipan, T. Gramberg, E. Heck, M. Geier, A. Wegele, A. Marzi, P. Bates, and S. Pohlmann. 2006. Highly conserved regions within the spike proteins of human coronaviruses 229E and NL63 determine recognition of their respective cellular receptors. Journal of Virology 80:8639-8652.

38. Howard, M. W., E. A. Travanty, S. A. Jeffers, M. K. Smith, S. T. Wennier, L. B. Thackray, and K. V. Holmes. 2008. Aromatic amino acids in the juxtamembrane domain of severe acute respiratory syndrome coronavirus

spike glycoprotein are important for receptor-dependent virus entry and cell-cell fusion. Journal of Virology 82:2883-2894.

39. Huang, I. C., B. J. Bosch, W. H. Li, M. Farzan, P. M. Rottier, and H. Choe. 2006. SARS-CoV, but not HCoV-NL63, utilizes cathepsins to infect cells - Viral entry, p. 335-338. *In* S. Perlamn and K. V. Holmes (ed.), Nidoviruses: Toward Control of Sars and Other Nidovirus Diseases, vol. 581.

40. Jeetendra, E., K. Ghosh, D. Odell, J. Li, H. P. Ghosh, and M. A. Whitt. 2003. The membrane-proximal region of vesicular stomatitis virus glycoprotein G ectodomain is critical for fusion and virus infectivity. Journal of Virology 77:12807-12818.

41. Jeetendra, E., C. S. Robison, L. M. Albritton, and M. A. Whitt. 2002. The membrane-proximal domain of vesicular stomatitis virus G protein functions as a membrane fusion potentiator and can induce hemifusion. Journal of Virology 76:12300-12311.

42. Jeffers, S. A., S. M. Tusell, L. Gillim-Ross, E. M. Hemmila, J. E. Achenbach, G. J. Babcock, W. D. Thomas, L. B. Thackray, M. D. Young, R. J. Mason, D. M. Ambrosino, D. E. Wentworth, J. C. DeMartini, and K. V. Holmes. 2004. CD209L (L-SIGN) is a receptor for severe acute respiratory syndrome coronavirus. Proceedings of the National Academy of Sciences of the United States of America 101:15748-15753.

43. Kemble, G. W., T. Danieli, and J. M. White. 1994. LIPID-ANCHORED INFLUENZA HEMAGGLUTININ PROMOTES HEMIFUSION, NOT COMPLETE FUSION. Cell 76:383-391.

44. Kielian, M., and F. A. Rey. 2006. Virus membrane-fusion proteins: more than one way to make a hairpin. Nature Reviews Microbiology 4:67-76.

45. Kliger, Y., S. A. Gallo, S. G. Peisajovich, I. Munoz-Barroso, S. Avkin, R. Blumenthal, and Y. Shai. 2001. Mode of action of an antiviral peptide from HIV-1 - Inhibition at a post-lipid mixing stage. Journal of Biological Chemistry 276:1391-1397.

46. Kroschewski, H., S. L. Allison, F. X. Heinz, and C. W. Mandl. 2003. Role of heparan sulfate for attachment and entry of tick-borne encephalitis virus. Virology 308:92-100.

47. Kuhn, J. H., W. Li, H. Choe, and M. Farzan. 2004. Angiotensin-converting enzyme 2: a functional receptor for SARS coronavirus. Cellular and Molecular Life Sciences 61:2738-2743.

48. Lamb, R. A., R. G. Paterson, and T. S. Jardetzky. 2006. Paramyxovirus membrane fusion: Lessons from the F and HN atomic structures. Virology 344:30-37.

49. Lewicki, D. N., and T. M. Gallagher. 2002. Quaternary structure of coronavirus spikes in complex with carcinoembryonic antigen-related cell adhesion molecule cellular receptors. Journal of Biological Chemistry 277:19727-19734.

50. Li, W. H., M. J. Moore, N. Vasilieva, J. H. Sui, S. K. Wong, M. A. Berne, M. Somasundaran, J. L. Sullivan, K. Luzuriaga, T. C. Greenough, H. Choe, and M. Farzan. 2003. Angiotensin-converting enzyme 2 is a functional receptor for the SARS coronavirus. Nature 426:450-454.

51. Li, W. H., C. S. Zhang, J. H. Sui, J. H. Kuhn, M. J. Moore, S. W. Luo, S. K. Wong, I. C. Huang, K. M. Xu, N. Vasilieva, A. Murakami, Y. Q. He, W. A. Marasco, Y. Guan, H. Y. Choe, and M. Farzan. 2005. Receptor and viral

determinants of SARS-coronavirus adaptation to human ACE2. Embo Journal 24:1634-1643.

52. Lin, X. X., C. A. Derdeyn, R. Blumenthal, J. West, and E. Hunter. 2003. Progressive truncations C terminal to the membrane-spanning domain of simian immunodeficiency virus Env reduce fusogenicity and increase concentration dependence of Env for fusion. Journal of Virology 77:7067-7077.

53. Madu, I. G., V. C. Chu, H. Lee, A. D. Regan, B. E. Bauman, and G. R. Whittaker. 2007. Heparan sulfate is a selective attachment factor for the avian coronavirus infectious bronchitis virus beaudette. Avian Diseases 51:45-51.

54. Madu, I. G., S. L. Roth, S. Belouzard, and G. R. Whittaker. 2009. Characterization of a Highly Conserved Domain within the Severe Acute Respiratory Syndrome Coronavirus Spike Protein S2 Domain with Characteristics of a Viral Fusion Peptide. Journal of Virology 83:7411-7421.

55. Markosyan, R. M., F. S. Cohen, and G. B. Melikyan. 2000. The lipid-anchored ectodomain of influenza virus hemagglutinin (GPI-HA) is capable of inducing nonenlarging fusion pores. Molecular Biology of the Cell 11:1143-1152.

56. Melikyan, G. B., R. M. Markosyan, H. Hemmati, M. K. Delmedico, D. M. Lambert, and F. S. Cohen. 2000. Evidence that the transition of HIV-1 gp41 into a six-helix bundle, not the bundle configuration, induces membrane fusion. Journal of Cell Biology 151:413-423.

57. Melikyan, G. B., J. M. White, and F. S. Cohen. 1995. GPI-ANCHORED INFLUENZA HEMAGGLUTININ INDUCES HEMIFUSION TO BOTH RED-BLOOD-CELL AND PLANAR BILAYER-MEMBRANES. Journal of Cell Biology 131:679-691.

58. Munoz-Barroso, I., K. Salzwedel, E. Hunter, and R. Blumenthal. 1999. Role of the membrane-proximal domain in the initial stages of human immunodeficiency virus type 1 envelope glycoprotein-mediated membrane fusion. Journal of Virology 73:6089-6092.

59. Owens, R. J., C. Burke, and J. K. Rose. 1994. MUTATIONS IN THE MEMBRANE-SPANNING DOMAIN OF THE HUMAN-IMMUNODEFICIENCY-VIRUS ENVELOPE GLYCOPROTEIN THAT AFFECT FUSION ACTIVITY. Journal of Virology 68:570-574.

60. Parrott, M. M., S. A. Sitarski, R. J. Arnold, L. K. Picton, R. B. Hill, and S. Mukhopadhyay. 2009. Role of Conserved Cysteines in the Alphavirus E3 Protein. Journal of Virology 83:2584-2591.

61. Perlman, S., and J. Netland. 2009. Coronaviruses post-SARS: update on replication and pathogenesis. Nature Reviews Microbiology 7:439-450.

62. Petit, C. M., V. N. Chouljenko, A. Iyer, R. Colgrove, M. Farzan, D. M. Knipe, and K. G. Kousoulas. 2007. Palmitoylation of the cysteine-rich endodomain of the SARS-coronavirus spike glycoprotein is important for spike-mediated cell fusion. Virology 360:264-274.

63. Petit, C. M., J. M. Melancon, V. N. Chouljenko, R. Colgrove, M. Farzan, D. M. Knipe, and K. G. Kousoulas. 2005. Genetic analysis of the SARS-coronavirus spike glycoprotein functional domains involved in cell-surface expression and cell-to-cell fusion. Virology 341:215-230.

64. Plemper, R. K., A. L. Hammond, D. Gerlier, A. K. Fielding, and R. Cattaneo. 2002. Strength of envelope protein interaction modulates cytopathicity of measles virus. Journal of Virology 76:5051-5061.

65. Pohlmann, S., F. Baribaud, and R. W. Doms. 2001. DC-SIGN and DC-SIGNR: helping hands for HIV. Trends in Immunology 22:643-646.

66. Qu, X. X., P. Hao, X. J. Song, S. M. Jiang, Y. X. Liu, P. G. Wang, X. Rao, H. D. Song, S. Y. Wang, Y. Zuo, A. H. Zheng, M. Luo, H. L. Wang, F. Deng, H. Z. Wang, Z. H. Hu, M. X. Ding, G. P. Zhao, and H. K. Deng. 2005. Identification of two critical amino acid residues of the severe acute respiratory syndrome coronavirus spike protein for its variation in zoonotic tropism transition via a double substitution strategy. Journal of Biological Chemistry 280:29588-29595.

67. Roche, S. 2006. Crystal structure of the low-pH form of the vesicular stomatitis virus glycoprotein G (vol 313, pg 187, 2006). Science 313:1389-1389.

68. Saez-Cirion, A., M. J. Gomara, A. Agirre, and J. L. Nieva. 2003. Pre-transmembrane sequence of Ebola glycoprotein - Interfacial hydrophobicity distribution and interaction with membranes. Febs Letters 533:47-53.

69. Sainz, B., J. M. Rausch, W. R. Gallaher, R. F. Garry, and W. C. Wimley. 2005. Identification and characterization of the putative fusion peptide of the severe acute respiratory syndrome-associated coronavirus spike protein. Journal of Virology 79:7195-7206.

70. Sainz, B., J. M. Rausch, W. R. Gallaher, R. F. Garry, and W. C. Wimley. 2005. The aromatic domain of the coronavirus class I viral fusion protein induces membrane permeabilization: Putative role during viral entry. Biochemistry 44:947-958.

71. Salzwedel, K., J. T. West, and E. Hunter. 1999. A conserved tryptophan-rich motif in the membrane-proximal region of the human immunodeficiency virus

type 1 gp41 ectodomain is important for Env-mediated fusion and virus infectivity. Journal of Virology 73:2469-2480.

72. Schibli, D. J., R. C. Montelaro, and H. J. Vogel. 2001. The membrane-proximal tryptophan-rich region of the HIV glycoprotein, gp41, forms a well-defined helix in dodecylphosphocholine micelles. Biochemistry 40:9570-9578.

73. Schultze, B., C. Krempl, M. L. Ballesteros, L. Shaw, R. Schauer, L. Enjuanes, and G. Herrler. 1996. Transmissible gastroenteritis coronavirus, but not the related porcine respiratory coronavirus, has a sialic acid (N-glycolylneuraminic acid) binding activity. Journal of Virology 70:5634-5637.

74. Sieczkarski, S. B., and G. R. Whittaker. 2002. Dissecting virus entry via endocytosis. Journal of General Virology 83:1535-1545.

75. Skehel, J. J., and D. C. Wiley. 2000. Receptor binding and membrane fusion in virus entry: The influenza hemagglutinin. Annual Review of Biochemistry 69:531-569.

76. Song, H. C., M. Y. Seo, K. Stadler, B. J. Yoo, Q. L. Choo, S. R. Coates, Y. Uematsu, T. Harada, C. E. Greer, J. M. Polo, P. Pileri, M. Eickmann, R. Rappuoli, S. Abrignani, M. Houghton, and J. H. Han. 2004. Synthesis and characterization of a native, oligomeric form of recombinant severe acute respiratory syndrome coronavirus spike glycoprotein. Journal of Virology 78:10328-10335.

77. Stiasny, K., and F. X. Heinz. 2006. Flavivirus membrane fusion. Journal of General Virology 87:2755-2766.

78. Sturman, L. S., C. S. Ricard, and K. V. Holmes. 1990. CONFORMATIONAL CHANGE OF THE CORONAVIRUS PEPLOMER GLYCOPROTEIN AT

PH 8.0 AND 37-DEGREES-C CORRELATES WITH VIRUS AGGREGATION AND VIRUS-INDUCED CELL-FUSION. Journal of Virology 64:3042-3050.

79. Suarez, T., S. Nir, F. M. Goni, A. Saez-Cirion, and J. L. Nieva. 2000. The pre-transmembrane region of the human immunodeficiency virus type-1 glycoprotein: a novel fusogenic sequence. Febs Letters 477:145-149.

80. Summerford, C., and R. J. Samulski. 1998. Membrane-associated heparan sulfate proteoglycan is a receptor for adeno-associated virus type 2 virions. Journal of Virology 72:1438-1445.

81. Sun, X., S. Belouzard, and G. R. Whittaker. 2008. Molecular architecture of the bipartite fusion loops of vesicular stomatitis virus glycoprotein G, a class III viral fusion protein. Journal of Biological Chemistry 283:6418-6427.

82. Taylor, G. M., and D. A. Sanders. 2003. Structural criteria for regulation of membrane fusion and virion incorporation by the murine leukemia virus TM cytoplasmic domain. Virology 312:295-305.

83. Thorp, E. B., and T. M. Gallagher. 2004. Requirements for CEACAMs and cholesterol during murine coronavirus cell entry. Journal of Virology 78:2682-2692.

84. Tong, S. X., and R. W. Compans. 2000. Oligomerization, secretion, and biological function of an anchor-free parainfluenza virus type 2 (PI2) fusion protein. Virology 270:368-376.

85. Wentworth, D. E., and K. V. Holmes. 2001. Molecular determinants of species specificity in the coronavirus receptor aminopeptidase N (CD13): Influence of N-linked glycosylation. Journal of Virology 75:9741-9752.

86. West, J. T., P. B. Johnston, S. R. Dubay, and E. Hunter. 2001. Mutations within the putative membrane-spanning domain of the simian immunodeficiency virus transmembrane glycoprotein define the minimal requirements for fusion, incorporation, and infectivity. Journal of Virology 75:9601-9612.

87. White, J. M., S. E. Delos, M. Brecher, and K. Schornberg. 2008. Structures and mechanisms of viral membrane fusion proteins: Multiple variations on a common theme. Critical Reviews in Biochemistry and Molecular Biology 43:189-219.

88. Winter, C., C. Schwegmann-Wessels, D. Cavanagh, U. Neumann, and G. Herrler. 2006. Sialic acid is a receptor determinant for infection of cells by avian Infectious bronchitis virus. Journal of General Virology 87:1209-1216.

89. Wyma, D. J., J. Y. Jiang, J. Shi, J. Zhou, J. E. Lineberger, M. D. Miller, and C. Aiken. 2004. Coupling of human immunodeficiency virus type 1 fusion to virion maturation: a novel role of the gp41 cytoplasmic tail. Journal of Virology 78:3429-3435.

90. Xiao, X. D., S. Chakraborti, A. S. Dimitrov, K. Gramatikoff, and D. S. Dimitrov. 2003. The SARS-CoV S glycoprotein: expression and functional characterization. Biochemical and Biophysical Research Communications 312:1159-1164.

91. Yamada, Y., and D. X. Liu. 2009. Proteolytic Activation of the Spike Protein at a Novel RRRR/S Motif Is Implicated in Furin-Dependent Entry, Syncytium Formation, and Infectivity of Coronavirus Infectious Bronchitis Virus in Cultured Cells. Journal of Virology 83:8744-8758.

CHAPTER 2

CHARACTERIZATION OF A HIGLY CONSERVED DOMAIN WITHIN THE SEVERE ACUTE RESPIRATORY SYNDROME CORONAVIRUS SPIKE PROTEIN S2 DOMAIN WITH CHARACTERISTICS OF A VIRAL FUSION PEPTIDE

Ikenna G. Madu, Shoshannah L. Roth, Sandrine Belouzard, and Gary R. Whittaker .2009. Journal of Virology, p. 7411-7421, Vol. 83, No. 15

Abstract

Many viral fusion proteins are primed by proteolytic cleavage near their fusion peptides. While the coronavirus (CoV) spike (S) protein is known to be cleaved at the S1/S2 boundary, this cleavage site is not closely linked to a fusion peptide. However, a second cleavage site has been identified in the severe acute respiratory syndrome CoV (SARS-CoV) S2 domain (R797). Here, we investigated whether this internal cleavage of S2 exposes a viral fusion peptide. We show that the residues immediately C-terminal to the SARS-CoV S2 cleavage site SFIEDLLFNKVTLADAGF are very highly conserved across all CoVs. Mutagenesis studies of these residues in SARS-CoV S, followed by cell-cell fusion and pseudotyped virion infectivity assays, showed a critical role for residues L803, L804, and F805 in membrane fusion. Mutation of the most N-terminal residue (S798) had little or no effect on membrane fusion. Biochemical analyses of synthetic peptides corresponding to the proposed S2 fusion peptide also showed an important role for this region in membrane fusion and indicated the presence of alpha-helical structure. We propose that proteolytic cleavage within S2 exposes a novel internal fusion peptide for SARS-CoV S, which may be conserved across the *Coronaviridae*.

Introduction

The severe acute respiratory syndrome coronavirus (SARS-CoV) emerged in 2003 as a significant threat to human health, and CoVs still represent a leading source of novel viruses for emergence into the human population. The CoV spike (S) protein mediates both receptor binding (via the S1 domain) and membrane fusion (via the S2 domain) and shows many features of a class I fusion protein, including the presence of distinct heptad repeats within the fusion domain (37). A critical feature of any viral fusion protein is the so-called "fusion peptide," which is a relatively apolar region of 15 to 25 amino acids that interacts with membranes and drives the fusion reaction (9, 34, 38).

Fusion peptides can be classified as N-terminal or internal, depending on their location relative to the cleavage site of the virus fusion protein (23). One key feature of viral fusion peptides is that within a particular virus family, there is high conservation of amino acid residues; however, there is little similarity between fusion peptides of different virus families (26). Despite these differences, some common themes do emerge, including a high level of glycine and/or alanine residues, as well as critical bulky hydrophobic amino acids. In several cases, the fusion peptide is known to contain a central "kink." In the case of influenza virus hemagglutinin (HA), which is a classic example of an N-terminal fusion peptide, the N- and C-terminal parts of the fusion peptide (which are alpha-helical) penetrate the outer leaflet of the target membrane, with the kink at the phospholipid surface. The inside of the kink contains hydrophobic amino acids, with charged residues on the outer face (18). Internal fusion peptides (such as Ebola virus [EBOV] GP) often contain a conserved proline near their centers but also require a mixture of hydrophobic and flexible residues similar to N-terminal fusion peptides (9, 11). It is believed that the kinked fusion peptide sits in the outer leaflet of the target membrane and possibly induces positive curvature to drive the fusion reaction (22). It is important to note that, despite the presence of key hydrophobic residues, viral fusion peptides often do not display extensive stretches of hydrophobicity and can contain one or more charged residues (8). Ultimately, fusion peptide identification must rely on an often complex set of criteria, including structures of the fusion protein in different conformations, biophysical measurements of peptide function in model membranes, and biological activity in the context of virus particles.

To date, the exact location and sequence of the CoV fusion peptide is not known (4); however, by analogy with other class I viral fusion proteins, it is predicted to be in the

S2 domain. Overall, three membranotropic regions in SARS-CoV S2 have been suggested as potential fusion peptides (14, 17). Based on sequence analysis and a hydrophobicity analysis of the S protein using the Wimley-White (WW) interfacial hydrophobic interface scale, initial indications were that the SARS-CoV fusion peptide resided in the N-terminal part of HR1 (heptad repeat 1) (5, 6), which is conserved across the *Coronaviridae*. Mutagenesis of this predicted fusion peptide inhibited fusion in syncytia assays of S-expressing cells (28). This region of SARS-CoV has also been analyzed by other groups in biochemical assays (16, 17, 29) and defined as the WW II region although Sainz et al. (29) identified another less conserved and less hydrophobic region (WW I) as being more important for fusion. Peptides corresponding to this region have also been studied in biochemical assays by other groups (13). In addition, a third, aromatic region adjacent to the transmembrane domain (the membrane-proximal domain) has been shown to be important in SARS-CoV fusion (15, 20, 25, 30). This membrane-proximal domain likely acts in concert with a fusion peptide in the S2 ectodomain to mediate final bilayer fusion once conformational changes have exposed the fusion peptide in the ectodomain. To date, there is little or no information on the fusion peptides of CoVs other than SARS-CoV, except for the identification of the N-terminal part of the mouse hepatitis virus (MHV) S HR1 domain as a putative fusion peptide based on sequence analysis (6). In none of these cases (for SARS-CoV or MHV) is the role of these sequences as bone fide fusion peptides established.

The majority of class I fusion proteins prime fusion activation by proteolytic processing, with the cleavage event occurring immediately N-terminal to the fusion peptide (21). In the case of SARS-CoV, early reports analyzing heterologously expressed SARS-CoV spike protein indicated that most of the protein was not cleaved

(31, 39) but that there was some possibility of limited cleavage at the S1-S2 boundary (39). However, it is generally considered that S1-S2 cleavage is not directly linked to fusion peptide exposure in the case of SARS-CoV or any other CoV (4). Recently, however, it has been shown that SARS-CoV S can be proteolytically cleaved at a downstream position in S2, at residue 797 (2, 36). Here, we investigated whether cleavage at this internal position in S2 might expose a domain with properties of a viral fusion peptide. We carried out a mutagenesis study of SARS-CoV S residues 798 to 815 using cell-cell fusion and pseudovirus assays, as well as lipid mixing and structural studies of an isolated peptide, and we show the importance of this region as a novel fusion peptide for SARS-CoV.

Materials and Methods

Cell culture. BHK-21, Vero E6, and 293T cells obtained from the American Type Culture Collection were used in this study. All cells were maintained in Dulbecco's modified Eagle's medium (DMEM; Cellgro) containing 10% fetal bovine serum, 100 units/ml penicillin, and 10 μg/ml streptomycin (complete DMEM).

Generation of mutant SARS-CoV spike glycoproteins. Site-directed mutagenesis was carried out on the spike protein expressing vector pcDNA3.1-SARS-CoV S (kindly provided by Michael Farzan, New England Primate Research Center) via PCR, using primers obtained from IDT Technologies. Mutations were then confirmed by sequencing using an Applied Biosystems Automated 3730 DNA Analyzer at the Cornell University Life Sciences Core Laboratories Center.

Analysis of SARS-CoV S cell surface expression. BHK-21 cells were grown on six-well plates and transfected with 1 μg of wild-type or mutant spike protein-expressing plasmids using Lipofectamine 2000 (Invitrogen) for 36 h at 32°C. Transfected cells

were washed twice with cold phosphate-buffered saline and then labeled with 250 μg/ml sulfo-NHS-SS-biotin [sulfosuccinimidyl 2-(biotinamido)-ethyl-1,3-dithiopropionate; Pierce] for 30 min on ice. Cold glycine solution (50 mM) was added to the cells three times at 5-min intervals to quench unlabeled free biotin, followed by a phosphate-buffered saline wash. The cells were lysed in 500 μl of lysis buffer (Tris-buffered saline containing 1% NP-40 and complete protease inhibitor mixture; Roche Applied Science). Surface proteins were affinity purified using immobilized NeutraAvidin beads (Pierce) overnight at 4°C. NeutraAvidin beads were then washed with lysis buffer, followed by the addition of sodium dodecyl sulfate-polyacrylamide gel electrophoresis (SDS-PAGE) sample loading buffer containing 100 mM dithiothreitol. The surface expression was analyzed by Western blotting using the anti-C9 epitope tag monoclonal antibody Rho 1D4 (National Cell Culture Center, Minneapolis, MN), and images were obtained and quantified using an LAS-3000 Mini Fuji film imaging system and software (Fuji Photo Film Co., Ltd). The biotinylation assay was repeated three times, and results from the Western blotting quantifications were plotted using Sigma Plot, version 9.0 (Systat Software).

Syncytia formation and visualization. BHK-21 cells in 24-well plates were cotransfected with pcDNA3.1-SARS-CoV S plasmid encoding wild-type or mutant spike protein and a plasmid encoding ACE2, the SARS-CoV receptor, using Lipofectamine 2000 (Invitrogen) for 24 h at 32°C. Cells were treated with 2 μg/ml of trypsin in serum free medium for 30 min to induce syncytia formation, and then the medium was replaced with complete DMEM for 1 h. The cells were then fixed using 3% paraformaldehyde and prepared for indirect immunofluorescence microscopy using the monoclonal SARS-CoV S antibody 341CD (NIH Biodefense and Emerging Infections Research Resources Repository) and Alexa Fluor 488-labeled anti-mouse

secondary antibody (Invitrogen-Molecular Probes). Images were captured using a Nikon E600 microscope 20x Plan Apo objective (numerical aperture, 0.75) equipped with a SensiCam EM camera (Cooke Corp.) and using IP Lab software (Scanalytics).

Quantitative cell-cell fusion assay. BHK-21 cells were grown in 24-well plates and cotransfected with wild-type or mutant spike protein-expressing plasmids and a plasmid encoding luciferase under the control of a T7 promoter, using Lipofectamine 2000 (Invitrogen) for 24 h at 32°C. Vero E6 cells in a 60-mm dish were also transfected with a plasmid encoding the T7 polymerase. After 24 h the BHK-21 cells were overlaid with Vero E6 cells and incubated for 3 h. Cells were treated with serum-free medium containing 2 μg/ml trypsin to induce fusion, the medium was replaced with complete DMEM after 30 min. At 6 h postinduction, cells were lysed and assayed for luciferase activity using a luciferase assay kit (Promega) and a Glomax 20/20 luminometer (Promega) to measure light emission.

Spike protein pseudotyped virion production. Pseudotyped virions were generated using plasmids kindly provided by Jean Dubuisson (Lille Pasteur Institute, France). 293T cells were cotransfected with a murine leukemia virus (MLV)-based transfer vector encoding luciferase, an MLV Gag-Pol packaging construct, and pcDNA3.1-SARS-CoV S, a plasmid encoding wild-type or mutant spike envelope glycoprotein, using Exgen 500 (Fermentas) as recommended. After incubation for 72 h at 32°C, supernatants were collected and filtered through a 0.45-μm-pore-size membrane. The level of spike protein incorporation was confirmed by polyethylene glycol (PEG) concentration, centrifugation, and Western blot analysis. A total of 600 μl of filtered supernatant was mixed with 200 μl of 40% PEG and centrifuged for 30 min at 4,000 rpm at 4°C. The pellet was redissolved in SDS-PAGE sample loading buffer

containing 100 mM dithiothreitol and blotted in the same manner as described above in the cell surface biotinylation assay.

Spike protein pseudotyped virion infectivity assays. Equal levels of pseudoparticles were used based on the level of spike protein pseudotype virions quantified by Western blotting, as described above. For a typical infection assay, spike protein pseudotype virions containing wild-type or mutant glycoproteins were bound for 2 h in RPMI medium containing 0.2% bovine serum albumin (BSA)-20 mM HEPES to Vero E6 cells at 4°C. Medium was exchanged for complete DMEM and incubated for 48 h at 37°C. The cells were then lysed, and luciferase activity was measured using the same methods as the quantitative cell-cell fusion assay. In a trypsin-mediated cell surface infectivity assay, Vero E6 cells were first preincubated with 25 mM NH_4Cl for 1 h at 37°C. Pseudotyped virions were then bound for 2 h in RPMI medium containing 0.2% BSA, 20 mM HEPES, and 25 mM NH_4Cl at 4°C. The cells were then warmed up with the addition of prewarmed RPMI medium containing 5 μg/ml trypsin, 0.2% BSA, 20 mM HEPES, and 25 mM ammonium chloride for 5 min at 37°C in a water bath.

Peptides.

The SARS-CoV S2 fusion peptides SFIEDLLFNKVTLADAGFMKQYGCGKKKK, SFIEDLLFGCGKKKK, and SFIEDAAAGCGKKKK were synthesized using solid-phase techniques by New England Peptide (Gardner, MA). The GCGKKKK linker was included to promote liposome association as described for the host-guest fusion peptide system of Han et al. (19). Purity as determined by high-performance liquid chromatography was greater than 95%, and mass identification was performed by matrix-assisted laser desorption ionization-time of flight mass spectrometry. Peptides

were resuspended to 5 mg/ml in sterile MilliQ water. Control peptides were treated identically and had the sequence SIRYSFCGNGRHV for circular dichroism (CD) spectroscopy experiments and GCGKKKK for lipid-mixing experiments.

Liposomes. 1-Palmitoyl-2-oleoyl-*sn*-glycero-3-phosphocholine (POPC), 1-palmitoyl-2-oleoyl-*sn*-glycero-3-[phospho-L-serine] (sodium salt) (POPS), and cholesterol were purchased from Avanti Polar Lipids (Alabaster, AL). Labeled phospholipids *N*-(7-nitrobenz-2-oxa-1,3-diazol-4-yl)-1,2-dihexadecanoyl-*sn*-glycero-3-phospho-ethanolamine, triethylammonium salt (NBD-PE) and lissamine rhodamine B 1,2-dihexadecanoyl-*sn*-glycero-3-phosphoethanolamine, triethylammonium salt (Rho-PE) were purchased from Invitrogen (Carlsbad, California). Large unilamellar vesicles were prepared according to the extrusion method. Lipid films were obtained by subjecting chloroform-dissolved lipid mixtures at a ratio of 1:3:1 of POPC-POPS-cholesterol to high vacuum overnight. Lipid films were resuspended by the addition of fusion buffer (5 mM HEPES, 5 mM morpholinethanesulfonic acid, 5 mM sodium succinate, 150 mM sodium chloride, pH 7) to a 5 or 10 mM lipid concentration and incubated for 15 min at room temperature, followed by vortexing for 15 min. Liposomes were then subjected to 10 freeze-thaw cycles, followed by 11 cycles of extrusion through a 0.1-μm-pore-size polycarbonate membrane using an Avanti mini-extruder. Liposomes labeled with the fluorescent resonance energy transfer (FRET) pairs Rho-PE and NBD-PE were made in the same manner with the addition of 0.6% each of NBD-PE and Rho-PE to the chloroform-dissolved lipid mixture.

Lipid-mixing assay. Lipid mixing was determined using the method of Struck et al. (32). Unlabeled and labeled liposomes were mixed at a 4:1 ratio to a total concentration of 110 μM lipid in fusion buffer at pH 7.0. Hydrochloric acid was added to the solution until the desired pH was achieved. To initiate fusion, peptide was added

to the specified concentration. To end the reaction and obtain a measurement of 100% lipid mixing, reduced Triton X-100 was added to a final concentration of 0.2%. Changes in fluorescence were measured using a QM-6SE spectrofluorimeter (Photon Technology International, Birmingham, NJ) with excitation set at 467 nm and emission monitored at 530 and 581 nm. The extent of lipid mixing was determined using the following formula: $F(\%) = [(f_t - f_0)/(f_{100} - f_0)] \times 100$, where f_t is the fluorescence measurement at time t, f_0 is the initial fluorescence, and f_{100} is the fluorescence after the addition of reduced Triton X-100. All measurements were taken in triplicate and averaged.

CD spectroscopy. Spectra were obtained using an Aviv Biomedical CD spectrometer, model 202-01, equipped with a thermoelectric temperature controller. Spectra were obtained at a 50 μM peptide concentration in 50% trifluoroethanol (TFE) at 37°C. A wavelength range of 190 to 260 nm and averaging time of 2 s were used. Alpha helical content was calculated using the following formula: $f_H = (\theta_{222} - \theta_C)/(\theta_H - \theta_C)$

Where θ_C =2220-53T and θ_H =(250T-44000)(1-3/n), T is the temperature in Celsius and n is the number of residues in the peptide.

Results

Bioinformatics and mutational analysis of the proposed CoV fusion peptide. Based on the internal S2 cleavage site of SARS-CoV at R797, a predicted fusion peptide exposed by such cleavage would start at residue serine 798 and extend to phenylalanine 815. One common feature of viral fusion peptides is that they show a high degree of conservation within a virus family (26). We therefore performed a multiple sequence alignment of the spike protein of representative CoVs. This bioinformatics analysis showed a very high degree of conservation in the site of the proposed S2 fusion peptide (residues 798 to 815) (Fig.2.1A). Indeed, residues 798 to

815 represent some of the most conserved spike protein residues across the *Coronaviridae*. In particular, the domain IEDLLF shows >95% identity, with only limited and very conservative substitutions (I-L/F, L-I/V, and F-Y) in the core hydrophobic residues and with 100% conservation of the initial serine residue (Fig. 2.1B). This highly conserved region is consistent with the requirements for a viral fusion peptide as it contains both small and bulky hydrophobic residues interspersed with more hydrophilic residues. While the juxtamembrane region is also highly conserved, the other proposed SARS-CoV S fusion peptides (WWI and WWII) show a much lower degree of conservation (Fig. 2.1B).

To test the fusogenic properties of the conserved S2 region (residues 798 to 815), mutations were introduced into a SARS-CoV S protein-expressing vector to generate the following mutants: S798A, F799A, I800A, E801A, D802A, L803A, L804A, F805A, N806A, K807A, V808A, T809A, L810A, D812A, G814A, and F815A (Fig. 2.1B). In order to evaluate the effect of point mutants on the fusogenic properties of SARS-CoV S protein, we first verified the cell surface expression of the mutants. The level of surface expression of the alanine point mutants was verified quantitatively after transfection of expression vectors bearing mutant or wild-type S protein in BHK-21 cells, at both 37°C and 32°C, followed by biotinylation and immunoblotting. At 37°C, we observed medium to low levels of surface expression of many of the mutants (data not shown), but at 32°C we were able to observe all mutants expressing at >65% of wild-type levels, and in most cases expression was >85% of wild-type levels (Fig.2.2).

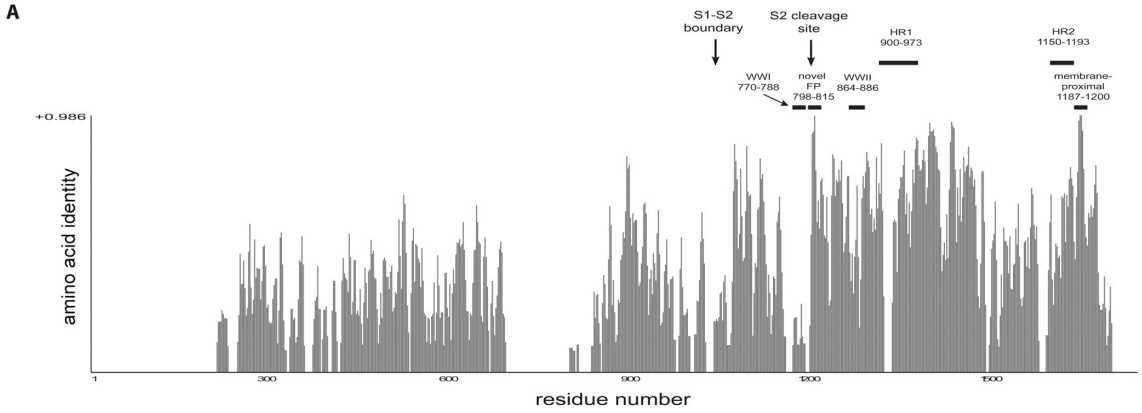

B

Group 2	SARS-CoV (TOR2)	SFIEDLLFNKVTLADAG-F 815	Group 1	HCoV-NL63 (Amsterdam)	SA**L**EDLLFS**K**V**V**TSG**L**G**T**V 889
	Sable Antelope CoV (US/OH1/03)	SAIEDLLFS**K**V**K**LSD**V**G-F 931		HCoV-229E	SAIED**I**LFS**K**L**V**TSG**L**G**T**V 708
	Giraffe CoV (US/OH3-TC/2006)	SAIEDLLFS**K**V**K**LSD**V**G-F 926		PEDV (LZC)	S**V**IEDLLFNK**V**V**T**NG**L**G**T**V 910
	Bovine CoV (R-AH187)	SAIEDLLFS**K**V**K**LSD**V**G-F 931		FIPV (79-1146)	SAIEDLLFD**K**V**V**TSG**L**G**T**V 980
	HCoV-OC43 (ATCC VR-759)	SAIEDLLFD**K**V**K**LSD**V**G-F 929		TGEV (Pur476-MAD)	SAIEDLLFD**K**V**V**TSG**L**G**T**V 977
	PHEV (VW572)	SAIEDLLFD**K**V**K**LSD**V**G-F 917		PRCoV (ISU-1)	SAIEDLLFS**K**V**V**TSG**L**G**T**V 750
	Equine CoV (NC99)	SAIEDLLFN**K**V**R**LSD**V**G-F 931		Bat CoV (BTCov/273/05)	SFIEDLL**Y**N**K**V**T**LADAG-F 801
	HCoV-HKU1 (N19)	SF**F**EDLLFD**K**V**K**LSD**V**G-F 922			
	MHV (A59)	SAIEDLLFD**K**V**K**LSD**V**G-F 887	Group 3	IBV (M41)	SFIEDLLFFTSVESVGLP- 708
	MHV-2	SAIED**V**LFD**K**V**K**LSD**V**G-F 925		IBV (Bdtte)	S**V**IEDLLFTS**V**ES**V**G**L**P-T 708

Figure. 2.1. Bioinformatics analysis of the CoV S protein and the proposed S2 fusion peptide. (A) A quantitative multiple sequence alignment of the S protein from representative CoVs was performed using the program AlignX, a component of Vector NTI 10.3.1 (Invitrogen), which uses a modified Clustal W algorithm. The proposed S2 fusion peptide and other regions of interest have been identified with bars or arrows to show their location within the S gene and their various degrees of conservation across the CoV family. (B) A multiple sequence alignment of the S protein from representative CoVs was performed using AlignX as above. Conserved residues within the proposed S2 fusion peptide region are indicated in bold. Underlining indicates residues showing conserved properties.

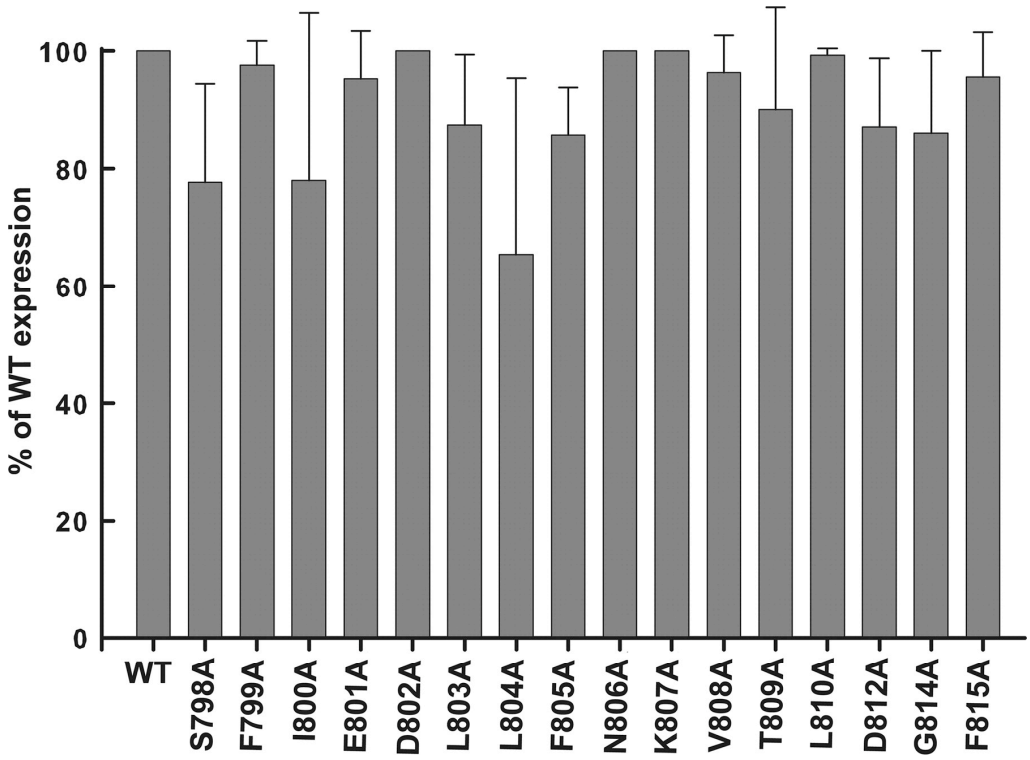

Figure 2.2. Effect of alanine point mutants on spike protein surface expression.

BHK cells were transfected with plasmids encoding wild-type SARS-CoV S or alanine mutants. The cells were labeled with sulfo-NHS-SS-biotin and lysed. Lysates were affinity purified with NeutraAvidin beads and resolved by SDS-PAGE and Western blotting using anti-S monoclonal antibody C9. The biotinylation assay was repeated three times, and the results from the Western blotting were quantified using IP Lab software and plotted in Sigma Plot, version 9.0. Error bars represent standard deviations of the means. WT, wild type.

With high-level expression at the cell surface verified, we were then able to evaluate how the mutated residues might affect membrane fusion. Taking advantage of trypsin as a fusion trigger for the spike protein, we employed two methods of determining cell-

cell fusion. The first method was a qualitative assessment of the mutant's ability to form syncytia in the presence of trypsin, which was performed by analyzing BHK-21 cells cotransfected with wild-type or mutant spike protein and ACE2, the SARS-CoV host cell receptor (Fig. 2.3). We observed a range of fusion events upon treatment with trypsin. In wild-type SARS-CoV S-expressing cells, trypsin treatment resulted in the production of large syncytia in comparison to nontreated cells expressing the spike protein. Mutation of the core conserved residues, i.e., I800A, L803A, L804A, F805A, K807A, and V808A, produced only limited fusion events in comparison to wild-type trypsin-treated cells, with the degree of syncytia comparable in some instances to wild-type levels in non-trypsin-treated cells. We also observed that the L810A, D812A, G814A, and F815A mutants in the C-terminal portion of the fusion peptide also displayed poor syncytia. In other alanine substitution mutants, i.e., S798A, D802A, N806A, and T809A, we saw similar levels of fusion in cells activated by trypsin and the wild-type protein.

In order to quantify the extent of the SARS S protein-mediated membrane fusion activity, a luciferase-based assay system was employed. In this assay, BHK-21 cells were cotransfected with wild-type or mutant spike protein along with a T7 polymerase-driven luciferase gene and overlaid with Vero E6 cells transfected with the T7 polymerase gene. Fusion was induced by trypsin treatment, and the degree of luciferase activity after induction of fusion was used as an indicator of the fusogenic ability of the mutant SARS-CoV S protein in comparison to the wild type (Fig.2.4). We observed a variation of activity in response to mutation of the conserved S2 region (residues 798 to 815).

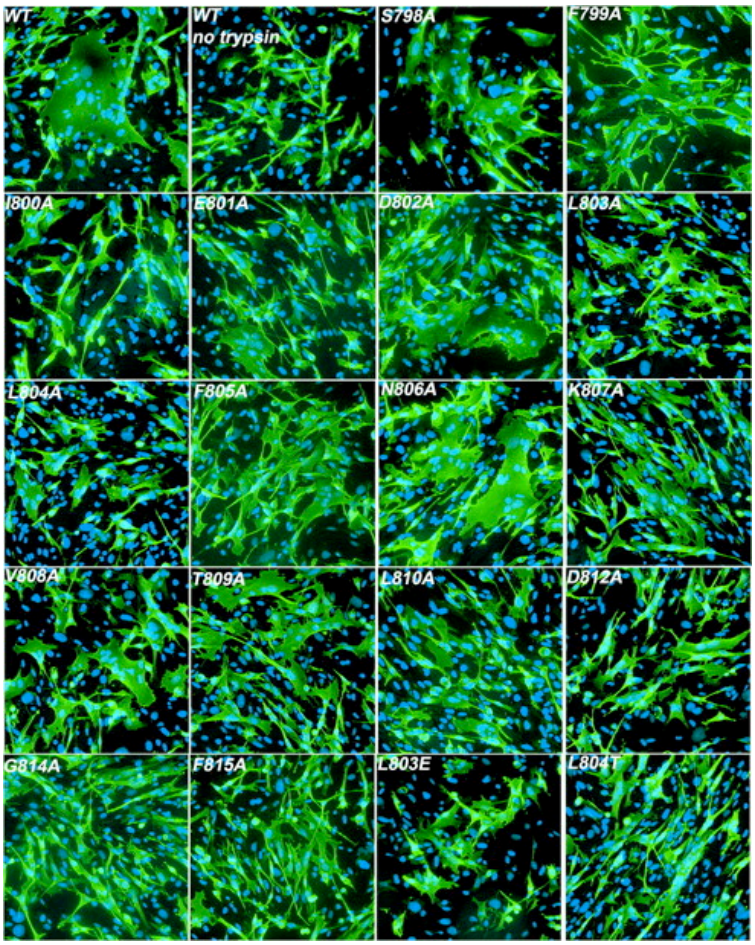

Figure 2.3. Syncytium formation mediated by mutant spike proteins.

BHK cells were transfected with plasmids encoding wild-type (WT) SARS-CoV S or alanine mutants and ACE2. Fusion was induced using medium containing 2 μg/ml trypsin as described in Materials and Methods, and syncytia were visualized by immunofluorescence microscopy using anti-S antibodies (green signal). Nuclei were counterstained with Hoechst 33264 (blue signal).

Mutation of the core conserved residues, such as I800, L803, L804, F805, K807, V808, L810, D812, G814, and F815, resulted in luciferase activity that was 20% or

less than wild-type activity, with the mutation at L804 producing activity close to background levels. Mutation of other residues, such as F799, E801, N806, and T809, showed 50% or less of wild-type activity. In contrast, mutations of residues S798 and D802 revealed no major differences from wild-type levels (fusion activity of >70%).

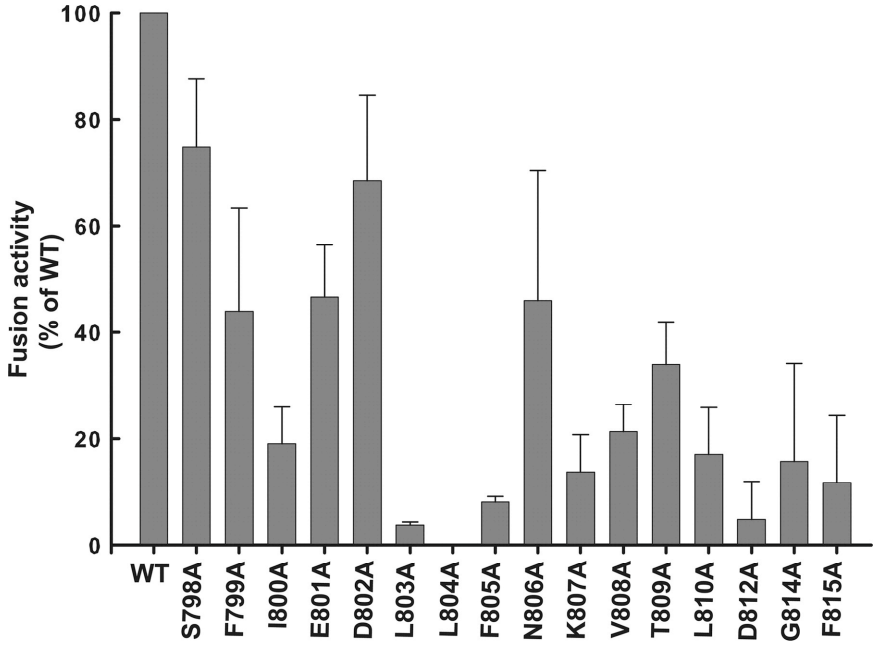

Figure 2.4. Quantitative assays of membrane fusion mediated by mutant spike proteins.

BHK cells were cotransfected with plasmids encoding wild-type (WT) SARS-CoV S or alanine mutants and also with luciferase cDNA under the control of a T7 promoter. At 24 h posttransfection, BHK cells were then overlaid with Vero cells previously transfected with a plasmid encoding T7 polymerase. After 3 h, fusion was induced using medium containing 2 μg/ml trypsin. The cells were lysed 6 h postfusion induction, and supernatants were measured for luciferase activity. Each bar is averaged from three individual experiments, and error bars represent standard deviations from the means.

Effects of SARS-CoV S fusion peptide mutants in MLV pseudotyped virions. To better understand the roles of these fusion peptide residues in the context of a virus particle, we employed a retrovirus-based pseudovirion system (1). Based on the cell-cell fusion assays described above, we selected the core conserved residues identified as being critical to the fusion process as candidates for SARS-CoV S-expressing pseudoviral particles. In this infectivity assay, 293T cells were first cotransfected with an MLV Gag-Pol and luciferase plasmid along with either the SARS-CoV wild-type or mutant S protein plasmid or with an empty vector control to generate SARS-CoV S or control pseudotyped viral particles. The transfected cells were then incubated for 72 h at 32°C as this temperature was optimal for surface expression of the mutants. We first confirmed that a suitable level of expression of mutant spike protein was incorporated in the viral particles, in comparison to wild type, by blotting for spike protein in the collected supernatant 72 h posttransfection (Fig. 2.5A). With many of the mutants expressing at levels greater than 60% of the wild type, we observed a relative lack of spike protein incorporation in the S798A, I800A, E801A, L803A, and L804A mutants. The level of cell surface expression in 293T cells was also confirmed by our biotinylation assay (data not shown). In order to counter this lack of incorporation, we generated additional point mutants with the goal of identifying mutations that would allow efficient incorporation into pseudoparticles. We generated the following mutations: S798G, S798L, S798H, I800G, I800S, E801L, L803E, L803T, L804E, and L804T. All of these mutants were tested for the level of surface expression and incorporation into pseudotyped viral particles; however, only L803E and L804T (Fig. 2.5B) showed incorporation above 60% in comparison to the wild type.

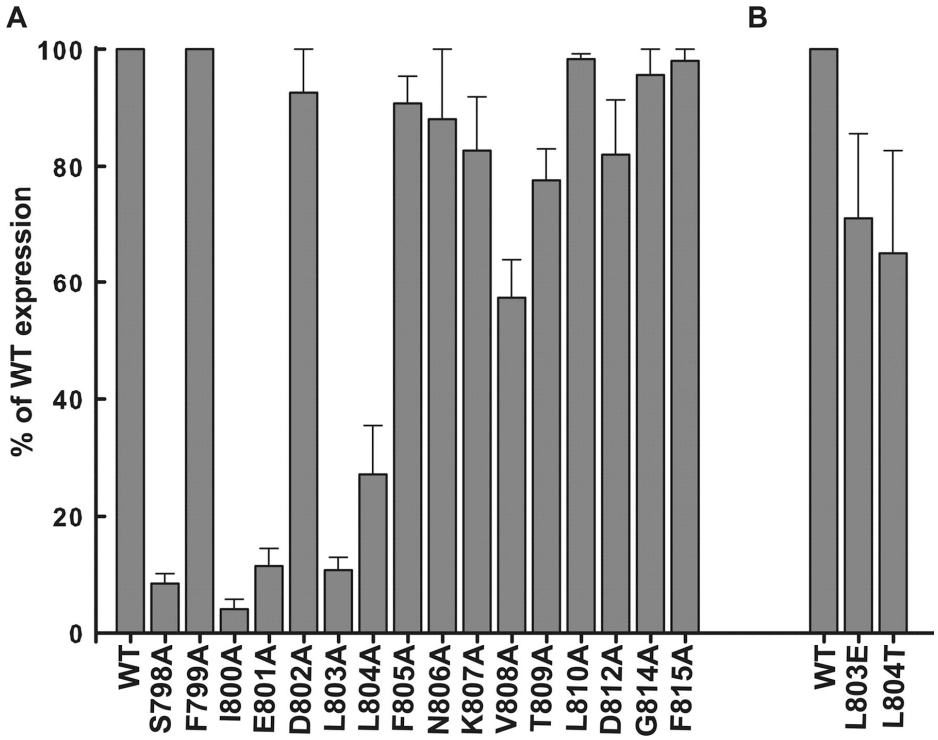

Figure 2.5. Incorporation of mutant spike proteins into MLV pseudotyped virions.

Spike protein-MLV pseudotyped virions were prepared as described in Materials and Methods. Virions were concentrated using a 10% PEG precipitation, diluted in SDS sample buffer, and resolved by SDS-PAGE and Western blotting using a monoclonal antibody specific for the C9 tag. The spike protein-MLV pseudotyped virions were generated three times for wild type (WT) or mutants, and the results from the Western blotting were quantified using IP Lab software and plotted in Sigma Plot, version 9.0. Error bars represent standard deviations from the means.

Upon confirmation of mutant spike protein incorporation, Vero E6 cells were then transduced with SARS-CoV S pseudovirions, ensuring that equal amounts of viral particles were used in the infectivity assay by adjusting the volume of the supernatant. At 72 h posttransduction, cells were lysed, and luciferase activity was measured as an indicator of the extent of viral infection. The luciferase activity of the wild type was normalized to 100%, and luciferase activities of the mutants were compared to those of the wild type. As shown in Fig. 2.6A, we observed a distinct pattern that was similar to the quantitative cell-cell fusion data (Fig.2.4). A marked reduction in infectivity in the core of the proposed fusion peptide, especially in mutants L803E, L804T, F805A, V808A, and L810A, was observed in the pseudovirus infectivity assay. We also observed that the mutation of residues flanking the core, such as F799A, K807A, G814A, and F815A, have less effect in virus entry assays than suggested by the corresponding cell-cell fusion data.

It is considered that SARS-CoV has the ability to fuse in both endocytic and nonendocytic compartments, and so we assessed any potential differences in the role of the proposed fusion peptide in each of these two pathways of virus entry. We therefore inhibited infection by the endocytic route using the lysosomotropic base NH_4Cl and induced fusion of surface-bound virions by trypsin activation. At 48 h after trypsin treatment, cells were assayed for luciferase activity. We observed that, with the exception of G814 and F815, almost all the residues highlighted in the trypsin-untreated assay as being important for infection were also critical in this assay of nonendosomal infection (Fig.2.6B).

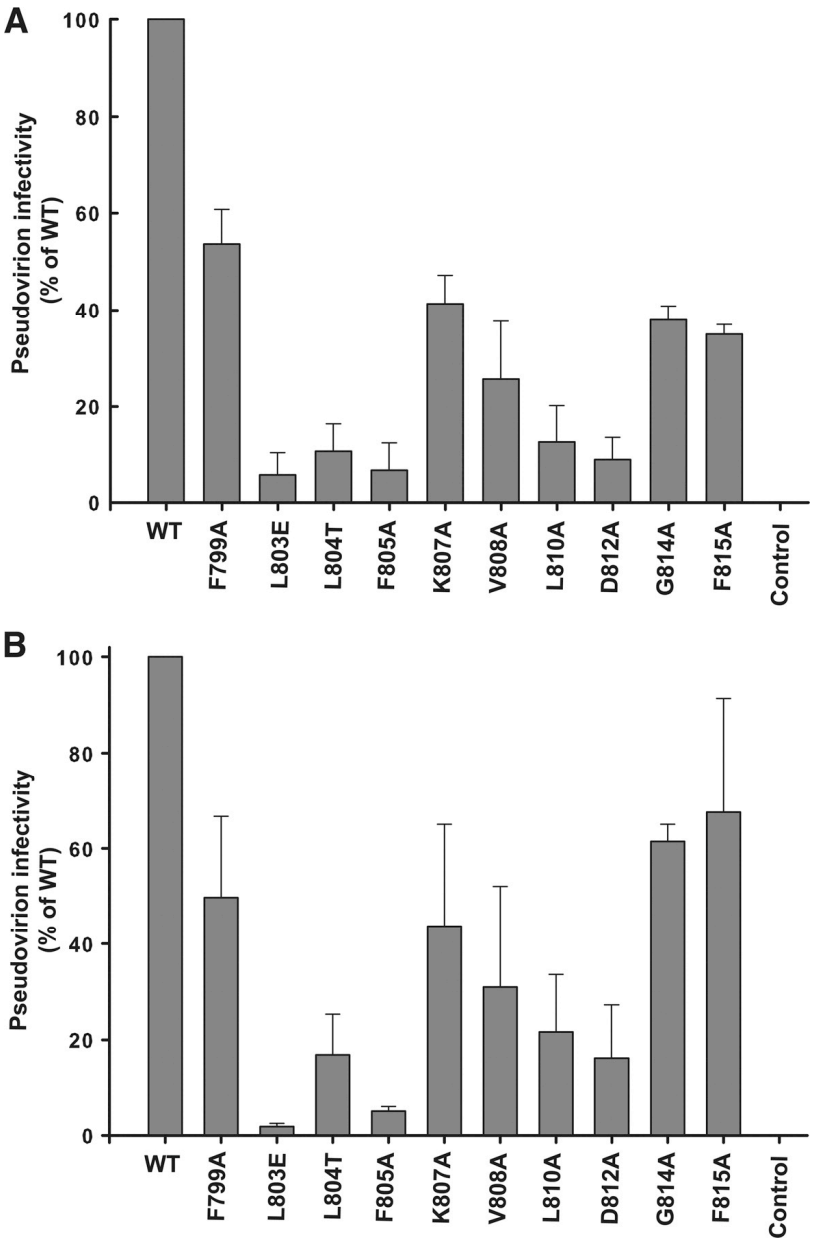

Figure 2.6. Infectivity of spike protein-MLV pseudotyped virions.

(A) Endosomal infectivity of spike protein-MLV pseudotyped virions. (B) Trypsin-mediated infectivity of spike protein-MLV pseudotyped virions. Each bar is averaged from three individual infectivity assays, and error bars represent standard deviations of the means. WT, wild type.

These residues show responses that vary from about 50% for F799A down to almost background levels, as observed in L803E. Data for cell-cell fusion and pseudovirus assays are summarized in Fig. 2.7.

		Cell-Cell fusion	Pseudotyped Virus infectivity	
			– trypsin	+ trypsin
SARS WT	SFIEDLLFNKVTLADAGF	+++	+++	+++
S798A	A----------	++	ND	ND
F799A	-A----------	+	++	+
I800A	--A----------	–	ND	ND
E801A	---A----------	+	ND	ND
D802A	----A----------	++	+++	+++
L803A	-----A----------	–	ND	ND
L803E	-----E----------	ND	–	–
L804A	------A----------	–	ND	ND
L804T	------T----------	ND	–	–
F805A	-------A----------	–	–	–
K807A	---------A--------	–	+	+
V808A	----------A-------	+	+	+
T809A	-----------A------	+	+++	+++
L810A	------------A-----	–	–	+
D812A	--------------A---	–	–	–
G814A	----------------A-	–	+	++
F815A	-----------------A	–	+	++

Figure 2.7. Summary of effects of S2 mutations on SARS-CoV S fusion activity.

The fusion activity of SARS-CoV S wild-type (WT) and mutants in cell-cell fusion assays, as well as in pseudovirus assays of endosomal (– trypsin) and nonendosomal (+ trypsin) infection are summarized. +++, 80 to 100% of wild-type level; ++, 79 to 50% of wild-type level; +, 49 to 20% of wild-type level; and –, <20% of wild-type level. ND, not determined.

Isolated peptides corresponding to the proposed SARS-CoV S2 fusion peptide promote lipid mixing. In order to determine the ability of our proposed fusion peptide to mediate membrane fusion, we utilized a FRET-based assay of lipid mixing (32). In this assay, if a peptide is able to mediate lipid mixing, labeled and unlabeled liposomes fuse, resulting in a dilution of FRET pairs present in the labeled liposomes and an increase in fluorescence of the donor chromophore. The extent of lipid mixing mediated by the SARS S2 peptide (SFIEDLLFNKVTLADAGFMKQYGCGKKKK) and a negative control are shown in Fig.2.8A. Lipid mixing was investigated at several concentrations of peptide, as well as at both pH 5 and pH 7. The SARS-CoV S2 peptide promoted a greater extent of lipid mixing at a lower pH. At higher concentrations of peptide, lipid mixing was also evident at pH 7. The negative control peptide showed no lipid mixing at any concentration or pH tested. The extent of lipid mixing of the SARS-CoV S2 peptide as a function of pH is shown in Fig. 2.8B. We also tested a shorter version of the peptide (SFIEDLLFGCGKKKK), which also showed efficient lipid mixing (Fig. 2.8C and D). The short peptide was also somewhat dependent on pH, but the effects of low pH were less pronounced than with the longer peptide. To examine the function of SARS-CoV S residues L803, L804, and F805 in the context of isolated peptides, we tested a modified short peptide (SFIEDAAAGCGKKKK). In contrast to wild-type sequence, the modified LLF-AAA peptide showed no ability to induce lipid mixing.

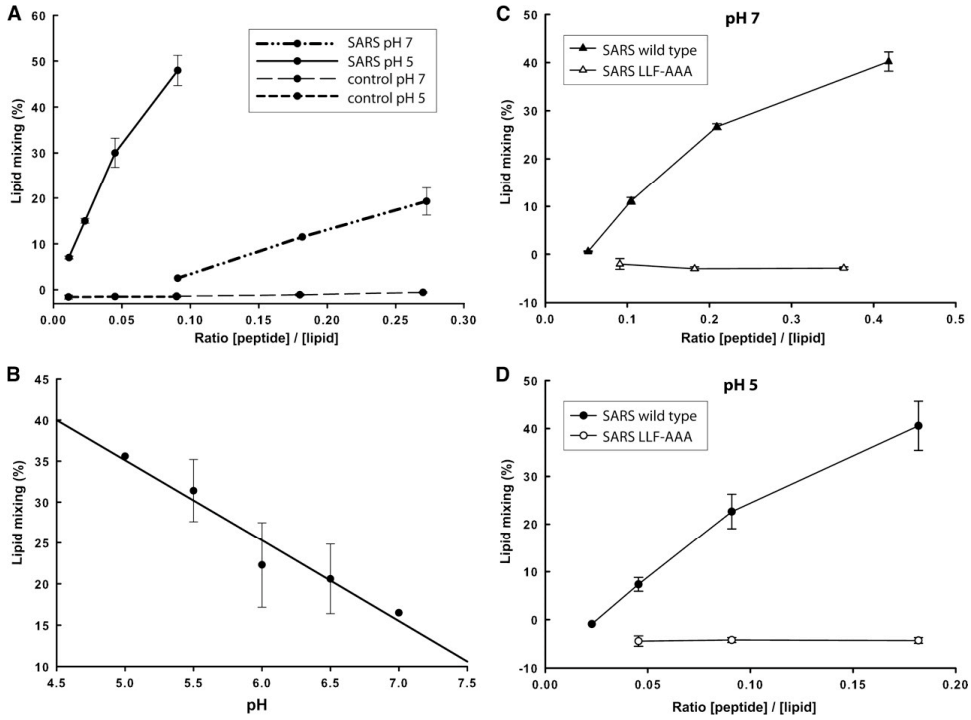

Figure 2.8. The proposed SARS-CoV S2 fusion peptide induces lipid mixing in liposomes.

(A) Extent of lipid mixing was determined by varying the ratios of the fusion peptide or control peptide concentrations with the total concentration of labeled and unlabeled liposomes at pH 5 and pH 7. (B) Effect of the fusion peptide on lipid mixing at various pH values. The kinetics of lipid mixing was followed by monitoring fluorescence intensity at 530 nm upon addition of peptide for A or in decreasing-pH environments (from pH 7.0 to pH 4.5) for B. (C) Extent of lipid mixing at pH 7 and pH 5 (D) were determined by varying the ratios of wild-type or modified LLF-AAA fusion peptide with liposomes at various ratios of peptide to lipid. Each data point is averaged from three individual assays, and error bars represent standard deviations of the means.

CD spectroscopy indicates that the proposed SARS-CoV S2 fusion peptide has a helical secondary structure.

With fusion peptides of many other class I fusion proteins, e.g., influenza virus HA, characterized to be predominantly alpha-helical in secondary structure, we were interested in the structure of the SARS-CoV S2 peptide and used CD spectroscopy as a way to resolve its secondary-structure content (Fig.2.9). The structure of the synthetic peptide SFIEDLLFNKVTLADAGFMKQYGCGKKKK was resolved in the presence and absence of TFE. TFE is a solvent used in many CD spectroscopy studies and functions to stabilize only structures that have the propensity to be helical (12). In the presence of TFE, the S2 fusion peptide gave a spectrum consistent with its having alpha-helical content; this was quantified to be approximately 37% alpha-helix. In the absence of TFE, the peptide maintained a structure in close resemblance to a random coil (Fig. 2.9A). A control peptide sequence downstream of the proposed S2 fusion peptide (residues 1021 to 1034) was used as a control. We also observed a major difference in the spectra of the proposed S2 fusion peptide compared to the control peptide, which maintained a structure closely resembling a random coil even in the presence of TFE (Fig. 2.9B). We also examined the structure of the shorter peptide SFIEDLLF. In the presence of TFE, the short S2 peptide also gave a spectrum consistent with its having a high degree of alpha-helical content, which was quantified to be approximately 77% alpha-helix (Fig. 2.9C).

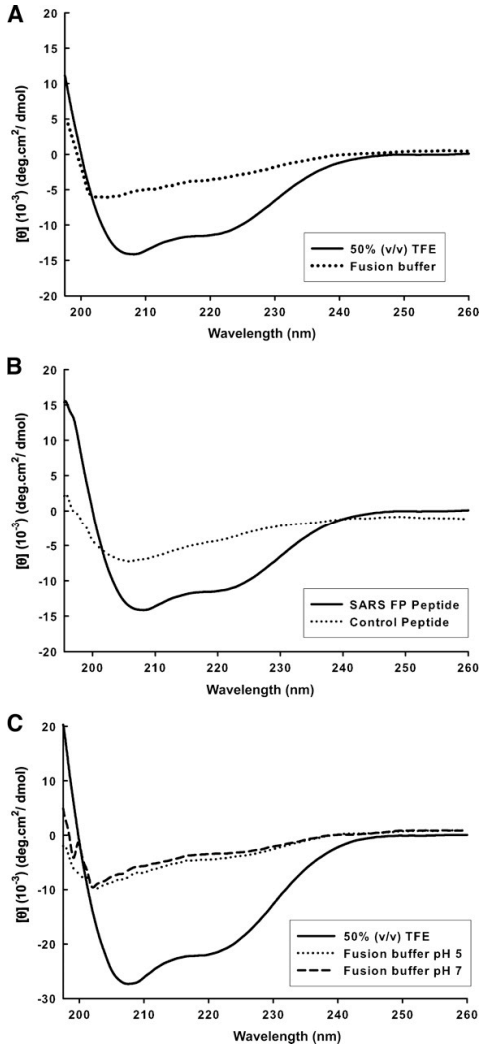

Figure 2.9. The proposed SARS-CoV S2 fusion peptide has the propensity to form helical secondary structure.

(A) CD spectrum of the fusion peptide (solid line) in a TFE/fusion buffer ratio of 50% (vol/vol) at 37°C or in fusion buffer alone (dotted line). (B) CD spectrum of the fusion peptide (FP; solid line) alongside a control peptide (dotted line) in a TFE/fusion buffer ratio of 50% (vol/vol) at 37°C. (C) CD spectrum of the short fusion peptide (solid

line) in a TFE/fusion buffer ratio of 50% (vol/vol) at 37°C or in fusion buffer alone at either pH 5.0 (dotted line) or pH 7.0 (dashed line). deg, degree.

Discussion

A common property of class I fusion proteins is that a proteolytic priming event is necessary for subsequent fusion activation that occurs following exposure to low pH and/or receptor binding. Proteolytic priming is classically associated with members of the trypsin or furin families (21), but more recently cathepsin family members have also been shown to prime fusion activation (38). In canonical class I fusion proteins, such as influenza virus HA or human immunodeficiency virus type 1 Env, proteolytic cleavage occurs directly N-terminal to the fusion peptide, in which case this is referred to as an "external," N-terminal fusion peptide (23, 38). In other cases, notably infection with avian leukosis sarcoma virus (ASLV) or EBOV, proteolytic priming still occurs with the cleavage site close to, but upstream from, the fusion peptide—in which case this is referred to as an "internal" fusion peptide (23, 38). Internal fusion peptides are generally considered to be relatively long (25 to 30 amino acids) and comprise an extended alpha-helix in the fusion-active state. In contrast, external class I fusion peptides are shorter (approximately 15 amino acids) and tend to have a helix-turn-helix structure, often with a central proline residue(s). In the case of CoV S proteins, proteolytic cleavage between the S1 and S2 domain often occurs, but there are no indications that this cleavage results in the exposure of a fusion peptide (4). Therefore, the S protein is generally considered to be a class I fusion protein with an internal fusion peptide.

Recently, it has become apparent that cleavage at a second position (R797) also occurs in the SARS-CoV protein (2, 36), and we hypothesized that this second cleavage event

might expose a critical fusion peptide for the S protein. The sequence immediately C-terminal to the R797 cleavage site of SARS-CoV S is SFIEDLLFNKVTLADAGF, and we assessed this peptide as a potential viral fusion peptide. The first factor we considered with regard to the potential of this peptide as a bona fide fusion peptide was the degree of conservation across the *Coronaviridae*. As shown in Fig.2.1, the peptide was extremely well conserved across all CoVs. In particular, the IEDLLF motif showed only minimal divergence, with occasional conservative substitutions (L to V and L to I). As viral fusion peptides are known to be highly conserved within a family (26), this gave us confidence to proceed with a comprehensive mutagenesis study of the putative fusion peptide, with fusion ability monitored by a cell-cell fusion assay. We initially took a conservative approach and carried out a replacement of individual amino acids with alanine residues. In all cases, mutations had limited or no effect on S protein assembly and cell surface expression; however, we saw marked effects on the ability to cause cell-cell fusion. In particular the L803A, L804A, and F805A substitutions had major effects on fusion, with fusion of the L804A mutant being undetectable in a highly sensitive luciferase-based fusion assay. Other residues with major effects on fusion (20% or less of wild-type levels) were K807A, D812A, and F815A. Notably, mutation of the new N terminus produced after cleavage at R797 (S798A) had very little effect on cell-cell fusion. To date, mutations to more hydrophilic residues, which may have more dramatic effects on fusion, have not been carried out for most of the residues within the S2 fusion peptide.

To confirm these results in the context of a virus particle, we created MLV pseudovirions containing wild-type and mutant SARS-CoV S proteins. In some cases, particularly for the apparently fusion-critical L803 and L804 residues, alanine substitutions could not be rescued in pseudovirus particles. In these cases, we made

additional substitutions, with the L803E and L803T mutations allowing efficient incorporation. The reasons for the differences in particle incorporation are currently unclear as both L803A and L804A showed nearly normal levels of cell surface expression. Pseudoparticle transduction was determined following both endosomal and nonendosomal routes, and in both cases results were essentially in line with cell-cell fusion data; i.e., fusion-critical residues (<20% of the wild-type level) were L803, L804, and F805, along with D812. The K807 and F815 residues seemed less critical in virus entry assays. Mutations at S798 failed to be incorporated into virus particles, and so the role of this residue could not be determined in this assay. Overall, these experiments appeared to point to L803, L804, and F805 as a fusion-active core of the proposed fusion peptide, with the N-terminal S798 residue being of only limited importance.

To examine the fusion peptide more biochemically, we carried out lipid-mixing and spectroscopy assays. We initially assessed a long version of the peptide (SFIEDLLFNKVTLADAGF), but due to the apparent importance of the more N-terminal hydrophobic resides (L803, L804, and F805), we also examined a short version of the peptide (SFIEDLLF) in lipid-mixing assays. By spectroscopy, the long and short peptides did not show any intrinsic structure but showed significant alpha-helical content in the presence of TFE. We were not able to assess the structure in the presence of liposomes due to fusion and aggregation of liposomes when peptide was added. In both cases, lipid-mixing experiments showed that the peptides were fusion active; both peptides were more active at pH 5 than at pH 7.

Notably, L803, L804, and F805 are the initial residues of a major antigenic determinant of SARS-CoV S (Leu 803-Ala 828) that is capable of inducing neutralizing antibodies (40). This SARS-CoV epitope is also homologous to an

immunodominant neutralizing domain on the MHV S2 subunit (7). It will be interesting to see if these neutralizing antibodies mediate their effects during membrane fusion, as found for the closely located 5B19 epitope of MHV S (33).

While a crystal structure of the SARS-CoV S ectodomain has not yet been solved, a predictive model of the quaternary structure is available (Protein Data Bank code 1T7G) (3). In the context of this model, the novel S2 fusion peptide is mainly helical (especially the conserved residues SXIEDLLF), with a short central unstructured region, and is in a relatively exposed position midway down the trimeric spike protein complex (Fig.2.10). This structure and position within the S trimer are consistent with its function as a viral fusion protein. In our initial bioinformatics analysis of the predicted SARS-CoV S fusion peptide, we were initially surprised by the presence of

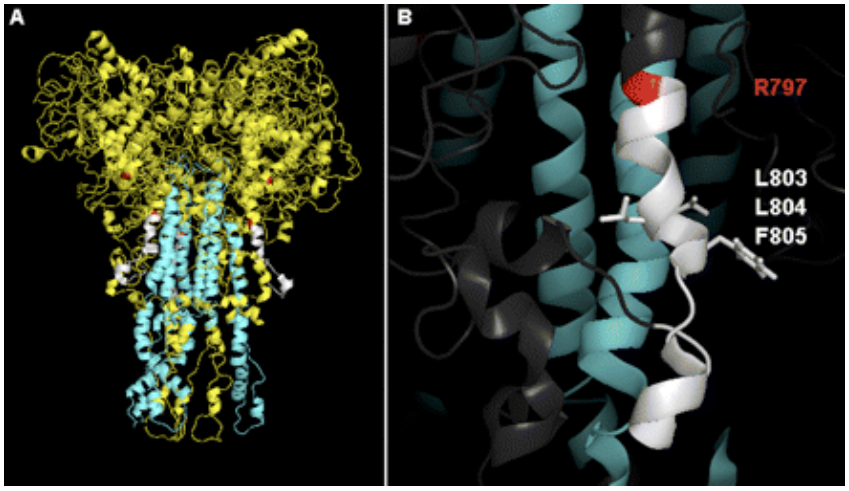

Figure 2.10. Structural model of the SARS-CoV S2.

(A) A three-dimensional model of the SARS-CoV S protein ectodomain trimer is shown in cartoon form with the proposed fusion peptide shown in white and the S2 cleavage site (R797) shown in magenta. (B) The side chains of the proposed fusion-active core (L803, L804, and F805) are shown in enlarged form.

several charged residues, i.e., E801, D802, K807, and D812. While fusion peptides from pH-dependent viruses, such influenza virus, often contain negatively charged residues, the presence of positively charged residues is unusual. The three-dimensional structure of the proposed S2 fusion peptide (SFIEDLLFNKVTLADAGF) in this model predicts two short helices separated by a short unstructured region. While there is no obvious proline-containing turn motif (as in ASLV or EBOV), we consider that the SARS-CoV S2 fusion peptide does not follow the N-terminal alpha-helix pattern of influenza virus or human immunodeficiency virus type 1 but, rather, comprises an internal fusion peptide more like that of ASLV or Ebola virus, which is exposed by a proximal cleavage event. The major difference for SARS-CoV S would be that the known S2 cleavage site is closer to the core residues of the proposed fusion peptide (6 to 8 amino acids away) rather than the 20 to 30 amino acids found for ASLV or EBOV (24, 27, 35, 38).

It is also possible that alternative cleavage sites within the S2 domain could result in exposure of the fusion peptide. In this scenario, the charged residues of the proposed SARS-CoV S fusion peptide (E801, D802, K807, and D812) would lie outside the membrane-penetrating region and would be cytosolic or interact with the phospholipid head groups. In terms of structure, the membrane-penetrating, fusion-active core of the SARS-CoV S2 fusion peptide would comprise residues L803, L804, and F805 and may be composed of a hydrophobic pocket in conjunction with a short 3_{10}-helix, as proposed for EBOV (10, 24) and for influenza virus at low pH (18), although this will need to be addressed experimentally.

The data presented here suggest the presence of a critical fusion peptide close to the S2 cleavage site; however, in the absence of a crystal structure of SARS-CoV S in both pre- and postfusion forms, as well as more biophysical measurements of peptide

intercalation into membranes in the context of the complete S protein, we do not have formal proof that the region SFIEDLLFNKVTLADAGF constitutes the only fusion peptide for SARS-CoV S. It is possible that the fusion peptide identified here functions in conjunction with other fusion peptides or membrane-intercalating regions of the spike protein identified in previous work.

While the low endosomal pH is important for SARS-CoV entry, other nonendosomal entry routes can occur. Thus, it is presently unclear whether low pH is needed only for activation of cathepsins priming the SARS-CoV S protein or whether low pH has a more direct role. Overall, however, it seems likely that CoVs in general can mediate membrane fusion at a range of pH values. The fusion peptide characterized here is highly conserved across the *Coronaviridae*, especially in the core IEDLLF sequence. It seems likely that this sequence, working in conjunction with other membrane-active regions of the spike protein, is an important feature of this diverse virus family at various pH values and with different cleavage events that could result in fusion peptide exposure.

Acknowledgements

We thank Ruth Collins, Holger Sondermann, and Brian Crane for their help and advice during the course of this work and Michael Farzan, Tom Gallagher, and Jean Dubuisson for their kind provision of reagents. We also thank A. Damon Ferguson for technical assistance and all members of the Whittaker laboratory for helpful suggestions. I.G.M. was the recipient of a fellowship from the National Institutes of Health (NIGMS), grant F31 GM082084. S.L.R. was the recipient of a Cornell University Provost's Diversity fellowship. This work was also supported by the Cornell University Nanobiotechnology Center, an STC program of the National Science Foundation under agreement number ECS-987677, and the National Institutes of Health (NIAID), grants R03 AI060946 and R21 AI076258.

REFERENCES

1. Bartosch, B., J. Dubuisson, and F. L. Cosset. 2003. Infectious hepatitis C virus pseudo-particles containing functional E1-E2 envelope protein complexes. J Exp Med 197:633-42.
2. Belouzard, S., V. C. Chu, and G. R. Whittaker. 2009. Activation of the SARS coronavirus spike protein via sequential proteolytic cleavage at two distinct sites. Proceedings of the National Academy of Sciences of the United States of America 106:5871-5876.
3. Bernini, A., O. Spiga, A. Ciutti, S. Chiellini, L. Bracci, X. Yan, B. Zheng, J. Huang, M. L. He, H. D. Song, P. Hao, G. Zhao, and N. Niccolai. 2004. Prediction of quaternary assembly of SARS coronavirus peplomer. Biochem Biophys Res Commun 325:1210-4.
4. Bosch, B. J., and P. J. Rottier. 2008. Nidovirus Entry into Cells, p. 157-178. *In* S. Perlman, T. Gallagher, and E. J. Snijder (ed.), Nidoviruses. ASM Press, Washington DC.
5. Bosch, B. J., R. van der Zee, C. A. de Haan, and P. J. Rottier. 2003. The coronavirus spike protein is a class I virus fusion protein: structural and functional characterization of the fusion core complex. J Virol 77:8801-11.
6. Chambers, P., C. R. Pringle, and A. J. Easton. 1990. Heptad repeat sequences are located adjacent to hydrophobic regions in several types of virus fusion glycoproteins. J Gen Virol 71 (Pt 12):3075-80.
7. Daniel, C., R. Anderson, M. J. Buchmeier, J. O. Fleming, W. J. Spaan, H. Wege, and P. J. Talbot. 1993. Identification of an immunodominant linear neutralization domain on the S2 portion of the murine coronavirus spike glycoprotein and

evidence that it forms part of complex tridimensional structure. J Virol 67:1185-94.

8. Durell, S. R., I. Martin, J. M. Ruysschaert, Y. Shai, and R. Blumenthal. 1997. What studies of fusion peptides tell us about viral envelope glycoprotein-mediated membrane fusion (review). Mol Membr Biol 14:97-112.
9. Earp, L. J., S. E. Delos, H. E. Park, and J. M. White. 2005. The many mechanisms of viral membrane fusion proteins. Curr. Top. Microbiol. Immunol. 285:25-66.
10. Freitas, M. S., L. P. Gaspar, M. Lorenzoni, F. C. Almeida, L. W. Tinoco, M. S. Almeida, L. F. Maia, L. Degreve, A. P. Valente, and J. L. Silva. 2007. Structure of the Ebola fusion peptide in a membrane-mimetic environment and the interaction with lipid rafts. J Biol Chem 282:27306-14.
11. Gomara, M. J., P. Mora, I. Mingarro, and J. L. Nieva. 2004. Roles of a conserved proline in the internal fusion peptide of Ebola glycoprotein. FEBS Lett 569:261-6.
12. Goodman, M., I. Listowsky, Y. Masuda, and F. Boardman. 1963. Conformational aspects of polypeptides. VIII. Helical assignments via far ultraviolet adsorption spectra and optical activity. Biopolymers 1:33-42.
13. Guillen, J., R. F. de Almeida, M. Prieto, and J. Villalain. 2008. Structural and dynamic characterization of the interaction of the putative fusion peptide of the S2 SARS-CoV virus protein with lipid membranes. J Phys Chem B 112:6997-7007.
14. Guillen, J., P. K. Kinnunen, and J. Villalain. 2008. Membrane insertion of the three main membranotropic sequences from SARS-CoV S2 glycoprotein. Biochim Biophys Acta.
15. Guillen, J., M. R. Moreno, A. J. Perez-Berna, A. Bernabeu, and J. Villalain. 2007. Interaction of a peptide from the pre-transmembrane domain of the severe acute respiratory syndrome coronavirus spike protein with phospholipid membranes. J Phys Chem B 111:13714-25.

16. Guillen, J., A. J. Perez-Berna, M. R. Moreno, and J. Villalain. 2008. A second SARS-CoV S2 glycoprotein internal membrane-active peptide. Biophysical characterization and membrane interaction. Biochemistry 47:8214-24.
17. Guillen, J., A. J. Perez-Berna, M. R. Moreno, and J. Villalain. 2005. Identification of the membrane-active regions of the severe acute respiratory syndrome coronavirus spike membrane glycoprotein using a 16/18-mer peptide scan: implications for the viral fusion mechanism. J Virol 79:1743-52.
18. Han, X., J. H. Bushweller, D. S. Cafiso, and L. K. Tamm. 2001. Membrane structure and fusion-triggering conformational change of the fusion domain from influenza hemagglutinin. Nat Struct Biol 8:715-20.
19. Han, X., and L. K. Tamm. 2000. A host-guest system to study structure-function relationships of membrane fusion peptides. Proc Natl Acad Sci U S A 97:13097-102.
20. Howard, M. W., E. A. Travanty, S. A. Jeffers, M. K. Smith, S. T. Wennier, L. B. Thackray, and K. V. Holmes. 2008. Aromatic amino acids in the juxtamembrane domain of severe acute respiratory syndrome coronavirus spike glycoprotein are important for receptor-dependent virus entry and cell-cell fusion. J Virol 82:2883-94.
21. Klenk, H. D., and W. Garten. 1994. Host cell proteases controlling virus pathogenicity. Trends Microbiol 2:39-43.
22. Lague, P., B. Roux, and R. W. Pastor. 2005. Molecular dynamics simulations of the influenza hemagglutinin fusion peptide in micelles and bilayers: conformational analysis of peptide and lipids. J Mol Biol 354:1129-41.
23. Lai, A. L., Y. Li, and L. K. Tamm. 2005. Interplay of proteins and lipids in virus entry by membrane fusion, p. 279-303. *In* L. K. Tamm (ed.), Protein–Lipid Interactions. Wiley-VCH Verlag GmbH & Co. KGaA, Weinheim, Germany.

24. Lee, J. E., M. L. Fusco, A. J. Hessell, W. B. Oswald, D. R. Burton, and E. O. Saphire. 2008. Structure of the Ebola virus glycoprotein bound to an antibody from a human survivor. Nature 454:177-82.
25. Lu, Y., T. L. Neo, D. X. Liu, and J. P. Tam. 2008. Importance of SARS-CoV spike protein Trp-rich region in viral infectivity. Biochem Biophys Res Commun 371:356-60.
26. Martin, I., and J. M. Ruysschaert. 2000. Common properties of fusion peptides from diverse systems. Biosci Rep 20:483-500.
27. Perez, L. G., and E. Hunter. 1987. Mutations within the proteolytic cleavage site of the Rous sarcoma virus glycoprotein that block processing to gp85 and gp37. J Virol 61:1609-14.
28. Petit, C. M., J. M. Melancon, V. N. Chouljenko, R. Colgrove, M. Farzan, D. M. Knipe, and K. G. Kousoulas. 2005. Genetic analysis of the SARS-coronavirus spike glycoprotein functional domains involved in cell-surface expression and cell-to-cell fusion. Virology 341:215-30.
29. Sainz, B., Jr., J. M. Rausch, W. R. Gallaher, R. F. Garry, and W. C. Wimley. 2005. Identification and characterization of the putative fusion peptide of the severe acute respiratory syndrome-associated coronavirus spike protein. J Virol 79:7195-206.
30. Sainz, B., Jr., J. M. Rausch, W. R. Gallaher, R. F. Garry, and W. C. Wimley. 2005. The aromatic domain of the coronavirus class I viral fusion protein induces membrane permeabilization: putative role during viral entry. Biochemistry 44:947-58.
31. Song, H. C., M. Y. Seo, K. Stadler, B. J. Yoo, Q. L. Choo, S. R. Coates, Y. Uematsu, T. Harada, C. E. Greer, J. M. Polo, P. Pileri, M. Eickmann, R. Rappuoli, S. Abrignani, M. Houghton, and J. H. Han. 2004. Synthesis and characterization of

a native, oligomeric form of recombinant severe acute respiratory syndrome coronavirus spike glycoprotein. J Virol 78:10328-35.

32. Struck, D. K., D. Hoekstra, and R. E. Pagano. 1981. Use of resonance energy transfer to monitor membrane fusion. Biochemistry 20:4093-9.
33. Taguchi, F., and Y. K. Shimazaki. 2000. Functional analysis of an epitope in the S2 subunit of the murine coronavirus spike protein: involvement in fusion activity. J Gen Virol 81:2867-71.
34. Tamm, L. K., and X. Han. 2000. Viral fusion peptides: a tool set to disrupt and connect biological membranes. Biosci Rep 20:501-18.
35. Volchkov, V. E., H. Feldmann, V. A. Volchkova, and H. D. Klenk. 1998. Processing of the Ebola virus glycoprotein by the proprotein convertase furin. Proc Natl Acad Sci U S A 95:5762-7.
36. Watanabe, R., S. Matsyama, K. Shirato, M. Maejima, S. Fukushi, S. Morikawa, and F. Taguchi. 2008. Entry from cell surface of SARS coronavirus with cleaved S protein as revealed by pseudotype virus bearing cleaved S protein. J Virol.
37. Wentworth, D. E., and K. V. Holmes. 2007. Coronavirus Binding and Entry, p. 3-31. *In* V. Thiel (ed.), Coronaviruses. Molecular and Cellular Biology. Caister Academic Press, Norfolk, UK.
38. White, J. M., S. E. Delos, M. Brecher, and K. Schornberg. 2008. Structures and mechanisms of viral membrane fusion proteins: multiple variations on a common theme. Crit Rev Biochem Mol Biol 43:189-219.
39. Xiao, X., S. Chakraborti, A. S. Dimitrov, K. Gramatikoff, and D. S. Dimitrov. 2003. The SARS-CoV S glycoprotein: expression and functional characterization. Biochem Biophys Res Commun 312:1159-64.
40. Zhang, H., G. Wang, J. Li, Y. Nie, X. Shi, G. Lian, W. Wang, X. Yin, Y. Zhao, X. Qu, M. Ding, and H. Deng. 2004. Identification of an antigenic determinant on the

S2 domain of the severe acute respiratory syndrome coronavirus spike glycoprotein capable of inducing neutralizing antibodies. J Virol 78:6938-45.

CHAPTER 3

SARS-CORONAVIRUS SPIKE S2 DOMAIN FLANKED BY CYSTEINE RESIDUES C822 AND C833 IS IMPORTANT FOR ACTIVATION OF MEMBRANE FUSION

Ikenna G. Madu, Sandrine Belouzard and Gary R. Whittaker. 2009. Virology, p. 265-271 Vol. 393, Issue 2

Abstract

The S2 domain of the coronavirus spike (S) protein is known to be responsible for mediating membrane fusion. In addition to a well-recognized cleavage site at the S1-S2 boundary, a second proteolytic cleavage site has been identified in the severe acute respiratory syndrome coronavirus (SARS-CoV) S2 domain (R797). C-terminal to this S2 cleavage site is a conserved region flanked by cysteine residues C822 and C833. Here, we investigated the importance of this well conserved region for SARS-CoV S-mediated fusion activation. We show that the residues between C822-C833 are well conserved across all coronaviruses. Mutagenic analysis of SARS-CoV S, combined with cell–cell fusion and pseudotyped virion infectivity assays, showed a critical role for the core-conserved residues C822, D830, L831, and C833. Based on available predictive models, we propose that the conserved domain flanked by cysteines 822 and 833 forms a loop structure that interacts with components of the SARS-CoV S trimer to control the activation of membrane fusion.

Introduction

The severe acute respiratory syndrome coronavirus (SARS-CoV) emerged in 2002 causing a global epidemic. The outbreak resulted in about 8,000 cases with a fatality of about 10% until it was quarantined (11, 14). SARS-CoV still maintains a significant threat to human health, as novel viruses such as these still present a possibility for re-emergence into the human population so an understanding of the mechanics of entry is crucial in order to develop effective treatment.

Coronaviruses are enveloped viruses with positive sense RNA genomes that commonly cause respiratory and enteric diseases within a wide host range (18). Entry of these viruses is mediated by the viral spike glycoprotein S and a receptor on the target cell. The viral spike glycoprotein can be cleaved into S1 and S2 domains (3, 12,

13, 19-21, 39, 42). The S1 domain of the viral spike protein dictates tropism and is responsible for mediating receptor binding (7, 15-17, 23-25, 34, 38, 40). The S2 domain is responsible for mediating membrane fusion between the virus and host cell, with strong sequence conservation within the family (5, 8)—hence the mechanics of fusion can be expected to be conserved across the *Coronaviridae*.

Based on structural similarities, the SARS-CoV S glycoprotein is a class 1 membrane fusion protein (33). The S2 domain contains two heptad repeat (14) regions, HR1 and HR2, as well as a fusion peptide. Following conformational changes based on receptor binding or change in pH, the S2 domain drives fusion of the viral and host cell membranes to allow virus entry. Observations of cell surface expressed SARS-CoV spike protein, indicated that most of the protein was not cleaved at the S1-S2 boundary, at best limited cleavage is possible (35, 41). It is generally considered that S1-S2 cleavage is not directly linked to fusion peptide exposure in the case of SARS-CoV, or any other coronavirus (6). However, it has recently been shown that SARS-CoV S can be proteolytically cleaved at a downstream position in S2, at residue 797 (2), and a highly conserved region C-terminal to the cleavage site has been characterized and identified as critical for fusion (26).

Downstream of these conserved core residues we observed another set of conserved residues flanked by cysteines 822 and 833. These flanks represent two of the 39 cysteines in S that are likely to form intra-disulfide bonds within S. Cysteine residues and their roles in mediating entry either in the receptor binding region or in the cytoplasmic tail have been well documented for coronaviruses (30, 31, 37, 43). For other families of viruses, cysteine residues have been key players for driving entry (27, 28) and fusion (9, 10, 29, 32) . In this study, we investigated the importance of a conserved domain in S2 flanked by cysteines 822 and 833 by carrying out a

comprehensive mutagenesis study. Using cell-cell fusion and pseudovirus assays, we show that this domain is critical for the activation of SARS-CoV S-mediated membrane fusion and virus entry.

Results

Bioinformatic analysis of the SARS-CoV S2 domain flanked by cysteine residues C822 and C833.

A common feature of regions within a viral glycoprotein that is required for entry is that they show a high degree of conservation within a virus family. We therefore performed a multiple sequence alignment of the spike protein of representative coronaviruses, with a focus on the domain flanked by cysteine residues C822 and C833. This bioinformatic analysis confirmed a high degree of conservation in the region (Fig. 3.1). Indeed, residues C822, D830, L831, and C833 of the SARS-CoV S represent some of the most conserved residues in that region and across the *Coronaviridae*.

Cloning and expression of WT and mutant SARS-CoV S glycoproteins.

To test the fusogenic properties of the conserved S2 domain flanked by cysteine residues C822 and C833, point, double, deletion and insertion mutants were introduced into a SARS-CoV S protein-expressing vector to generate the following mutants: C822S, G824A, D825A, N827A, A828S, D830L, L831D, C833S, double cysteine mutant (C822S/ C833S), a deletion of the residues between the cysteines (Δ823-832) and a Gly-Ala-Gly (GAG) loop mutant to replace the residues between the cysteines. The rationale for the mutants was as follows: residues G824, D825, N827, and A828 were mutated to alanine (or serine in the case of A828) to modify their chemical nature in an innocuous manner. The conserved residue C822 and C833 were mutated to serines to change the chemical nature of the cysteines and prevent normal

disulfide bond formation; the C822S/C833S double mutant was designed to curb the possibility of spurious disulfide bonding occurring with unpaired cysteines; D830L, and L831D mutants were also generated to modify the chemistry of each original residue with the corresponding conserved residue, as both are 100% conserved; and to further address how residues within the proposed loop might be important, we generated a loop deletion mutant Δ823-832, and a flexible tripeptide GAG loop (22) between the flanking cysteines.

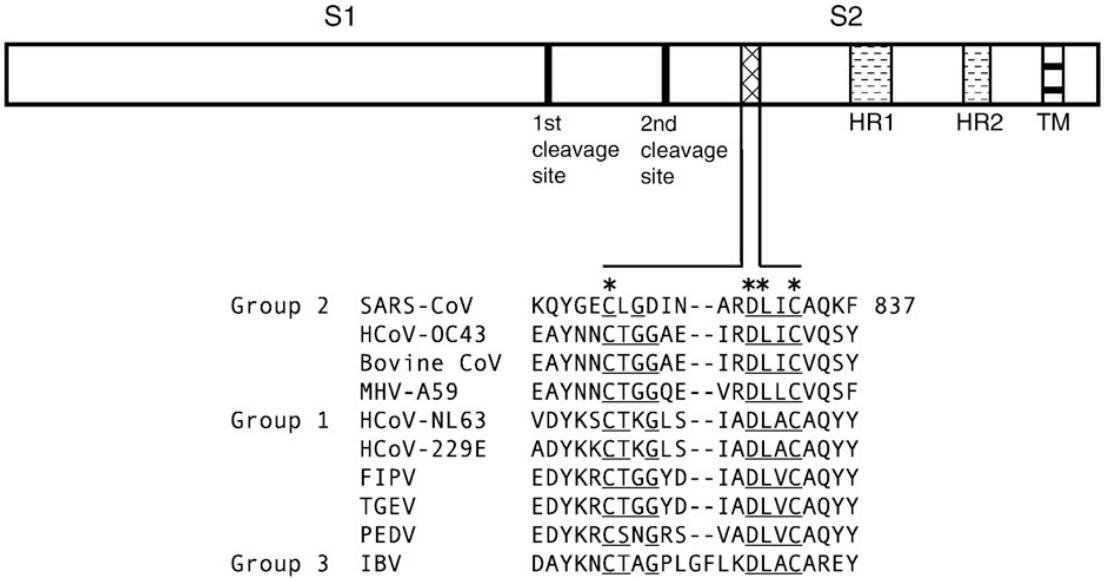

Figure 3.1. Schematic and alignment of the cysteine flanked region

A schematic representation of the coronavirus spike with hallmark domains alongside the region of interest. A multiple sequence alignment of the S protein from representative coronavirus groups was performed. Residues that are conserved directly or in terms of properties are underlined and asterisked residues represent 100% conservation within the CoV family.

In order to evaluate the effect of the mutations on the fusogenic properties of SARS-CoV S protein, we first verified the cell surface expression of the mutants. The level of surface expression of the point mutants was verified quantitatively after transfection of expression vectors bearing mutant or wild type S protein in BHK-21 cells, at both 37°C and 32°C, followed by biotinylation and immunoblotting. At 37°C, with the exception of the N827A mutant, we observed a tolerable surface expression of many of the mutants (Fig. 3.2A), but at 32°C we observed an overall better surface expression of all mutants expressing at > 65% of wild-type levels (Fig. 3.2B) so this temperature was used in the corresponding surface expression fusion assays as well as in the generation of pseudotyped virions.

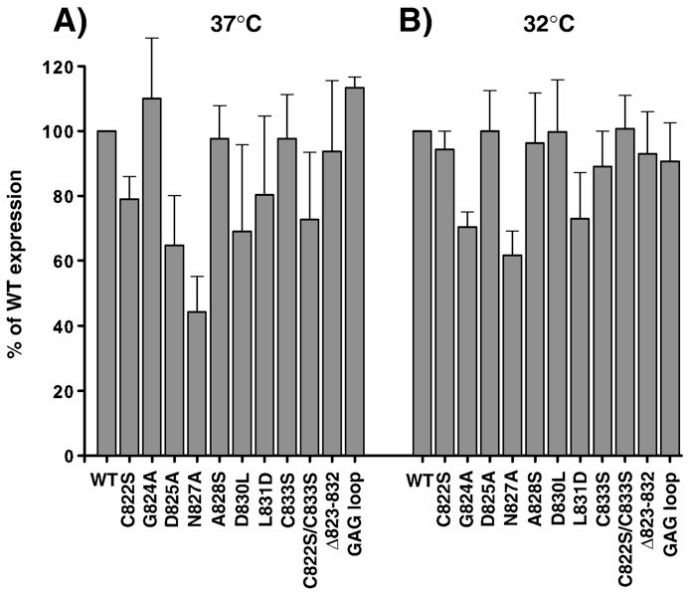

Figure 3.2. Effect of point mutants on spike protein surface expression

BHK cells were transfected with plasmids encoding wild type SARS-CoV S or mutants at (A) 37°C and (B) 32°C. The cells were labeled with biotin, proteins were affinity purified with NeutraAvidin beads and resolved by SDS-PAGE and analyzed by Western blot using anti C9 tag antibody. The biotinylation assay was repeated three times and the results plotted. The Error bars represent standard deviation of the mean.

Binding of soluble hACE2-Fc to wild type or mutant SARS-CoV S.

With point mutants introduced into the viral glycoprotein, it was important to confirm that the binding to ACE2 the SARS-CoV receptor is not altered. To confirm this, we cotransfected 293T cells with a construct expressing human ACE2 fused to the Fc-domain of human IgG (hACE2-Fc) and wild type or mutant spike vectors. 48 h post transfection, cells were lysed and affinity purified for hACE2-Fc, and then immunoblotted for SARS-CoV S to confirm interactions between receptor and spike. The levels of binding were observed to be comparable with mutants binding ACE2 at an average > 70% of wild type levels (Fig. 3.3).

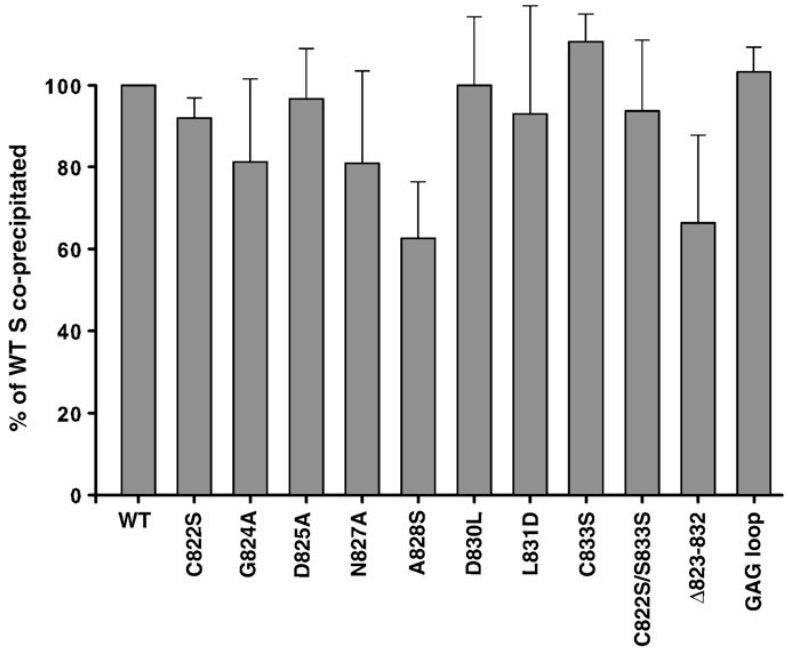

Figure 3.3. Effect of point mutants on receptor binding

293-T cells were co-transfected with plasmids expressing wild type or mutant spike protein and human ACE2-Fc.The lysates were affinity purified using immobilized Protein A beads. Protein A beads were then washed and resolved via SDS-PAGE and Western blot. The binding assay was repeated three times and results from the western blot quantifications were plotted.

Fusion assays of cells expressing WT or mutant SARS-CoV S and ACE2.

With a tolerable level expression at the cell surface verified, we were then able to evaluate how the mutations might affect membrane fusion. Taking advantage of trypsin as a fusion trigger for the spike protein, we employed a quantitative method of determining SARS-CoV S protein-mediated membrane fusion activity, by using a luciferase-based assay system to measure cell–cell fusion. In this assay, BHK-21 cells were cotransfected with wild type or mutant spike protein along with T7 polymerase-driven luciferase gene and overlayed with Vero E6 cells transfected with the T7 polymerase gene. Fusion was induced by trypsin treatment, and the degree of luciferase activity after induction of fusion was used as an indicator of the fusogenic ability of the mutant SARS-CoV S protein, in comparison to wild type (Fig. 3.4).

We observed that while alanine substitution of less conserved residues G824A, D825A, N827A, and A828S, displayed activity close to or better than wild type, mutation of the core conserved residues, as well as the loop deletion and mini-loop mutants resulted in luciferase activity that was close to background levels in comparison to wild type activity.

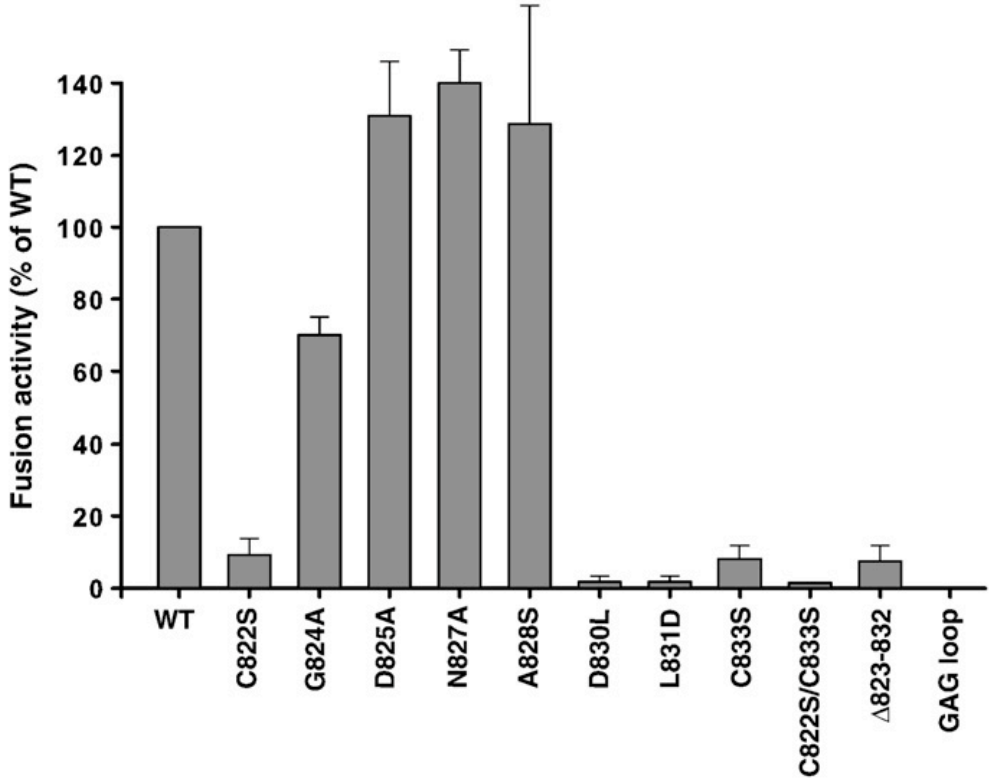

Figure 3.4. Quantitative assays of membrane fusion mediated by mutant spike proteins

BHK cells were cotransfected with plasmids encoding wild type SARS-CoV S or alanine mutants and also with luciferase cDNA under the control of a T7 promoter. At 24 h post transfection, BHK cells were then overlaid with Vero cells previously transfected with a plasmid encoding T7 polymerase. After 3 h, fusion was induced using media containing 2 μg/ml trypsin. The cells were lysed 6 h post fusion induction and supernatants measured for luciferase activity. Each bar is averaged from three individual repeats and error bars represent standard deviation from the mean.

Characterization of SARS-CoV S mutants in MLV-pseudotyped virions.

To better understand the roles of S2 domain flanked by cysteine residues C822 and C833 in the context of a virus particle, we employed a retrovirus-based pseudovirion system (1). In this infectivity assay, 293T cells are first cotransfected with a murine leukemia virus (MLV) Gag-Pol and luciferase plasmid along with either the SARS-CoV wild type or mutant S protein plasmid, or an empty vector control, to generate control-pseudotyped viral particles missing the SARS-CoV S. The transfected cells were then incubated for 72 h at 32°C, as this temperature was optimal for surface expression of the mutants. We first confirmed that a suitable level of expression of mutant spike protein was incorporated in the viral particles, in comparison to wild type, by blotting for spike protein in the collected supernatant 72 h post transfection (Fig. 3.5).

Although mutant N827A showed a low level of spike incorporation, the other mutants expressing at levels greater than 60% of the wild type the level of cell surface expression in 293T was also confirmed by our biotinylation assay (data not shown). Upon confirmation of mutant spike protein incorporation, Vero E6 cells were then transduced with SARS-CoV S pseudovirions with comparable levels of detected spike by adjusting the volume of the supernatant to ensure that equal amounts of S protein were used in the infectivity assay. At 72 h post transduction, cells were lysed and luciferase activity measured as an indicator of the extent of viral infection. The luciferase activity of the wild type construct was set to 100% and luciferase activities of the mutants were normalized to wild type. As shown in Fig. 3.6A, we observed a pattern that was similar to the quantitative cell–cell fusion data (see Fig. 3.4) although the level activity of the D825A mutant is at an average of about 70% of the WT.

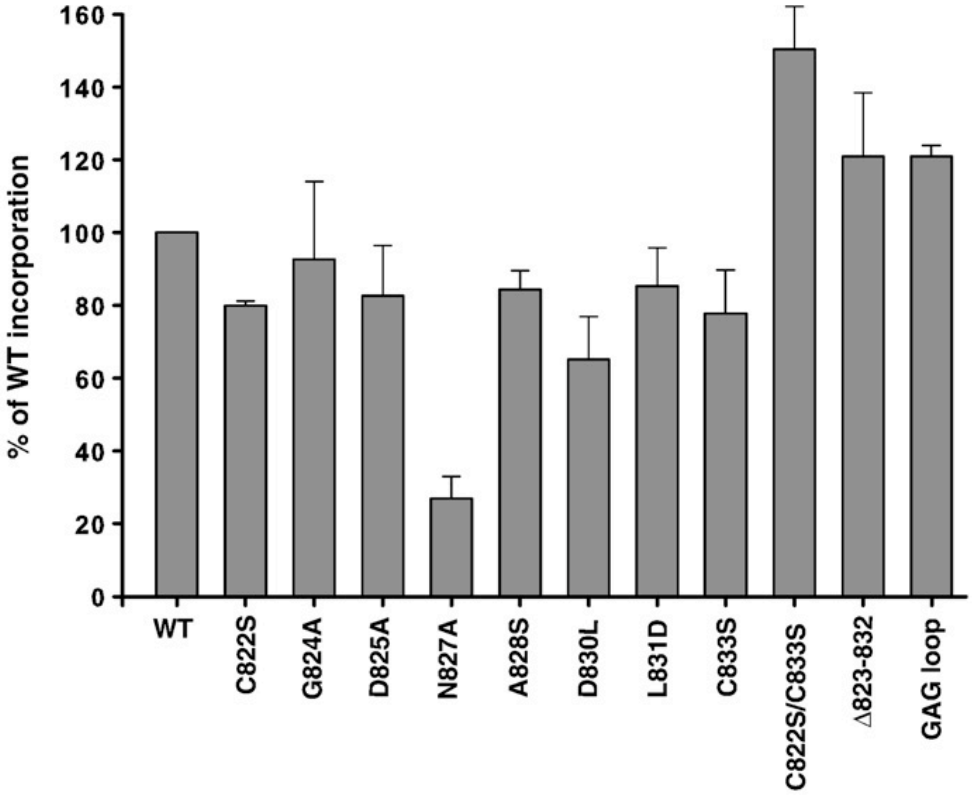

Figure 3.5. Incorporation of mutant spike proteins into MLV pseudotyped virions

Spike protein-MLV pseudotyped virions were prepared as described in the methods. Virions were concentrated using a 10% PEG precipitation, diluted in SDS sample buffer, and resolved by SDS-PAGE and Western blot using a monoclonal antibody specific for the C9 tag. The spike protein-MLV pseudotyped virions were generated three times for wild type or mutants, and the results from the Western blots were quantified using IP lab software and plotted in Sigma Plot 9.0. Error bars represent standard deviation from the mean.

It is considered that SARS-CoV has the ability to fuse in both endocytic and non-endocytic compartments, and as such we assessed any potential differences in the role of this cysteine-flanked region in each of these two pathways of virus entry. We therefore inhibited infection by the endocytic route using the lysosomotropic base NH_4Cl, and induced fusion of surface-bound virions by trypsin activation. At 48 h post trypsin-treatment, cells were assayed for luciferase activity. We observed that in this assay of non-endosomal infection that the overall results reflect both trypsin-untreated assay and the cell-cell fusion data (Fig. 3.6B).

Discussion

The coronavirus spike protein is responsible for mediating both the attachment and fusion that is required to deliver the viral genome. Binding of the virus to the host cell receptor sets in motion a series of rearrangements of the fusion protein in preparation for fusion. The fusion event as directed by the S2 domain requires a concerted cooperation within the domains of the fusion protein. In this study, we describe another region essential to the S2 function of fusing host and viral membrane.

It has been recently published that a critical cleavage event at R797 occurs in SARS-CoV S (2), which might expose a viral fusion peptide (26). 25 residues C-terminal to the cleavage site, we observed an interesting conserved domain flanked by cysteine residues C822 and C833. Given its proximity to a cleavage site and the proposed fusion peptide, we set out to characterize this domain. Sequence alignment of this domain showed a strong conservation particularly in the C-terminus of the region. We set out to carry out a series of mutagenic studies in a comprehensive manner. Our investigation entailed the replacing of core-conserved residues with residues to modify the chemistry of the wild type, and substituting or deleting the residues between the cysteines. This comprehensive investigation of the residues

between C822 and C833 allowed us to gauge the extent of involvement of this region

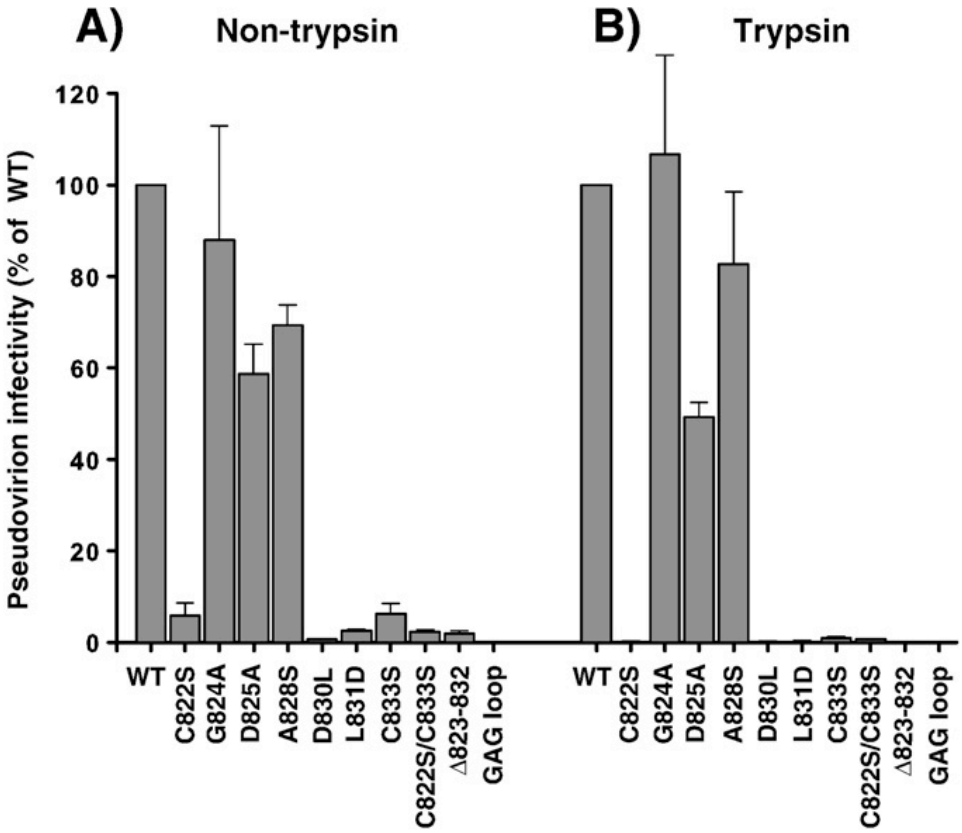

Figure 3.6. Infectivity of spike protein-MLV pseudotyped virions

A. Endosomal infectivity of spike protein-MLV pseudotyped virions. Virions were bound to Vero cells at 4°C in RPMI media for 2hrs. After binding, cells were rinsed in RPMI media before replaced with complete DMEM and incubated at 37°C. 48 h post-binding cells were lysed and assayed for luciferase activity. B. Trypsin-mediated infectivity of spike protein-MLV pseudotyped virions. Virions were bound to Vero cells at 4°C in RPMI media and treated with 25mM ammonium chloride. Fusion was induced using serum-free media containing 2 μg/ml trypsin. The cells were lysed 48 h post fusion induction and supernatants assayed for luciferase activity. Each bar is averaged from three individual infectivity assays and error bars represent standard deviation of the mean.

in the membrane fusion process. In all cases, we observed very limited to no effects on either surface expression or receptor binding, but observed drastic loss in fusogenic ability in the mutants of the core conserved residues, in comparison to the wild type SARS-CoV S in cell-cell fusion assays.

In the context of a virus particle, we generated MLV-pseudovirions containing either WT or mutant S proteins. The mutant proteins were found to incorporate into MLV-pseudovirions at a level suitable for assessment of S function during virus entry. Upon pseudoparticle transduction, a drastic loss in the ability to infect cells was observed for both "endosomal" and "non-endosomal" routes of infection. The manner of sensitivity for these MLV-S mutants was very similar to the cell-cell fusion data thus indicating the importance of this region for fusion.

We hypothesize that this region acts a means of relaying the signal for fusion within the subunit of S2, presumably based on comformational changes induced by low pH and /or receptor binding. One possible way the domain flanked by cysteine residues C822 and C833 may do so is by forming a disulfide bond-anchored loop that interacts with an as yet undisclosed part of the fusion protein to promote membrane fusion. In the absence of a crystal structure of the SARS-CoV S ectodomain, a predictive model of the quaternary structure is available: PDB code 1T7G (4, 36) (Fig. 3.7A). In the context of this model, the cysteine-flanked region is represented as a loop region with the cysteines 822 and 833 positioned directly next to each other, which we predict to form a disulfide bond (Fig. 3.7B).

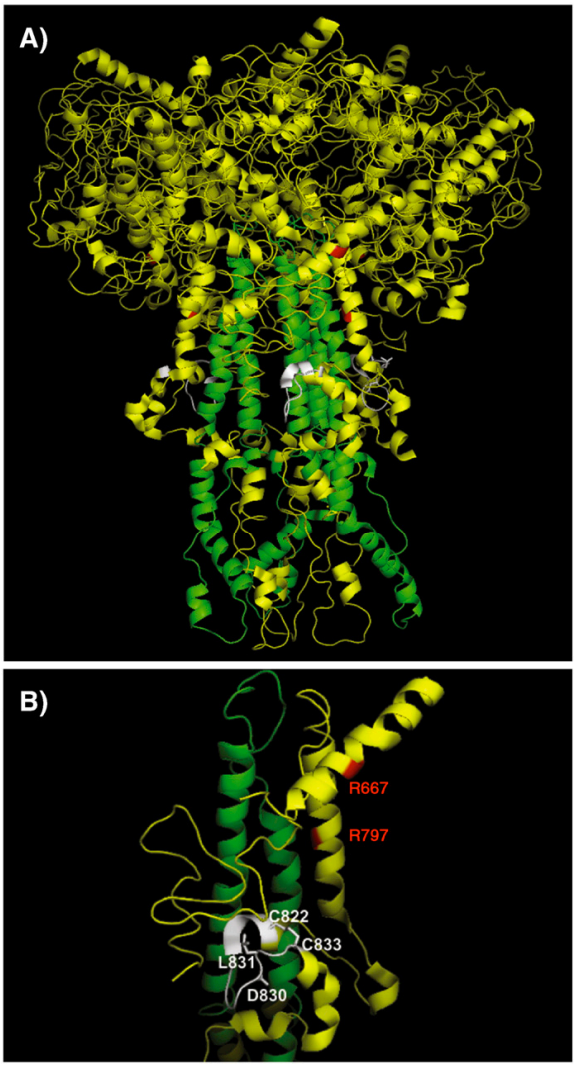

Figure 3.7. Predicted structural model of the Cysteine flanked region

A. A three dimensional model of the SARS-CoV S protein ectodomain trimer with the cysteine-flanked region colored white, both the S1 and S2 cleavage sites (R667 and R797) colored red and HR1 in green.

B. A monomer of the spike depicting the environment of the cysteine flanked region. The side chains of conserved residues C822, D830, L831 and C822 are shown.

The environment is one that might hint at further interactions with other parts of the spike protein. Of particularly interest is the finding that residues C822, L823, G824, D825, I826, N827 and A828 within the loop are part of a major antigenic determinant

of SARS-CoV S (Leu 803 - Ala 828) capable of inducing neutralizing antibodies (44) . In conclusion, we present data of a critical domain of SARS-CoV S2 that is required for the successful function of S-mediated fusion. We propose this region functions by interactions with other domain(s) in S to activate membrane fusion. It is important to point out that in the absence of a "true" crystal structure, we cannot rule out the fact that this region may function through many other possible roles within SARS-CoV S to aid in membrane fusion.

Materials and methods

Cell culture

BHK-21, Vero E6 and 293T cells obtained from the American Type Culture Collection were used in this study. All cells were maintained in Dulbecco's modified Eagle's medium (DMEM, Cellgro) containing 10% fetal bovine serum, 100 units/ml penicillin and 10 μg/ml streptomycin (complete DMEM).

Generation of mutant SARS-CoV spike glycoproteins

Site-directed mutagenesis was carried out on the spike protein-expressing vector pcDNA3.1-SARS-CoV S (kindly provided by Dr. Michael Farzan, New England Primate Research Center) via PCR, using primers obtained from IDT technologies. Mutations were then confirmed by sequencing using an Applied Biosystems Automated 3730 DNA Analyzer at the Cornell University Life Sciences Core Laboratories Center.

Analysis of SARS-CoV S cell surface expression

BHK-21 cells were grown on 6 well plates and transfected with 1 μg of wild type or mutant spike protein expressing plasmids using Lipofectamine 2000 (Invitrogen) for

36 h at 32°C or 24 h at 37°C. Transfected cells were washed twice with cold phosphate buffered saline (PBS) and then labeled with 250 µg/ml Sulfo-NHS-SS-biotin (Pierce) for 30 min on ice. 50 mM cold glycine solution was added to the cells three times at 5 min intervals to quench unlabelled free biotin followed by a PBS wash. The cells were lysed in 500 µl of lysis buffer (Tris-buffered saline (TBS) containing 1% NP-40 and complete protease inhibitor mixture (Roche Applied Science)). The lysates were affinity purified using immobilized NeutraAvidin beads (Pierce) overnight at 4°C. NeutraAvidin beads were then washed with lysis buffer followed by addition of SDS-PAGE sample loading buffer containing 100mM dithiothreitol. The surface expression was analyzed by Western blot using the anti-C9 epitope tag monoclonal antibody Rho 1D4 (National Cell Culture Center, Minneapolis MN) and images were obtained and quantified using a LAS-3000 mini Fuji film imaging system and software (Fuji Photo Film Co., Ltd). The biotinylation assay was repeated three times and results from the western blot quantifications were plotted using Sigma Plot 9.0 (Systat Software).

Human ACE2-Fc binding Assay

293-T cells were grown on 6cm dishes and co-transfected with 2 µg each of wild type or mutant spike protein expressing plasmids and human ACE2-Fc expressing plasmids using Lipofectamine 2000 (Invitrogen) for 48 h at 32°C. Transfected cells were washed with cold phosphate buffered saline (PBS) and the cells were lysed in 500 µl of lysis buffer (Tris-buffered saline (TBS) containing 1% CHAPS and complete protease inhibitor mixture (Roche Applied Science)). The lysates were affinity purified using immobilized Protein A beads (Pierce) overnight at 4°C. Protein A beads were then washed three times with 0.5% CHAPS lysis buffer followed by addition of SDS-PAGE sample loading buffer containing 100mM dithiothreitol. The SARS CoV

S binding to precipitated ACE2-Fc was analyzed by Western blot using the anti-C9 epitope tag monoclonal antibody Rho 1D4 (National Cell Culture Center, Minneapolis MN) and images were obtained and quantified using a LAS-3000 mini Fuji film imaging system and software (Fuji Photo Film Co., Ltd). The binding assay was repeated three times and results from the western blot quantifications were plotted using Sigma Plot 9.0 (Systat Software).

Quantitative cell-cell fusion assay

BHK-21 cells were grown in 24 well plates and co-transfected with wild type or mutant spike protein-expressing plasmids and a plasmid encoding luciferase under the control of a T7 promoter, using Lipofectamine 2000 (Invitrogen) for 24 h at 32°C. Vero E6 cells in a 60 mm dish were also transfected with a plasmid encoding the T7 polymerase. After 24 h the BHK-21 cells were overlaid with Vero E6 cells and incubated for 3 h. Cells were treated with serum-free media containing 2 μg/ml trypsin to induce fusion and replaced with complete DMEM after 30mins. At 6 h post induction, cells were lysed and assayed for Luciferase activity using a Luciferase assay kit (Promega) and a Glomax 20/20 luminometer (Promega) to measure light emission.

Spike protein-pseudotyped virion production

Pseudotyped virions were generated using plasmids kindly provided by Dr. Jean Dubuisson (Lille Pasteur Institute, France). 293T cells were cotransfected with a murine leukemia virus (MLV)-based transfer vector encoding luciferase, a MLV Gag-Pol packaging construct and a pcDNA3.1-SARS-CoV S plasmid encoding wildtype or mutant spike envelope glycoprotein, using Exgen 500 (Fermentas) as recommended. After incubation for 72 h at 32°C, supernatants were collected and filtered through a 0.45 μm pore size membrane. The level of spike protein incorporation was confirmed

by polyethylene glycol (PEG) concentration, centrifugation and western blot analysis. 600 µl of filtered supernatant was mixed with 200 µl 40% PEG and centrifuged for 30 min at 4000 rpm at 4°C. The pellet was redissolved in SDS-PAGE sample loading buffer containing 100 mM dithiothreitol and blotted in the same manner as described above in the cell surface biotinylation assay.

Spike protein-pseudotyped virion infectivity assays

Equal levels of pseudoparticles were used based on the level of spike protein-pseudotyped virions quantified by Western blot, as described above. For a typical infection assay, spike protein-pseudotype virions containing wild-type or mutant glycoproteins were bound for 2 h in RPMI media containing 0.2% BSA, 20 mM HEPES to Vero E6 cells at 4°C. Media was exchanged for complete DMEM and incubated for 48 h at 37°C. The cells were then lysed and luciferase activity measured using the same methods as the quantitative cell-cell fusion assay. In a trypsin-mediated cell surface infectivity assay, Vero E6 cells were first pre-incubated with 25 mM NH_4Cl for 1 h at 37°C. Pseudotyped virions were then bound for 2 h in RPMI media containing 0.2% BSA, 20mM HEPES, and 25 mM NH_4Cl at 4°C. The cells were then warmed up with the addition of pre-warmed RPMI media containing 5 µg/ml trypsin, 0.2% BSA, 20 mM HEPES, and 25 mM ammonium chloride for 5 min at 37°C in a water bath.

Acknowledgements

We thank Ruth Collins and all members of the Whittaker laboratory for helpful discussions and input during the course of this work and Michael Farzan, Tom Gallagher and Jean Dubuisson for their kind provision of reagents. I.G.M. was the recipient of a fellowship from the National Institutes of Health (NIGMS), grant # F31 GM082084. The National Institutes of Health (NIAID) grants R03 AI060946 and R21 AI1076258 also supported this work.

REFERENCES

1. Bartosch, B., J. Dubuisson, and F. L. Cosset. 2003. Infectious hepatitis C virus pseudo-particles containing functional E1-E2 envelope protein complexes. J Exp Med 197:633-42.

2. Belouzard, S., V. C. Chu, and G. R. Whittaker. 2009. Activation of the SARS coronavirus spike protein via sequential proteolytic cleavage at two distinct sites. Proceedings of the National Academy of Sciences of the United States of America 106:5871-5876.

3. Bergeron, E., M. J. Vincent, L. Wickham, J. Hamelin, A. Basak, S. T. Nichol, M. Chretien, and N. G. Seidah. 2005. Implication of proprotein convertases in the processing and spread of severe acute respiratory syndrome coronavirus. Biochemical and Biophysical Research Communications 326:554-563.

4. Bernini, A., O. Spiga, A. Ciutti, S. Chiellini, L. Bracci, X. Yan, B. Zheng, J. Huang, M. L. He, H. D. Song, P. Hao, G. Zhao, and N. Niccolai. 2004. Prediction of quaternary assembly of SARS coronavirus peplomer. Biochem Biophys Res Commun 325:1210-4.

5. Bosch, B. J., B. E. E. Martina, R. van der Zee, J. Lepault, B. J. Haijema, C. Versluis, A. J. R. Heck, R. de Groot, A. Osterhaus, and P. J. M. Rottier. 2004. Severe acute respiratory syndrome coroavirus (SARS-CoV) infection inhibition using spike protein heptad repeat-derived peptides. Proceedings of the National Academy of Sciences of the United States of America 101:8455-8460.

6. Bosch, B. J., and P. J. Rottier. 2008. Nidovirus Entry into Cells, p. 157-178. *In* S. Perlman, T. Gallagher, and E. J. Snijder (ed.), Nidoviruses. ASM Press, Washington DC.

7. Chen, D. S., M. Asanaka, F. S. Chen, J. E. Shively, and M. M. C. Lai. 1997. Human carcinoembryonic antigen and biliary glycoprotein can serve as mouse hepatitis virus receptors. Journal of Virology 71:1688-1691.

8. Chu, V. C., L. J. McElroy, V. Chu, B. E. Bauman, and G. R. Whittaker. 2006. The avian coronavirus infectious bronchitis virus undergoes direct low-pH-dependent fusion activation during entry into host cells. Journal of Virology 80:3180-3188.

9. Delos, S. E., M. B. Brecher, Z. Y. Chen, D. C. Melder, M. J. Federspiel, and J. M. White. 2008. Cysteines flanking the internal fusion peptide are required for the avian sarcoma/leukosis virus glycoprotein to mediate the lipid mixing stage of fusion with high efficiency. Journal of Virology 82:3131-3134.

10. Delos, S. E., and J. M. White. 2000. Critical role for the cysteines flanking the internal fusion peptide of avian sarcoma/leukosis virus envelope glycoprotein. Journal of Virology 74:9738-9741.

11. Drosten, C., S. Gunther, W. Preiser, S. van der Werf, H. R. Brodt, S. Becker, H. Rabenau, M. Panning, L. Kolesnikova, R. A. M. Fouchier, A. Berger, A. M. Burguiere, J. Cinatl, M. Eickmann, N. Escriou, K. Grywna, S. Kramme, J. C. Manuguerra, S. Muller, V. Rickerts, M. Sturmer, S. Vieth, H. D. Klenk, A. Osterhaus, H. Schmitz, and H. W. Doerr. 2003. Identification of a novel coronavirus in patients with severe acute respiratory syndrome. New England Journal of Medicine 348:1967-1976.

12. Du, L. Y., R. Y. Kao, Y. S. Zhou, Y. X. He, G. Y. Zhao, C. Wong, S. B. Jiang, K. Y. Yuen, D. Y. Jin, and B. J. Zheng. 2007. Cleavage of spike protein of SARS coronavirus by protease factor Xa is associated with viral infectivity. Biochemical and Biophysical Research Communications 359:174-179.

13. Follis, K. E., J. York, and J. H. Nunberg. 2006. Furin cleavage of the SARS coronavirus spike glycoprotein enhances cell-cell fusion but does not affect virion entry. Virology 350:358-369.

14. Fouchier, R. A. M., T. Kuiken, M. Schutten, G. van Amerongen, J. van Doornum, B. G. van den Hoogen, M. Peiris, W. Lim, K. Stohr, and A. Osterhaus. 2003. Aetiology - Koch's postulates fulfilled for SARS virus. Nature 423:240-240.

15. Han, D. P., M. Lohani, and M. W. Cho. 2007. Specific asparagine-linked glycosylation sites are critical for DC-SIGN- and L-SIGN-Mediated severe acute respiratory syndrome coronavirus entry. Journal of Virology 81:12029-12039.

16. Hensley, L. E., and R. S. Baric. 1998. Human biliary glycoproteins function as receptors for interspecies transfer of Mouse Hepatitis virus, p. 43-52. *In* L. Enjuanes, S. G. Siddell, and W. Spaan (ed.), Coronaviruses and Arteriviruses, vol. 440.

17. Hofmann, H., G. Simmons, A. J. Rennekamp, C. Chaipan, T. Gramberg, E. Heck, M. Geier, A. Wegele, A. Marzi, P. Bates, and S. Pohlmann. 2006. Highly conserved regions within the spike proteins of human coronaviruses 229E and NL63 determine recognition of their respective cellular receptors. Journal of Virology 80:8639-8652.

18. Holmes, K. V. 2003. SARS-associated coronavirus. New England Journal of Medicine 348:1948-1951.

19. Huang, I. C., B. J. Bosch, F. Li, W. H. Li, K. H. Lee, S. Ghiran, N. Vasilieva, T. S. Dermody, S. C. Harrison, P. R. Dormitzer, M. Farzan, P. J. M. Rottier, and H. Choe. 2006. SARS coronavirus, but not human coronavirus NL63, utilizes cathepsin L to infect ACE2-expressing cells. Journal of Biological Chemistry 281:3198-3203.

20. Jackwood, M. W., D. A. Hilt, S. A. Callison, C. W. Lee, H. Plaza, and E. Wade. 2001. Spike glycoprotein cleavage recognition site analysis of infectious bronchitis virus. Avian Diseases 45:366-372.

21. Kawase, M., K. Shirato, S. Matsuyama, and F. Taguchi. 2009. Protease-Mediated Entry via the Endosome of Human Coronavirus 229E. Journal of Virology 83:712-721.

22. Kwong, P. D., R. Wyatt, J. Robinson, R. W. Sweet, J. Sodroski, and W. A. Hendrickson. 1998. Structure of an HIV gp120 envelope glycoprotein in complex with the CD4 receptor and a neutralizing human antibody. Nature 393:648-659.

23. Lewicki, D. N., and T. M. Gallagher. 2002. Quaternary structure of coronavirus spikes in complex with carcinoembryonic antigen-related cell adhesion molecule cellular receptors. Journal of Biological Chemistry 277:19727-19734.

24. Li, W. H., M. J. Moore, N. Vasilieva, J. H. Sui, S. K. Wong, M. A. Berne, M. Somasundaran, J. L. Sullivan, K. Luzuriaga, T. C. Greenough, H. Choe, and M. Farzan. 2003. Angiotensin-converting enzyme 2 is a functional receptor for the SARS coronavirus. Nature 426:450-454.

25. Li, W. H., J. H. Sui, I. C. Huang, J. H. Kuhn, S. R. Radoshitzky, W. A. Marasco, H. Choe, and M. Farzan. 2007. The S proteins of human coronavirus NL63 and severe acute respiratory syndrome coronavirus bind overlapping regions of ACE2. Virology 367:367-374.

26. Madu, I. G., S. L. Roth, S. Belouzard, and G. R. Whittaker. 2009. Characterization of a Highly Conserved Domain within the Severe Acute Respiratory Syndrome Coronavirus Spike Protein S2 Domain with Characteristics of a Viral Fusion Peptide. Journal of Virology 83:7411-7421.

27. Matthias, L. J., and P. J. Hogg. 2003. Redox control on the cell surface: Implications for HIV-1 entry. Antioxidants & Redox Signaling 5:133-138.

28. Matthias, L. J., P. T. W. Yam, X. M. Jiang, N. Vandegraaff, P. Li, P. Poumbourios, N. Donoghue, and P. J. Hogg. 2002. Disulfide exchange in domain 2 of CD4 is required for entry of HIV-I. Nature Immunology 3:727-732.

29. Parrott, M. M., S. A. Sitarski, R. J. Arnold, L. K. Picton, R. B. Hill, and S. Mukhopadhyay. 2009. Role of Conserved Cysteines in the Alphavirus E3 Protein. Journal of Virology 83:2584-2591.

30. Petit, C. M., V. N. Chouljenko, A. Iyer, R. Colgrove, M. Farzan, D. M. Knipe, and K. G. Kousoulas. 2007. Palmitoylation of the cysteine-rich endodomain of the SARS-coronavirus spike glycoprotein is important for spike-mediated cell fusion. Virology 360:264-274.

31. Petit, C. M., J. M. Melancon, V. N. Chouljenko, R. Colgrove, M. Farzan, D. M. Knipe, and K. G. Kousoulas. 2005. Genetic analysis of the SARS-coronavirus spike glycoprotein functional domains involved in cell-surface expression and cell-to-cell fusion. Virology 341:215-230.

32. Rai, T., D. Marble, K. Rihani, and L. J. Rong. 2004. The spacing between cysteines two and three of the LDL-A module of Tva is important for subgroup A avian sarcoma and leukosis virus entry. Journal of Virology 78:683-691.

33. Schibli, D. J., and W. Weissenhorn. 2004. Class I and class II viral fusion protein structures reveal similar principles in membrane fusion (Review). Molecular Membrane Biology 21:361-371.

34. Schultze, B., C. Krempl, M. L. Ballesteros, L. Shaw, R. Schauer, L. Enjuanes, and G. Herrler. 1996. Transmissible gastroenteritis coronavirus, but not the related

porcine respiratory coronavirus, has a sialic acid (N-glycolylneuraminic acid) binding activity. Journal of Virology 70:5634-5637.

35. Song, H. C., M. Y. Seo, K. Stadler, B. J. Yoo, Q. L. Choo, S. R. Coates, Y. Uematsu, T. Harada, C. E. Greer, J. M. Polo, P. Pileri, M. Eickmann, R. Rappuoli, S. Abrignani, M. Houghton, and J. H. Han. 2004. Synthesis and characterization of a native, oligomeric form of recombinant severe acute respiratory syndrome coronavirus spike glycoprotein. Journal of Virology 78:10328-10335.

36. Spiga, O., A. Bernini, A. Ciutti, S. Chiellini, N. Menciassi, F. Finetti, V. Causarono, F. Anselmi, F. Prischi, and N. Niccolai. 2003. Molecular modelling of S1 and S2 subunits of SARS coronavirus spike glycoprotein. Biochemical and Biophysical Research Communications 310:78-83.

37. Thorp, E. B., J. A. Boscarino, H. L. Logan, J. T. Goletz, and T. M. Gallagher. 2006. Palmitoylations on murine coronavirus spike proteins are essential for virion assembly and infectivity. Journal of Virology 80:1280-1289.

38. Thorp, E. B., and T. M. Gallagher. 2004. Requirements for CEACAMs and cholesterol during murine coronavirus cell entry. Journal of Virology 78:2682-2692.

39. Watanabe, R., S. Matsuyama, K. Shirato, M. Maejima, S. Fukushi, S. Morikawa, and F. Taguchi. 2008. Entry from the Cell Surface of Severe Acute Respiratory Syndrome Coronavirus with Cleaved S Protein as Revealed by Pseudotype Virus Bearing Cleaved S Protein. Journal of Virology 82:11985-11991.

40. Wentworth, D. E., and K. V. Holmes. 2001. Molecular determinants of species specificity in the coronavirus receptor aminopeptidase N (CD13): Influence of N-linked glycosylation. Journal of Virology 75:9741-9752.

41. Xiao, X. D., S. Chakraborti, A. S. Dimitrov, K. Gramatikoff, and D. S. Dimitrov. 2003. The SARS-CoV S glycoprotein: expression and functional characterization. Biochemical and Biophysical Research Communications 312:1159-1164.

42. Yamada, Y. K., K. Takimoto, M. Yabe, and F. Taguchi. 1998. Requirement of proteolytic cleavage of the murine coronavirus MHV-2 spike protein for fusion activity, p. 89-93. *In* L. Enjuanes, S. G. Siddell, and W. Spaan (ed.), Coronaviruses and Arteriviruses, vol. 440.

43. Ye, R., C. Montalto-Morrison, and P. S. Masters. 2004. Genetic analysis of determinants for spike glycoprotein assembly into murine coronavirus virions: Distinct roles for charge-rich and cysteine-rich regions of the endodomain. Journal of Virology 78:9904-9917.

44. Zhang, H., G. W. Wang, H. Li, Y. C. Nie, X. L. Shi, G. W. Lian, W. Wang, X. L. Yin, Y. Zhao, X. X. Qu, M. X. Ding, and H. K. Deng. 2004. Identification of an antigenic determinant on the S2 domain of the severe acute respiratory syndrome coronavirus spike glycoprotein capable of inducing neutralizing antibodies. Journal of Virology 78:6938-6945.

CHAPTER 4

HEPARAN SULFATE IS A SELECTIVE ATTACHMENT FACTOR FOR THE AVIAN CORONAVIRUS IBV BEAUDETTE

Ikenna G. Madu, Victor C. Chu, Hwajin Lee, Andrew D. Regan, Beverley E. Bauman and Gary R. Whittaker. 2007. *Avian Diseases:* Vol. 51, No. 1, pp.45-51.

Summary

The avian coronavirus infectious bronchitis virus (IBV) strain Beaudette is an embryo-adapted virus that has extended species tropism in cell culture. In order to understand the acquired tropism of the Beaudette strain, we compared the S protein sequences of several IBV strains. The Beaudette strain was found to contain a putative heparan sulfate (HS)-binding site, indicating that the Beaudette virus may use HS as a selective receptor. To ascertain the requirements of cell surface HS for Beaudette infectivity, we assayed for infectivity in the presence of soluble heparin as a competitor, and determined infectivity in mutant cell lines with no HS or glycosaminoglycan expression. Our results indicate that HS plays a role as an attachment factor for IBV, working in concert with other factors like sialic acid to mediate virus binding to cells, and may explain in part the extended tropism of IBV Beaudette.

Introduction

Coronaviruses show strong species and tissue tropism, and a major factor in this specificity is the virus receptor on host cells (19). The viral S protein mediates receptor binding, and has been studied in some detail for many coronaviruses, a principal exception being group 3 coronaviruses such as IBV. Group 1 coronaviruses (e.g., HCoV 229E, transmissible gastroenteritis virus, and feline infectious peritonitis virus) are well established to use aminopeptidase N (CD13) as a primary receptor (14,22,36,42); indeed most, if not all, members of this group can apparently use the feline aminopeptidase N (fAPN) for productive entry (35). An exception to this is the recently identified human coronavirus NL63, which uses angiotensin-converting enzyme 2 (ACE2), the severe acute respiratory syndrome (SARS)-CoV receptor (18). In the case of group 2 coronaviruses, glycoproteins in the carcinoembryonic antigen-related glycoprotein family act as receptors (12,39) and SARS-CoV uses ACE2 likely

in combination with CD209L (20,25). There is one published report that fAPN may act as a receptor for the IBV strain Arkansas 99 (30); however, it is unclear whether APN is a general receptor for IBV. Recently, sialic acid has been identified as a receptor determinant for the IBV strains Massachusetts 41 and Beaudette-US (40). The coronavirus receptor is generally considered to be the primary determinant of host range, and this has recently been shown in some detail for SARS-CoV. Viruses isolated during the 2002–2003 SARS outbreak, during the much less severe 2003–2004 outbreak, and from palm civets were analyzed. All three S proteins bound to and used palm civet ACE2 efficiently, but the latter two S proteins used human ACE2 markedly less efficiently, and the lower affinity S proteins could be complemented by incorporating specific mutations (26).

Like most coronaviruses, clinical isolates of IBV show distinct tropism both *in vivo* and in cell culture. The prototype IBV strain (Massachusetts 41 [M41]) causes an acute, highly contagious respiratory disease in chickens. The virus can also replicate in the gastrointestinal tract, oviduct, and kidney, where it can be highly nephropathogenic with the potential to cause up to 44% mortality (8,11); in some cases infection of the proventriculus leads to 75%–100% mortality in young birds (43). IBV is distributed worldwide, and in the United States several serotypes (e.g., Arkansas and Delaware) are currently circulating in addition to the originally identified Massachusetts type. Most isolates of IBV replicate well in the developing chicken embryo following inoculation of the allantoic cavity, and high titers of virus can be isolated from the allantoic fluid. The IBV strain Beaudette was derived from the prototypic M41 strain following at least 150 passages in chick embryos (2,16,29). IBV Beaudette is no longer pathogenic for adult birds but rapidly kills embryos. In terms of host cells, IBV M41 is normally restricted to infection of primary chicken

cells; however, the Beaudette strain of IBV is known to be able to infect a range of cells in culture, including Vero and baby hamster kidney (BHK) (1,17,31). IBV Beaudette therefore represents a significant virus that has extended its host range based on very limited changes in its S protein. IBV M41 and Beaudette are closely homologous (having 96% amino acid identity in their S proteins) and the replacement of the Beaudette S protein with that of M41 shows that the S protein (and by implication the receptor-binding properties of the virus) is the sole determinant of its extended species tropism (7).

Here we carried out a bioinformatic analysis of the S protein of IBV M41 and Beaudette and identified a unique heparin-binding consensus sequence on the Beaudette S protein. We show that IBV Beaudette infection is specifically inhibited by soluble heparin and is restricted for infection in heparan sulfate (HS)-deficient cells, indicating that the specific use of heparan sulfate as an attachment factor is involved in the extended species tropism of IBV Beaudette, most likely in conjunction with sialic acid moieties as well as an additional specific, but unidentified, receptor protein used by all strains of IBV.

Materials and Methods

Virus Growth and Cell culture

IBV (strains Beaudette 42 and Massachusetts 41) were obtained from Dr. Benjamin Lucio-Martinez, Unit of Avian Health Cornell University and propagated in 11 day-old embryonated chicken eggs. Virus was harvested from the allantoic fluid after 24 h of infection for Beaudette and 48 h of infection for Massachusetts 41). BHK cells were obtained from ATCC and grown in DMEM containing 10% fetal calf serum. Wild type CHO cells, as well as the GAG-deficient mutants CHO-677 and CHO-745, were

obtained from ATCC and grown in alpha MEM containing 10% fetal calf serum. Heparin, sodium salt, was obtained from Sigma. Neuraminidase (from Vibrio cholera) was obtained from Roche Applied Science.

Preparation of primary chick kidney (CK) and chick embryo kidney (CEK) cells

For preparation of CK cells, SPF White Leghorn Chicks (11-14 days of age) were placed in a CO_2 chamber and kidneys removed from each side of the chick. Kidney tissue was placed in 25-50 ml sterile PBS and the container shaken gently to remove clots and red blood cells. The supernatant containing the cells was removed and cells rinsed a second time with an equivalent volume of sterile PBS. 25 ml trypsin/EDTA was added and allowed to rinse/digest for approx. 2 min with a stir bar on a stir plate (or by hand-swirling). The trypsin/EDTA was decanted or aspirated and a further 10 ml trypsin/EDTA added. This was then allowed to digest for 2 min with a stir bar on stir plate (or by hand-swirling). The supernatant was poured through sterile cheese-cloth into a sterile beaker with 1 ml FBS on ice, and the trypsin/EDTA digest repeated 1-2 more times until all chunks of tissue were digested. The supernatant was placed into a 50 ml Falcon tube and centrifuged at 1,000 r.p.m. for 2 min. Cells were resuspended in 25 ml M20 media and counted on a hemocytometer. Cells were adjusted to a concentration of 1-1.5 $x10^6$/ml with M25 media containing 5% FBS.

Preparation of CEK cells was essentially as for CK cells, except that kidneys were removed from 19 day chick embryos.

RT-PCR reaction and DNA sequencing

vRNA was extracted from 0.2 mg of sucrose purified virus stock using an RNeasy Plus Mini kit (Qiagen). 10 ng of vRNA was subjected to RT-PCR reaction using the forward primer (5'-TGAAAACTGAACAAAAGACAG-3') and reverse primer (5'-

CTTGTATTAGTTGTTGGAGCG-3') using a OneStep RT-PCR kit (Qiagen) according to manufacturer's instructions. The full-length cDNA product of the IBV spike glycoprotein gene was then purified using QIAquick Gel Extraction kit (Qiagen) and sequenced by the Biotechnology Resource Center (Cornell University). Individual sequences were further analyzed and aligned using the ClustalW online software from the European Bioinformatics Institute (http://www.ebi.ac.uk/clustalw).

Immunofluorescence microscopy

This was essentially performed as described previously (34), except with methanol fixation for IBV antibodies. IBV was identified using anti-S1 monoclonal antibody 15:88 (21). Secondary antibodies used were Alexa 488-labeled or Alexa 568-labeled goat anti-mouse or chicken IgG (Molecular Probes). Nuclei were counterstained with 7.5 mg/ml Hoechst 33258 (Molecular Probes). Cells were viewed on a Nikon Eclipse E600 fluorescence microscope and images captured with a Sensicam EM camera and IPLab software before transfer into Adobe Photoshop 7 and determination of infection frequency.

Flow cytometry

For flow cytometry preparation, cells were scraped gently from the dish, washed in PBS, fixed in 3% paraformaldehyde/PBS, permeabilized in 0.1% Triton X-100 and blocked in 10% goat serum/PBS. To detect virus infection cells were incubated with the monoclonal antibody 15:88 for 30 min, followed by Alexa 488-labeled goat anti-mouse IgG for 30 min. Cells were analyzed on a FACSCalibur cytometer using CellQuest 3.1f software (Becton Dickinson Immunocytometry Systems). Data analysis was performed with Flow Jo 4.6 software (Treestar Inc.). At least 10^4 cells were analyzed for each sample.

Results

Whereas most strains of IBV have restricted tropism, and only efficiently infect embryonated eggs and primary chicken cells in tissue culture, IBV Beaudette has extended species tropism in cell culture. As a way to examine possible differences in tropism, we carried out a bioinformatics analysis of the spike protein sequences for these viruses, with the goal of identifying possible novel receptor-binding sites on the Beaudette virus. We first performed DNA sequence analysis of the Beaudette and prototype Massachusetts (M41) viruses used in our laboratory. The S gene from each virus was reverse-transcribed and then PCR amplified from purified virions, and sequenced. These sequences were designated Bddt_Cornell and Mass41_Cornell and showed a high degree of similarity to published Beaudette and M41 sequences. Sequence information for these viruses is available at NCBI (accession number DQ664534). The predicted amino acid sequences of Bddt_Cornell and Mass41_Cornell were then aligned with the S protein sequences from a number of other representative IBV strains (Fig. 4.1). We observed that IBV Beaudette encoded a novel sequence (SRRKRS or SRRRRS) between residues 686 and 691 that may comprise a heparin-binding site—having a consensus sequence of XBBXBX, where B is a basic residue and X is any amino acid (6). This consensus was present in all Beaudette sequences available in the database, but not present for any other IBV strain analyzed. Because of the known propensity of heparan sulphate (HS) to act as a viral co-receptor (28), we therefore investigated the possible role of the HS as a co-factor in the extended tropism of IBV Beaudette. We first examined whether IBV Beaudette infection could be competed by soluble exogenous heparin. BHK cells were infected with approximately 1 FFU/cell IBV Beaudette, and infection was analyzed at 8 h post infection by immunofluorescence microscopy using an anti-IBV S1 monoclonal

antibody.

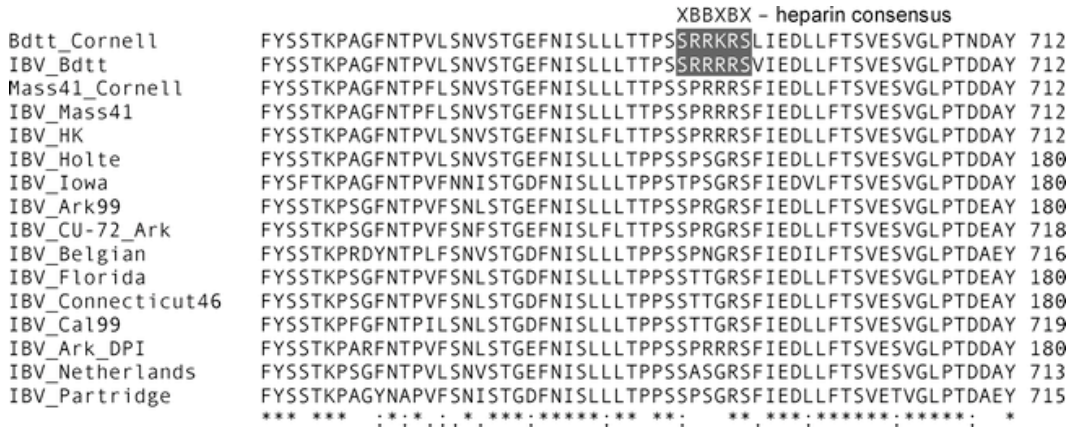

Figure 4.1. Sequence alignment of the region including the potential heparin-binding site of IBV Beaudette.

The single letter amino acid code is used. Asterisk indicates that the residues are identical in all sequences in the alignment, colon indicates that conserved substitutions are present relative to Bdtt_Cornell, period indicates that semiconserved substitutions are present relative to Bdtt_Cornell. The heparin-binding consensus sequence, XBBXBX, is indicated with a gray box, where B = a basic residue and X = any residue. Amino acid residue numbers based on the GenBank submissions are indicated.

In the absence of soluble heparin, approximately 90% of the cells were infected, however in the presence of excess soluble heparin, infectivity was not detectable (Fig 4.2A). To quantify the effect of soluble heparin, we carried out a dose-response experiment of IBV Beaudette infection in BHK cells by flow cytometry (Fig 4.2B). We found that whereas 15 mg/ml soluble heparin gave a complete inhibition of viral

infectivity, 12 mg/ml gave an approximately 50% block, and 8mg/ml or lower gave only a limited or undetectable inhibition of infection.

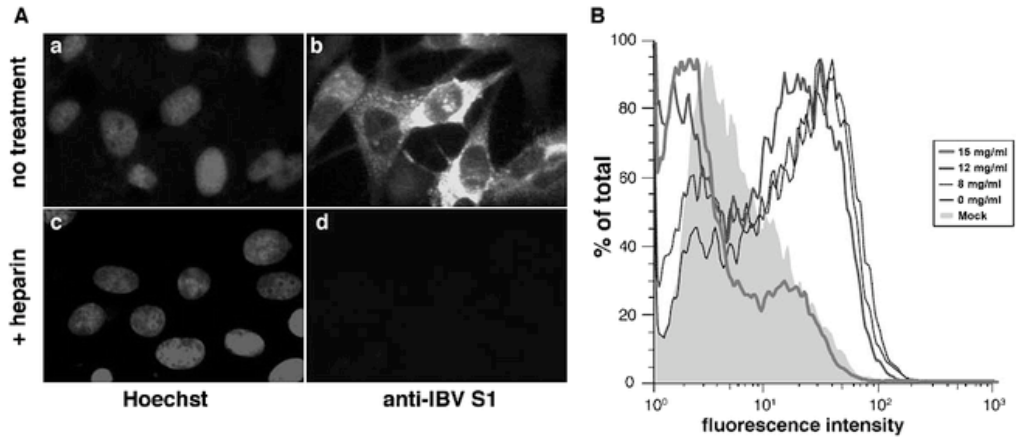

Figure 4.2. Soluble heparin prevents infection by IBV Beaudette

(A) BHK cells were infected with IBV Beaudette that had been treated with 15 mg/ml heparin (c and d) or were untreated (a and b). Cells were analyzed at 8 hr after infection by immunofluorescence microscopy using an anti-S1 monoclonal antibody to detect IBV infection (b and d) and nuclei counterstained with Hoechst 33258. (B) BHK cells were infected with IBV Beaudette that had been treated with varying concentrations of heparin, or were untreated. Cells were also mock infected. Cells were analyzed at 8 hr after infection by flow cytometry using an anti-S1 monoclonal antibody.

To confirm that the effects of the higher levels of soluble heparin were specific for virus entry, we repeated the experiments adding the heparin after the first 60 min of virus infection. Under these conditions, we observed no significant inhibition of IBV infection (data not shown).

To determine whether the effects of soluble heparin were specific for IBV Beaudette, we repeated the experiments in primary chicken kidney (CK) cells and compared the infectivity of IBV Beaudette with the prototype Massachusetts 41 (M41) strain. In the absence of soluble heparin, addition of approximately 1 FFU/cell IBV M41 gave approximately 60-70% infectivity of CK cells, a level of infection that was essentially unchanged incubation with excess soluble heparin (Fig. 4.3). As with BHK cells, approximately 90% of the CK cells were infected by IBV Beaudette in the absence of excess soluble heparin, whereas infectivity of CK cells with IBV was not detectable after incubation with heparin (Fig 4.3). These data show a specific requirement of HS for infection by IBV Beaudette.

Heparan sulphate (HS) is an abundant cell-surface glycosaminoglycan (GAG) that is widely used as a viral attachment factor (28), however other cell-surface GAGs are also expressed at high levels (notably chondroitin sulphate, CS) and can be used as viral receptor moieties (32). To assess the specific contribution of cell surface HS for infection by IBV Beaudette we utilized two mutant CHO cells lines; CHO-745, which is deficient in overall GAG biosynthesis due to a mutation in the xylotransferase I gene, and CHO-677, which is specifically deficient in HS biosynthesis due to mutations in the N-acetylglucosaminyl transferase and glucuronosyl transferase genes (15, 37).

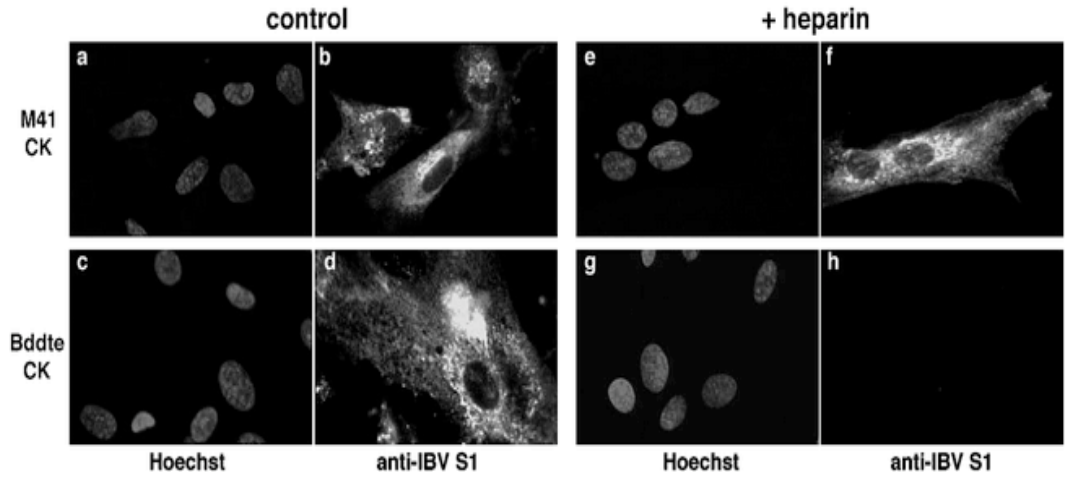

Figure 4.3. Soluble heparin does not prevent infection by IBV M41

Approximately 1 FFU/cell IBV Massachusetts 41 (M41) (a, b, e and f) or Beaudette (Bddte) (c, d, g and h) was used to infect primary chick kidney (CK) cells that had been treated with 15mg/ml heparin (e-h)) or were untreated (a-d)). Cells were analyzed at 8 h post infection by immunofluorescence microscopy using an anti-S1 monoclonal antibody to detect IBV infection (b, d, f and h)) and nuclei counterstained with Hoechst 33258 (a, c, e and g).

We first examined CHO-677 cells, which express no detectable cell-surface HS, but have a three fold-higher expression of CS (15). Infection of wild-type CHO cells with approximately 1 FFU/cell IBV Beaudette resulted in an approximately 70% of the cells being infected. However, infection of CHO-677 cells was significantly reduced or undetectable (<5% infection) (Fig 4.4), confirming the important role for HS in infection by IBV Beaudette.

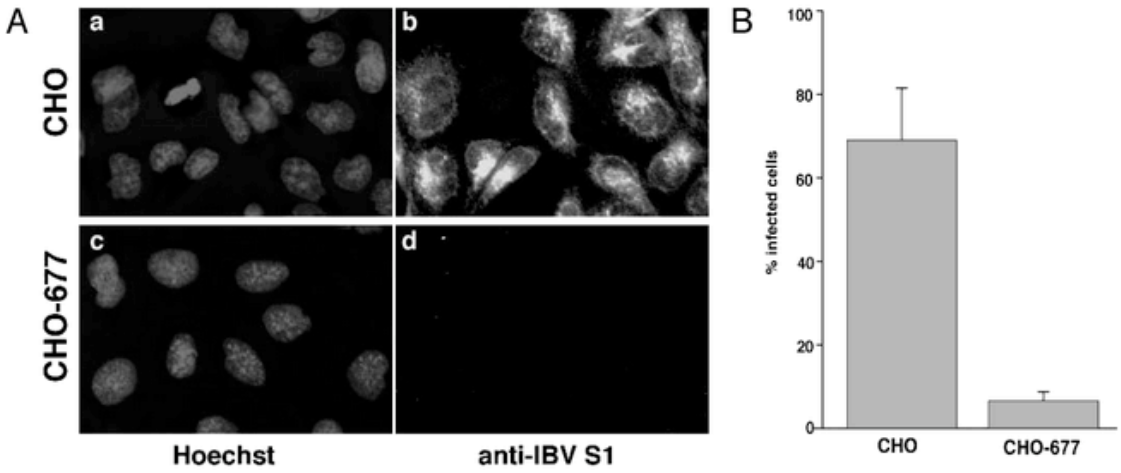

Figure 4.4. IBV Beaudette does not infect heparan sulphate deficient cells

Approximately 1 FFU/cell IBV Beaudette was used to infect CHO-677 cells (panels c and d) or wild type CHO cells (panels a and b). Cells were analyzed at 8 h post infection by immunofluorescence microscopy using an anti-S1 monoclonal antibody to detect IBV infection (panels b and d) and nuclei counterstained with Hoechst 33258 (panels a and and c). B) Quantification of immunofluorescence data. > 300 cells were scored for infection. Error bars represent the standard deviation of the mean.

We next examined CHO-745 cells, which have no detectable cell-surface GAG (15). Unexpectedly, these cells showed no significant reduction in the level of IBV Beaudette infection; for both wild-type and CHO-745 cells we observed approximately 70-75% infection (Fig 4.5). To account for the apparent discrepancy in the data from CHO-677 vs. CHO-745 cells, we considered the possibility that whereas elimination of specific HS-binding sites led to a reduction in IBV Beaudette infection by virtue of the fact that IBV Beaudette–HS interactions were prevented, elimination of all cell surface GAGs in CHO-745 cells exposed an alternative virus binding site(s)

which could act as a virus receptor.

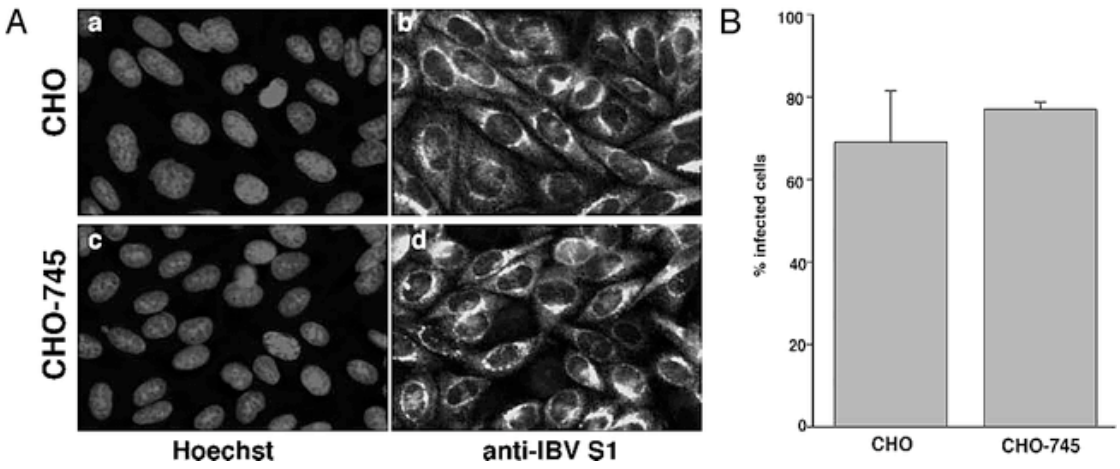

Figure 4.5. IBV Beaudette infects glycosaminoglycan-deficient cells

A) Approximately 1 FFU/cell IBV Beaudette was used to infect CHO-745 cells (c and d) or wild type CHO cells (a and b). Cells were analyzed at 8 h post infection by immunofluorescence microscopy using an anti-S1 monoclonal antibody to detect IBV infection (b and d) B) Quantification of immunofluorescence data. > 300 cells were scored for infection. Error bars represent the standard deviation of the mean.

As sialic acid residues have recently been shown to be involved in binding and entry of IBV (40), we reasoned that CHO-745 cells may have increased sialic acid binding capacity, which overcomes the lack of HS. We therefore assessed the effect of neuraminidase (NA) treatment on infection of CHO-745 cells, along with the effects of NA on CHO-677, wild type CHO and BHK cells. Cells were infected with approximately 1 FFU/cell IBV Beaudette. In all cases treatment with NA reduced infection to a level <5% of that in the absence of NA (Fig. 4.6). Therefore, we consider that HS acts in conjunction with sialic acid for infection of cells by IBV

Beaudette.

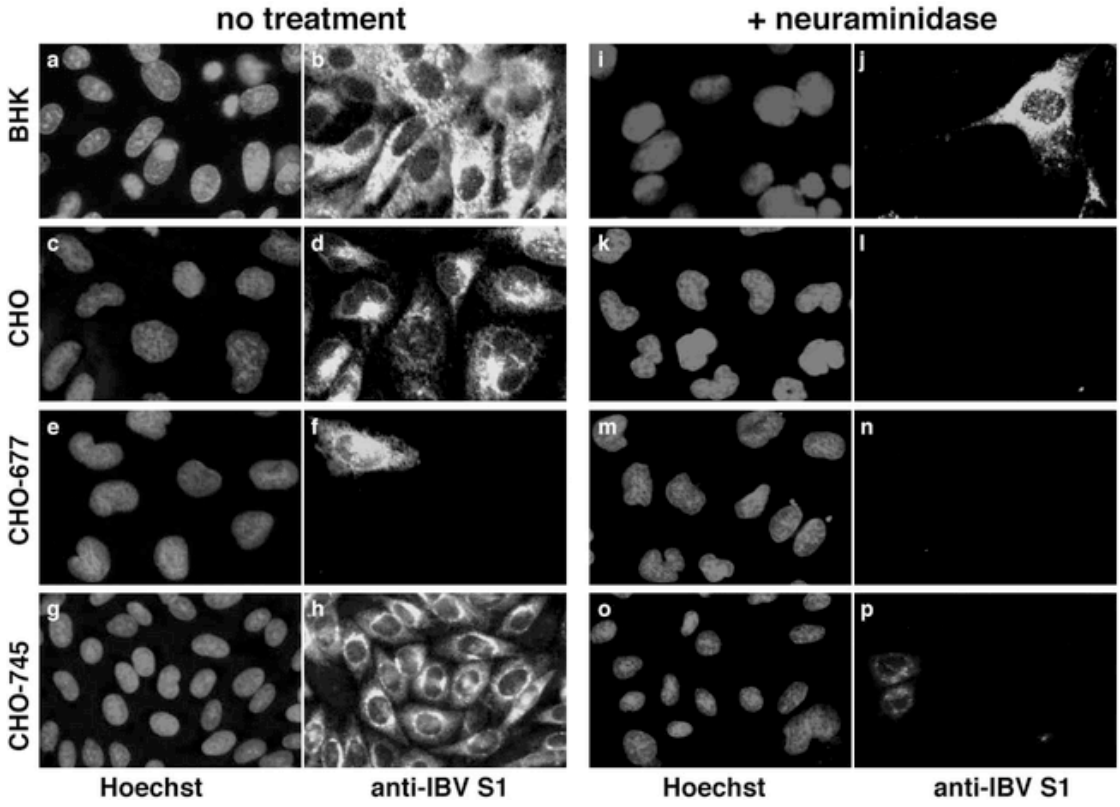

Figure 4.6. Neuraminidase treatment prevents IBV Beaudette infection of glycosaminoglycan-deficient cells

Approximately 1 FFU/cell IBV Beaudette was used to infect BHK (a, b, i and j), wild type CHO (c, d, k and l), CHO-677 (e, f, m and n) or CHO-745 cells (p g, h, o and p) that had been treated with 200 mU/ml neuraminidase (i-p) or were untreated (a-h). Cells were analyzed at 8 h post infection by immunofluorescence microscopy using an anti-S1 monoclonal antibody to detect IBV infection (b, d, f, h, j, l, n and p) and nuclei counterstained with Hoechst 33258 (a, c, e, g, i, k, m and o)

To confirm a general role for sialic acid in IBV infection, we analyzed infection by IBV M41 and Beaudette of chicken embryo kidney (CEK) cells that had been treated with NA. Cells were infected with approximately 1 FFU/cell IBV Beaudette or IBV M41, and in both cases pre-treatment of cells with NA reduced infection to undetectable levels compared to untreated cells (Fig. 4.7). Identical results were obtained with primary CK cells (data not shown). Overall, these data confirm a general role for sialic acid as an attachment factor for IBV, acting in concert with specific HS-mediated binding of IBV Beaudette.

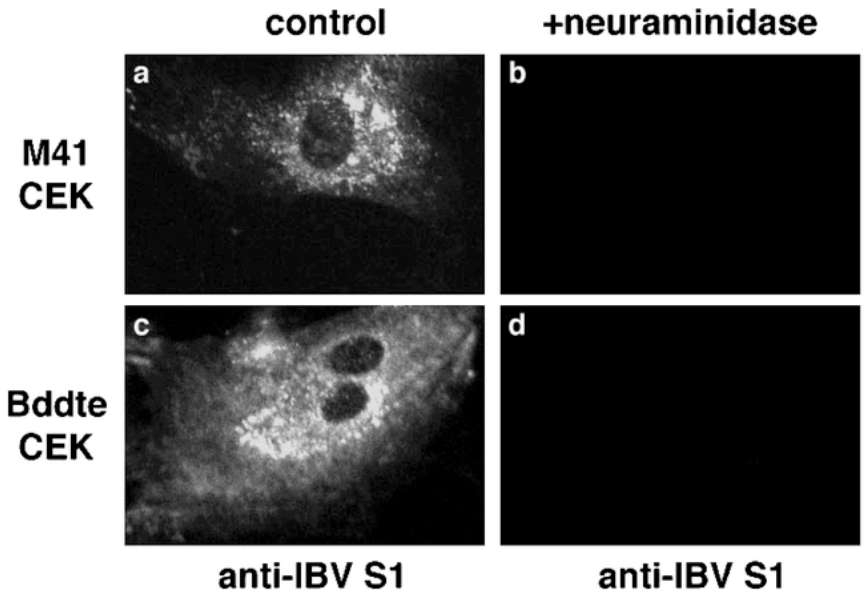

Figure 4.7. Neuraminidase treatment prevents IBV M41 and Beaudette infection of primary chick cells

Approximately 1 FFU/cell IBV Massachusetts 41 (M41) (a and b) or Beaudette (Bddte) (c and d) was used to infect primary chick embryo kidney (CEK) cells that had been treated with 200 mU/ml neuraminidase (b and d)) or were untreated (a and b)). Cells were analyzed at 8 h post infection by immunofluorescence microscopy using an anti-S1 monoclonal antibody to detect IBV infection.

Discussion

IBV Beaudette is an embryo-adapted avian coronavirus with an extended host range in cell culture. We show here that this extended tropism may in part be due to the use of HS as a selective attachment factor; excess soluble heparin competed with IBV Beaudette infection. Excess soluble heparin competed with IBV M41 infection. HS is well established as a cofactor in entry of a wide variety of viruses (28,32). However the levels of heparin needed for inhibition of IBV Beaudette infection were relatively high (approximately 12 mg/ml), which is significantly higher than for other viruses where heparin typically gives inhibition of infectivity, for example with Dengue virus and herpes simplex virus (27,41). However, in other cases, virus binding is only inhibited by high levels of heparan sulfate, e.g., a human rhinovirus type 89 variant was inhibited at heparin concentrations of 2 mg/ml (38) and adeno-associated virus type 3H required pretreatment of cells with 50–100 mg/ml to prevent infections (4). Our data indicate that the affinity of IBV Beaudette–HS interactions is quite low. However, owing to the multivalent nature of virus–cell interactions, it is not possible to determine a value for this low-affinity interaction.

To further characterize the heparin binding of IBV Beaudette, we carried out experiments with CHO cells that are deficient in HS/GAG expression, as well as carrying out experiments on BHK cells where surface HS was enzymatically removed with heparinase treatment (data not shown). However, in contrast to the situation where the virus receptor–binding sites are blocked by excess soluble heparin, we believe that the absence of HS/GAG on the cells surface can expose additional binding sites for the virus (i.e., sialic acid), and so these treatments do not inhibit infection with IBV Beaudette. In other words, blockage of a HS-binding site on the virus is not equivalent to removal of HS from the cell surface.

One distinctive feature of IBV Beaudette that may account for the specific interaction with HS is the presence of a novel sequence (SRRKRS or SRRRRS) between residues 686 and 691, which fits the heparin-binding consensus sequence of XBBXBX, where B is a basic residue and X is any amino acid (6). This consensus was present in all Beaudette sequences available in the database but not present for any other IBV strain analyzed. It is presently unclear whether this sequence is responsible for HS binding of IBV Beaudette. The consensus sequence identified by Cardin and Weintraub is based on the assumption that all GAG-binding proteins interact with the same oligosaccharides within heparin, a strategy that has been suggested to be overly simplistic (37). In fact examination of the consensus binding sites for heparin in basic fibroblast growth factor turned out to be incorrect once the crystal structure was determined. In the case of IBV Beaudette, the SRRKRS or SRRRRS motif is actually present in the S2 domain of the spike protein and not the S1 domain typically associated with receptor interactions. However, in the absence of detailed structural information, it cannot be ruled out that this region of S2 (between 686 and 691) is not exposed for use in viral attachment; the use of this as a receptor-binding site awaits experimental analysis.

As shown recently by Winter and colleagues (40), we confirm that sialic acid is an attachment factor for both IBV Beaudette and M41 and likely acts in a similar manner for all IBV strains. This is unusual, since most IBV strains do not ordinarily hemagglutinate red blood cells unless the virions themselves are pretreated with NA (3,9,33), and IBV Beaudette does not hemagglutinate red blood cells at all (3). Unlike some other coronaviruses that use sialic acid receptors, IBV does not encode a hemagglutinin-esterase protein that might act to cleave the receptor moities and allow efficient virus release and spread (8). Ultimately it is likely that despite acting as low-

affinity attachment factors, neither HS nor sialic acid comprise the critical receptor for IBV entry into cells. The identification of this receptor is currently unknown. Like Winter *et al.* (40), we have been unable to rescue IBV M41 infection in BHK cells by expression of feline or human aminopeptidase N (J. Aronson, V. Chu, and G. Whittaker, unpubl. data), suggesting that aminopeptidase N is not a functional IBV receptor. The entry and receptor binding of IBV is likely to be complex process, and the specific use of HS by IBV Beaudette clearly demonstrates one important piece of the complex picture for IBV entry—the initial use of heparin sulfate by IBV Beaudette, which may play a critical role in the pathogenesis and host range of the virus. It is presently unclear whether HS binding accounts for differential tissue tropism of IBV Beaudette within the infected embryo, in addition to its possible role in extended species tropism. Experiments to determine the role of HS for IBV Beaudette of the chick embryo are currently underway.

Acknowledgements

We thank Benjamin Lucio-Martinez for virus isolates, Damon Ferguson for technical assistance, and Elizabeth Buckles and all members of the Whittaker lab for helpful discussions. This work was supported in part by grant R03 AI060946 from the National Institutes of Health.

REFERENCES

1. Alonso-Caplen, F. V., Y. Matsuoka, G. E. Wilcox, and R. W. Compans. 1984. Replication and morphogenesis of avian coronavirus in Vero cells and their inhibition by monensin. Virus Res 1:153-67.

2. Beaudette, F. R., and C. R. Hudson. 1937. Cultivation of the virus of infectious bronchitis. J. Amer. Vet. Med. Ass. 90:51-60.

3. Bingham, R. W., M. H. Madge, and D. A. Tyrrell. 1975. Haemagglutination by avian infectious bronchitis virus-a coronavirus. J Gen Virol 28:381-90.

4. Blackburn, S. D., R. A. Steadman, and F. B. Johnson. 2006. Attachment of adeno-associated virus type 3H to fibroblast growth factor receptor 1. Arch Virol 151:617-23.

5. Bosch, B. J., R. van der Zee, C. A. de Haan, and P. J. Rottier. 2003. The coronavirus spike protein is a class I virus fusion protein: structural and functional characterization of the fusion core complex. J Virol 77:8801-11.

6. Cardin, A. D., and H. J. Weintraub. 1989. Molecular modeling of protein-glycosaminoglycan interactions. Arteriosclerosis 9:21-32.

7. Casais, R., B. Dove, D. Cavanagh, and P. Britton. 2003. Recombinant avian infectious bronchitis virus expressing a heterologous spike gene demonstrates that the spike protein is a determinant of cell tropism. J Virol 77:9084-9.

8. Cavanagh, D. 2005. *Coronaviridae*: a review of coronaviruses and toroviruses, p. 1-54. *In* A. Schmidt, M. H. Wolff, and O. Weber (ed.), Coronaviruses with Special Emphasis on First Insights Concerning SARS. Birkhauser Verlag, Basel/Switzerland.

9. Cavanagh, D., and P. J. Davis. 1986. Coronavirus IBV: removal of spike glycopolypeptide S1 by urea abolishes infectivity and haemagglutination but not attachment to cells. J Gen Virol 67 (Pt 7):1443-8.

10. Cavanagh, D., P. J. Davis, D. J. Pappin, M. M. Binns, M. E. Boursnell, and T. D. Brown. 1986. Coronavirus IBV: partial amino terminal sequencing of spike polypeptide S2 identifies the sequence Arg-Arg-Phe-Arg-Arg at the cleavage site of the spike precursor propolypeptide of IBV strains Beaudette and M41. Virus Res 4:133-43.

11. Cavanagh, D., and S. A. Naqi. 2003. Infectious Bronchitis, p. 101-119. *In* S. M. Saif (ed.), Diseases of Poultry. Iowa State Press, Ames, Iowa.

12. Chen, D. S., M. Asanaka, F. S. Chen, J. E. Shively, and M. M. Lai. 1997. Human carcinoembryonic antigen and biliary glycoprotein can serve as mouse hepatitis virus receptors. J Virol 71:1688-91.

13. de Haan, C. A., K. Stadler, G. J. Godeke, B. J. Bosch, and P. J. Rottier. 2004. Cleavage inhibition of the murine coronavirus spike protein by a furin-like enzyme affects cell-cell but not virus-cell fusion. J Virol 78:6048-54.

14. Delmas, B., J. Gelfi, R. L'Haridon, L. K. Vogel, H. Sjostrom, O. Noren, and H. Laude. 1992. Aminopeptidase N is a major receptor for the entero-pathogenic coronavirus TGEV. Nature 357:417-20.

15. Esko, J. D., T. E. Stewart, and W. H. Taylor. 1985. Animal cell mutants defective in glycosaminoglycan biosynthesis. Proc Natl Acad Sci U S A 82:3197-201.

16. Fabricant, J. 1951. Studies on the diagnosis of Newcastle disease and infectious bronchitis. IV. The use of the serum neutralization test in the diagnosis of infectious bronchitis. Cornell Vet. 61:68-80.

17. Fang, S. G., S. Shen, F. P. Tay, and D. X. Liu. 2005. Selection of and recombination between minor variants lead to the adaptation of an avian coronavirus to primate cells. Biochem Biophys Res Commun 336:417-23.

18. Hofmann, H., K. Pyrc, L. van der Hoek, M. Geier, B. Berkhout, and S. Pohlmann. 2005. Human coronavirus NL63 employs the severe acute respiratory

syndrome coronavirus receptor for cellular entry. Proc Natl Acad Sci U S A 102:7988-93.

19. Holmes, K. V., and S. R. Compton. 1995. Coronavirus receptors, p. 55-71. *In* S. G. Siddell (ed.), The Coronaviridae. Plenum Press, New York.

20. Jeffers, S. A., S. M. Tusell, L. Gillim-Ross, E. M. Hemmila, J. E. Achenbach, G. J. Babcock, W. D. Thomas, Jr., L. B. Thackray, M. D. Young, R. J. Mason, D. M. Ambrosino, D. E. Wentworth, J. C. Demartini, and K. V. Holmes. 2004. CD209L (L-SIGN) is a receptor for severe acute respiratory syndrome coronavirus. Proc Natl Acad Sci U S A 101:15748-53.

21. Karaca, K., S. Naqi, and J. Gelb, Jr. 1992. Production and characterization of monoclonal antibodies to three infectious bronchitis virus serotypes. Avian Dis 36:903-15.

22. Kolb, A. F., A. Hegyi, and S. G. Siddell. 1997. Identification of residues critical for the human coronavirus 229E receptor function of human aminopeptidase N. J Gen Virol 78 (Pt 11):2795-802.

23. Lai, M. M. C., and K. V. Holmes. 2001. *Coronaviridae:* The Viruses and Their Replication. *In* D. M. Knipe and P. M. Howely (ed.), Fields Virology. Lippincott Wilkins and Williams, Philadelphia.

24. Li, F., W. Li, M. Farzan, and S. C. Harrison. 2005. Structure of SARS coronavirus spike receptor-binding domain complexed with receptor. Science 309:1864-8.

25. Li, W., M. J. Moore, N. Vasilieva, J. Sui, S. K. Wong, M. A. Berne, M. Somasundaran, J. L. Sullivan, K. Luzuriaga, T. C. Greenough, H. Choe, and M. Farzan. 2003. Angiotensin-converting enzyme 2 is a functional receptor for the SARS coronavirus. Nature 426:450-4.

26. Li, W., C. Zhang, J. Sui, J. H. Kuhn, M. J. Moore, S. Luo, S. K. Wong, I. C. Huang, K. Xu, N. Vasilieva, A. Murakami, Y. He, W. A. Marasco, Y. Guan, H. Choe, and M. Farzan. 2005. Receptor and viral determinants of SARS-coronavirus adaptation to human ACE2. Embo J 24:1634-43.

27. Lin, Y. L., H. Y. Lei, Y. S. Lin, T. M. Yeh, S. H. Chen, and H. S. Liu. 2002. Heparin inhibits dengue-2 virus infection of five human liver cell lines. Antiviral Res 56:93-6.

28. Liu, J., and S. C. Thorp. 2002. Cell surface heparan sulfate and its roles in assisting viral infections. Med Res Rev 22:1-25.

29. McMartin, D. 1993. Infectious Bronchitis. *In* J. B. McFerran and M. S. McNulty (ed.), Virus Infections of Birds. Elsevier, Amsterdam.

30. Miguel, B., G. T. Pharr, and C. Wang. 2002. The role of feline aminopeptidase N as a receptor for infectious bronchitis virus. Brief review. Arch Virol 147:2047-56.

31. Otsuki, K., K. Noro, H. Yamamoto, and M. Tsubokura. 1979. Studies on avian infectious bronchitis virus (IBV). II. Propagation of IBV in several cultured cells. Arch Virol 60:115-22.

32. Rostand, K. S., and J. D. Esko. 1997. Microbial adherence to and invasion through proteoglycans. Infect Immun 65:1-8.

33. Schultze, B., L. Enjuanes, D. Cavanagh, and G. Herrler. 1993. N-acetylneuraminic acid plays a critical role for the haemagglutinating activity of avian infectious bronchitis virus and porcine transmissible gastroenteritis virus. Adv Exp Med Biol 342:305-10.

34. Sieczkarski, S. B., and G. R. Whittaker. 2002. Influenza virus can enter and infect cells in the absence of clathrin-mediated endocytosis. J. Virol. 76:10455-10464.

35. Tresnan, D. B., and K. V. Holmes. 1998. Feline aminopeptidase N is a receptor for all group I coronaviruses. Adv Exp Med Biol 440:69-75.

36. Tresnan, D. B., R. Levis, and K. V. Holmes. 1996. Feline aminopeptidase N serves as a receptor for feline, canine, porcine, and human coronaviruses in serogroup I. J Virol 70:8669-74.

37. Varki, A., R. Cummings, J. D. Esko, H. Freeze, G. Hart, and J. Marth (ed.). 1999. Essentials of Glycobiology. Cold Spring Harbor Press, Cold Spring Harbor, NY.

38. Vlasak, M., I. Goesler, and D. Blaas. 2005. Human rhinovirus type 89 variants use heparan sulfate proteoglycan for cell attachment. J Virol 79:5963-70.

39. Williams, R. K., G. S. Jiang, and K. V. Holmes. 1991. Receptor for mouse hepatitis virus is a member of the carcinoembryonic antigen family of glycoproteins. Proc Natl Acad Sci U S A 88:5533-6.

40. Winter, C., C. Schwegmann-Wessels, D. Cavanagh, U. Neumann, and G. Herrler. 2006. Sialic acid is a receptor determinant for infection of cells by avian Infectious bronchitis virus. J Gen Virol 87:1209-1216.

41. WuDunn, D., and P. G. Spear. 1989. Initial interaction of herpes simplex virus with cells is binding to heparan sulfate. J Virol 63:52-8.

42. Yeager, C. L., R. A. Ashmun, R. K. Williams, C. B. Cardellichio, L. H. Shapiro, A. T. Look, and K. V. Holmes. 1992. Human aminopeptidase N is a receptor for human coronavirus 229E. Nature 357:420-2.

43. Yu, L., Y. Jiang, S. Low, Z. Wang, S. J. Nam, W. Liu, and J. Kwangac. 2001. Characterization of three infectious bronchitis virus isolates from China associated with proventriculus in vaccinated chickens. Avian Dis 45:416-24.

CHAPTER 5

SUMMARY AND CONCLUSIONS

Coronaviruses like SAR-CoV have had a negative impact on humans while the poultry industry has suffered financial losses due to the avian coronavirus IBV. In both cases, coronaviruses utilize their envelope spike glycoprotein S to gain entry in to the target cell. The S protein binds to a host cell receptor and this triggers conformational changes that make the S protein fusion ready. The S protein, a class 1 fusion protein is capable of juxtaposing, destabilizing and fusing viral and host membranes. The coronavirus S protein has been the topic of a lot of research especially since the SARS outbreak, I have set out to characterize domains in S protein of the avian coronavirus the infectious bronchitis virus (IBV) and the severe acute respiratory coronavirus (SARS-CoV) utilized for entry.

In Chapter 2, we introduce residues S798 to F815 corresponding with the S protein sequence as a putative fusion peptide. The region of the S protein was in close proximity to a newly identified cleavage site within S as well as highly conserved across the coronavirus family. Our studies showed that key conserved residues: L803, L804, F805 were important for fusion assays. Point mutants of the key residues drastically altered the fusiogenic potential of S in cell-cell fusion assays. Also in the pseudo-viral infection assays we observed that while pseudo-particles bearing the wildtype S were able to infect cells either at the cell surface or by the endosomal pathway, the pseudo-particles bearing point mutants of the key residues could not afford the same level of infection. We also took our studies a step further to show that synthetic peptides corresponding to the wildtype putative FP sequence were able to interact with membranes in a manner that promotes fusion and lipid mixing between labeled and unlabelled liposomes, while mutants peptides corresponding to the conserved residues highlighted in both cell-cell fusion and pseudovirus infection assays could not fuse.

In chapter 3, we try to extend our understanding of the requirements for S mediated membrane fusion. We introduce conserved cysteine flanked domain (CFD) that we propose is part of the part of the machinery responsible for relaying the message of fusion. We hypothesize that the mechanism by which the signal for fusion is relayed within S might include cysteine disulfide loops formed between the flanking residues. Through mutations and deletions to the CFD, we were able to assay for function in fusion and infection assays, to demonstrate the importance of this region.

Finally in chapter 4, we investigated the possible role of heparan sulfate (HS) a Glycosaminoglycan (GAG) as possible attachment factor for IBV. We observed that in the S protein of the IBV Beaudette, an avian coronavirus with extended host range was the presence of a novel sequence (SRRKRS or SRRRRS) between residues 686 and 691, which fits the heparin-binding consensus sequence of XBBXBX, where B is a basic residue and X is any amino acid. We set out to show that this extended tropism might be due to the use of HS as a selective attachment factor with the use of soluble heparin in competitive infection assays and CHO cells deficient in HS/GAG expression.

In terms of the current state of affairs regarding S protein mediated CoV entry, our studies though quite recent, have been met with consensus in recent literature. Most interesting is the consensus idea on the importance of the role of cleavage in the activation of the spike protein for membrane fusion (3, 4). Even better is the observation that the cleavage occurring directly upstream of our proposed fusion peptide has been implicated to be important for fusion in the avian coronavirus IBV (5). Also in unpublished data from our lab we observe an interesting flexibility in cleavage of the region N-terminal to the proposed fusion peptide. The indications from the results might further support the argument that this fusion peptide region might be

internal and a host of proteases can act on the spike either in close proximity to the fusion peptide or further upstream akin to the same situation observed in ASLV or EBOV.

With all indications in the literature on the need for proteolytic activity for S protein function in membrane fusion and particularly as observed in IBV, it is more possible that our initial assessment of the region of the IBV Beaudette S protein as having a heparin sulfate (HS) binding site might take a backseat to the observation that the region is a designated furin cleavage site. We are already familiar with the advantage of furin cleavability and heparin sulfate binding in CoVs (1, 2) so it is possible that this novel region might work to extend the host range through HS binding and then increase cell-cell spread through furin cleavage.

Future Directions

In Chapter 2, we put forth a significant argument why the region S798-F815 corresponding to the S2 portion of the SARS-CoV could be a coronavirus fusion peptide. In support of our claim, we observed that mutations made to select residues within the proposed sequence and in the context of the full length fusion protein showed decreased fusion activity and the synthetic peptides to the fusion peptide could promote fusion.

A possible step to conclusively prove that this is the fusion peptide would be to show experimentally that cleavage exposes this fusion peptide. An antibody prepared against the fusion peptide can be used to detect the exposure of the fusion peptide upon cleavage. Also if the antibody is able to block infection, it can be proposed that the antibody inhibits the fusion peptide from properly inserting in to the host membrane. Also confirmation that the fusion peptide actually interacts with the host

membrane in context with the full length fusion protein can be achieved by identifying sequences that can be labeled by cross-linking probes embedded in the target membrane. All these suggestions are currently being pursued in our laboratory.

Finally, it is my belief that we stand to gain a lot of information if the structure of the S protein can be solved as we have benefited immensely from the amount of information gained from solved structures of other viral protein. Ultimately a solved structure would help shed light on the claims put forth in its absence and perhaps further aid in the development of potent therapeutics.

REFERENCES

1. de Haan, C. A. M., B. J. Haijema, P. Schellen, P. W. Schreur, E. T. Lintelo, H. Vennema, and P. J. M. Rottier. 2008. Cleavage of group 1 coronavirus spike proteins: How furin cleavage is traded off against heparan sulfate binding upon cell culture adaptation. Journal of Virology 82:6078-6083.
2. de Haan, C. A. M., Z. Li, E. T. Lintelo, B. J. Bosch, B. J. Haijema, and P. J. M. Rottier. 2005. Murine coronavirus with an extended host range uses heparan sulfate as an entry receptor. Journal of Virology 79:14451-14456.
3. Kawase, M., K. Shirato, S. Matsuyama, and F. Taguchi. 2009. Protease-Mediated Entry via the Endosome of Human Coronavirus 229E. Journal of Virology 83:712-721.
4. Watanabe, R., S. Matsuyama, K. Shirato, M. Maejima, S. Fukushi, S. Morikawa, and F. Taguchi. 2008. Entry from the Cell Surface of Severe Acute Respiratory Syndrome Coronavirus with Cleaved S Protein as Revealed by Pseudotype Virus Bearing Cleaved S Protein. Journal of Virology 82:11985-11991.
5. Yamada, Y., and D. X. Liu. 2009. Proteolytic Activation of the Spike Protein at a Novel RRRR/S Motif Is Implicated in Furin-Dependent Entry, Syncytium Formation, and Infectivity of Coronavirus Infectious Bronchitis Virus in Cultured Cells. Journal of Virology 83:8744-8758.